Feasibility Study of a Fast Electric Passenger Ferry

Moreno Alexander Johannes Francis

CoCo Yachts

TUDelft

Feasibility Study of
a Fast Electric Passenger Ferry

By

Moreno Alexander Johannes Francis

to obtain the degree of
Master of Science in **Marine Technology**
in the specialization of
Ship Design
at the
Delft University of Technology
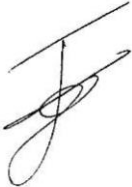
CoCo Yachts

The undersigned approves, in name of CoCo Yachts B.V., the publication of this report on http://repository.tudelft.nl/ in August 2019.

Name: T. Frijters

Date: 29-07-2019

Signature:

Preface

During my time at the **Delft University of Technology**, I've had some setbacks, leading to a study carrier of almost ten years. For a long time, graduating seemed like a faraway dream, but the fact that you are reading this means that I succeeded. So I am proud to present this document to you, which is the report of my master thesis project, the final challenge of the master Marine Technology (specialization Ship Design) at the Delft University of Technology.

I carried out my project at **CoCo Yachts B.V.**, a ship designing company specialized in high speed vessels. These are built by various shipyards, for customers all over the world. CoCo Yachts was founded in November 2011, and currently has 21 employers. At the start of this thesis they were working on a design for a low speed electric ferry to operate in the waters of Gorinchem, the Netherlands, which is the place where their office is located. As most of the ships in their portfolio are classified as fast ferries, CoCo Yachts wanted to know if a high speed electric ferry is feasible as well. My project is a case study that looked at the feasibility of replacing one of their ferries with an electric version.

The only thing left to say: enjoy…

Moreno
Gorinchem, July 2019

Summary

Negative effects of global warming can already be noticed. The burning of fossil fuels not only contributes to this global warming, but also to a reduction of air quality, especially in urban areas. In order to limit the climate change, as well as to improve the air quality, more and more vehicles are replaced by emission free versions. In practice, as well as in this report, an emission free vehicle is an electric vehicle. Therefore, the terms 'electric' and 'emission free' are used interchangeably throughout this report.

The revolution of electrifying vehicles also takes place in Shenzhen, China, the first city in the world that has a fully electric public bus fleet. A lot of people travel by water, so there are many fast ferries in the region of Shenzhen, such as CoCo Yachts' Coastal Cruiser 300. Since Shenzhen is motivated to decrease pollution, it makes sense to replace these passenger ferries with emission free versions as well.

This thesis is a case study in which the feasibility of replacing the Coastal Cruiser 300 by an emission free ferry was investigated. One of the first steps was an exploration of different methods of emission free propulsion. The next step was to look at the effect of implementing these methods into the design of the current ferry. Because the feasibility is limited, different ways of reducing the energy consumption of the ferry were analysed. Because a more severe reduction is desirable, the last analysis of this project was a hydrofoil supported catamaran.

Exploration of Emission Free Propulsion Methods

Two options remained after analysing different methods for emission free propulsion: battery powered and hydrogen fuel cell powered. Operating on supercapacitors is similar to operating on batteries, but because they are heavier and more expensive than batteries, supercapacitors were not chosen as an option. Solar cells were also not be implemented in the concept design, as their contribution is negligibly small.

The main problem of batteries is its large mass, and the hydrogen powered ferry suffers from a large increase in fuel costs, as hydrogen is much more expensive than diesel fuel. So in both cases, the energy consumption must be sufficiently low.

Costs related to the power and propulsion system were also analysed. It is however important to keep in mind that costs is not the most important aspect of the emission free ferry. The reduction in emissions might be worth the additional costs. Furthermore, it might lead to a reduction in indirect costs related to pollution.

Implementing the Electric Propulsion Systems into the Design

A battery powered version is not feasible, because the weight of the vessel is too large, resulting in a too large increase in resistance and energy consumption. Thus a reduction in energy consumption is desirable to achieve a feasible battery powered fast ferry.

The hydrogen powered ferry is feasible, but the higher costs make a reduction in energy consumption desirable.

Analysis of Ways to Reduce the Energy Consumption

Energy consumption can be influenced by changes in design (i.e. elongated hull, lighter structure and improved system performance in the future), as well as by changes in the operational profile (i.e. sailing at a lower speed and operating on a shorter distance). The effect of changing these parameters was analysed for both the battery and hydrogen powered ferry.

Battery Powered Concept Ferry

In case of the battery powered catamaran, operating on the 25 NM crossing is only possible with an elongated hull. A lighter structure improves the feasibility of the elongated version, but it has no effect on the concept with the original length. Looking at costs, the battery powered ferry is likely to be more expensive than the diesel powered ferry, but this depends on the electricity price and diesel fuel price.

If the battery performance improves in the future, the feasibility increases. With 1,000 Wh/kg batteries, feasibility exists for all estimations, with a strong indication that operating on batteries is cost competitive with operating on diesel fuel.

Decreasing the design speed does not significantly reduce energy consumption, as the reduction in resistance is roughly proportional to the increase in travel time. Furthermore, without changing the timetable, the charging time at quay gets smaller if the travel time increases, making this option not feasible.

Operating on a shorter distance increases the feasibility. It can be advised to consider a battery powered ferry for short crossings, roughly shorter than 25 NM.

Hydrogen Powered Ferry

For the hydrogen powered ferry, all analysed concepts are feasible, but all are more expensive than the diesel powered ferry. The same is true in the future, when the fuel cell performance has improved.

Lowering the design speed also has little effect on the costs of the hydrogen powered ferry, for the same reason as it has little effect for the battery powered ferry.

Changing the design crossing's distance also does not have any significant impact on the total costs of the hydrogen powered ferry in comparison to the diesel powered ferry.

For the case study crossing of 25 NM, the hydrogen powered version is likely to be the better choice, as the battery powered version is on the edge of feasibility. So it can be advised to consider a hydrogen fuel cell powered ferry for long crossings, roughly longer than 25 NM.

As mentioned before, costs is not the most important aspect of this analysis. The reduction in pollution, and all other negative effects of emissions, might be worth the extra costs. Because the costs of the hydrogen powered ferry are likely to be higher than that of the battery powered version, it makes sense to only consider hydrogen for distances beyond 25 NM, which cannot be reached by the battery powered version.

Analysis of a Hydrofoil Supported Concept Catamaran

The final topic that was analysed in this project is the hydrofoil supported concept, because a more severe reduction in energy consumption is still desirable. Multiple fast ferries operate on hydrofoils, because these underwater wings can significantly lower the resistance.

Compared to the existing hydrofoil vessels, there are two major differences: the electric concept ship has relatively more weight, and the design speed is lower. Both these differences require larger hydrofoils, which suffer from stronger 3D and interference effects. As a result, the effective lift coefficient goes down and no feasible solution exists.

The study shows that only at higher speeds, the hydrofoil has a positive impact on the resistance. But in absolute terms, this does not improve the energy consumption with respect to the electric version of the Coastal Cruiser 300 at 30 knots. It can therefore be concluded that hydrofoils are not suited for the electric concept ferry.

Conclusion

This project was a case study for a 300 passenger ferry on a 25 NM crossings, operating at 30 knots. The results show that the battery powered concept is on the edge of feasibility, but for shorter crossings, the feasibility is higher. In general, a battery powered ferry, when feasible, is less expensive than a hydrogen powered ferry, but the latter is feasible over a larger range of distances.

So fast electric passenger ferries are feasible, but the direct costs are currently higher than for a comparable diesel powered ferry. The higher price can be seen as an investment, because it will improve the liveability on this planet, as well as limit the increase of the indirect costs of pollution, which is estimated to be over four trillion euro globally, each year. This shows that we have to pay the price either way. So the remaining question is:

Do we want to invest now, or pay for the damage afterwards?

…

Contents

x

List of Figures

List of Tables

Nomenclature

Abbreviations

3D	Three dimensional
A	(planform) area, or ampere
AC	Alternating Current
Ah	Ampere-hour
AR	Aspect Ratio
add	Additional
aux	Auxiliary
B	Beam
	B_{oa} *Overall beam*
C	Coefficient
	C_B *Block coefficient*
	C_D *Drag coefficient*
	C_F *Frictional resistance coefficient*
	C_L *Lift coefficient*
	C_R *Residual resistance coefficient*
CC199	Coastal Cruiser 199 (CoCo Yachts's fast ferry with a 199 passenger capacity)
CC300	Coastal Cruiser 300 (CoCo Yachts's fast ferry with a 300 passenger capacity)
CFD	Computational Fluid Dynamics
CO_2	Carbon Dioxide
CO_2-eq	Carbon Dioxide equivalent
c	Cents or centi- (10^{-2}), or chord length of a hydrofoil
D	Depth of the vessel, or 'diesel'
DC	Direct Current
E_{1c}	Energy consumption of one crossing
EM	Electric Motor
EP	Electric Powertrain
ESS	Energy Storage System (battery system)
EU	European Union
F	Force
	F_D *Drag*
	F_L *Lift*
FC	Fuel Cell
FEM	Finite Element Method
Fn	Froude number
	Fn_h *Submergence Froude number*
f	(safety) factor
ft.	Foot (1 ft. = 0.3048 m)
G	Giga- (10^9)
GHI	Global Horizontal Irradiance
GWh	Gigawatt-hour

g	Gravitational acceleration (g = 9.81 m/s^2 on earth)
H	Hydrogen
h	Hour, or hydrofoil submergence
IM	Induction Machine
k	Kilo- (10^3)
kV	Kilo volt
kWh	Kilowatt-hour
L	Litre
Li-ion	Lithium-ion
M	Million or mega- (10^6), or mass:

M_{DC} *Mass of the DC-DC converter*

M_{EM} *Mass of the electric motor*

M_{ESS} *Mass of the energy storage system*

M_{FC} *Mass of the fuel cell system*

M_{HS} *Mass of the hydrogen storage system*

M_{PC} *Mass of the propulsion converter*

M_{PP} *Mass of the power and propulsion system*

M_S *Structural mass*

M_{SB} *Mass of the switchboard*

M_{SS} *Mass of the superstructure*

M_{wj} *Mass of the waterjet*

MCR	Maximum Continuous Rating
MF	Motor Ferry
MWh	Megawatt-hour
max	maximum
min	minimum
NM	Nautical mile (1 NM = 1,852 m)
NO$_X$	Nitrogen Oxides
n	Number
P	Power

P_i *Installed propulsion power*

P_P *Required propulsion power*

PAX	Passengers
PC	Propulsion Converter
PEMFC	Proton-Exchange Membrane Fuel Cell, or Polymer Electrolyte Membrane Fuel Cell
PMSM	Permanent Magnet Synchronous Machine
ppm	Parts per million
RMB	Renminbi (RMB 1 = CNY 1 = € 0.13 [exchange-rates.org, June 2019])
Rn	Reynolds number

Rn_c *Chord length Reynolds number*

rpm	Rounds per minute
SE	Specific energy
SI	Système International (d'unités); French for 'International System of Units'
s	Span of a hydrofoil
T	Draft of the vessel
TU	Technical University
t	thickness
t$_t$	Time at transit speed

USD   United States Dollar (1 USD = $ 1 = € 0.89 [exchange-rates.org, May 2019])
V   Velocity or volt
W   Watt

X   Due to confidentiality, some values are replaced by this 'X'.

Greek Letters and Symbols

Δ Displacement mass
        Δ_{cat} *Total displacement of the catamaran*
∇ Displacement volume
α Angle of attack
ζ Loss factor
η Efficiency
ρ Fluid density
σ Stress or yield strength
∞ Infinity
C Costs
        C_i *Investment costs*
        C_o *Operational costs*
€   Euro
$ Dollar (USD)

xx

1
Introduction

Negative effects of global warming can already be noticed; extreme weather conditions, such as heat waves, droughts and heavy downpours, have increased in number and in strength [1]. Studies indicate a 97% consensus among climate scientist that humans are the main cause of recent global warming [2]. Since the start of the industrialisation, carbon dioxide (CO_2) levels have risen to above 400 ppm, a concentration level that last occurred three million years ago; a period with a higher average temperature, humidity and seawater level than today [3]. The burning of fossil fuels is a major source of CO_2, and the influence of carbon dioxide on the climate was already documented over a century ago (by S. Arrhenius in 1896 [4]). In order to limit the climate change, measures are taken to reduce emissions, e.g. more and more electricity originates from renewable resources, and the number of electric vehicles is growing.

The burning of fossil fuels does not only result in CO_2 and other greenhouse gasses, but also in hazardous particulates such as soot. Diesel powered vehicles also result in smog, which is an increasing problem in urban areas. Studies have shown that air pollution causes an increase in hospitalizations and deaths [5]. It is even estimated that pollution is the highest risk factor for humanity, e.g. more people die due to pollution than due to tobacco smoking: in 2015, nine million globally compared to seven million [6]. These nine million premature deaths were 16% of all global deaths [7].

Worldwide, the number of people in urban areas is constantly rising [8]. Cities keep growing and thus the problem keeps getting bigger, as more and more people get in contact with air pollution. Furthermore, an increase in people means an increase in vehicle movements, and thus an increase in pollution. Therefore it is important to replace polluting vehicles with emission-free electric versions.

The revolution of electrifying vehicles also takes place in China, with Shenzhen as the frontrunner. In 2018, after a timeframe of only eight years, Shenzhen had replaced all its 16,000 public busses, and became the first city in the world to electrify 100% of all its public busses. This transit to fully electric transport is realized with support from the Chinese government. Shenzhen also invested part of the subsidies into a robust charging infrastructure, with enough outlets to charge half the fleet at a time. Besides busses, there are other ways of transportation; a lot of people travel by water, so there are many fast ferries in the region of Shenzhen. One such ferry is CoCo Yachts' Coastal Cruiser 300. Since Shenzhen is motivated to decrease pollution, it makes sense to replace these passenger ferries with emission free versions as well. [9]

This thesis is a case study in which the feasibility of replacing the Coastal Cruiser 300 by an emission free ferry is investigated. Because the concept will be an electric ferry, the terms 'electric' and 'emission free' are used interchangeably.

1.1 Background Information on Emission Free Ferries

In 2013, a supercapacitor powered ferry was taken into service in France [10]. The first battery powered ferry was taken into service in Norway in 2015 [11]. Since then, more electric ferries became operational. However, these types of emission free vessels are low speed vessels, while many fast ferries are operational around the globe.

Fast ships require relatively more power and energy to operate. This makes it more difficult to convert them into an electric version, as an electric powertrain has relatively more weight than a diesel powertrain [appendix A.1.10]. Even so, more and more effort is put into the development of fast emission free ferries.

In 2016, a commuter vessel was launched by BB Green, an EU funded development project. The battery powered vessel, as seen in figure 1.1, is capable of transporting 80 passengers with a speed of 28 knots. [12]

Another project is the SF-BREEZE, a hydrogen fuel cell powered fast ferry concept for the San Francisco Bay, California, USA. This ship should be capable of transporting 150 passengers with a speed of 35 knots. Its feasibility was examined in 2016, and the conclusion is that it is feasible, if one is willing to pay the higher costs that accompany a hydrogen fuel cell powered vessel. [13]

Flying Foil, a Norwegian start-up company, also started to investigate fast electric ferries. Their goal is to have a 28 m long battery powered ferry sail with 35 knots in 2022. In order to reach that speed, the vessel will be supported by hydrofoils, as seen in figure 1.2. [14]

Figure 1.1: AiriEl, BB Green's fully electric demonstrator vessel.   [12]

Figure 1.2: concept art of Flying Foil's hydrofoil supported electric catamaran ferry.   © Flying Foil

This thesis project is a case study for an emission free replacement for the Coastal Cruiser 300, a fast 39.5 m long passenger ferry with a 300 passenger capacity [15]. This is more than the passenger capacities of the other studies. Furthermore, the other projects mainly focused on either batteries or fuel cells, while this thesis will take both systems into consideration.

1.2 Research Objective and Structure of this Report

The purposes of this report is to present the feasibility study of an electric fast ferry concept, in which the following main research question will be answered:

**How feasible is an emission free catamaran
as a replacement for the Coastal Cruiser 300,
operating as a fast passenger ferry in Shenzhen, China?**

Because the feasibility of the concept depends on many factors, it is not possible to simply say if it is or is not feasible. Instead, this report will analyse under which circumstances the ferry is feasible, e.g. the batter powered ferry is only feasible on short crossings.

Answering the main research question is done in multiple steps, and an overview of the project approach can be seen in figure 1.3. First the current Coastal Cruiser 300 is discussed in **chapter 2**, as well as the route on which it operates. Replacing this ferry with an emission free vessel might be possible in multiple ways, so the first question to be answered is the following:

*What are suitable methods of emission free propulsion,
and what is the main problem when implementing them into a ferry?*

Answering this question will be done in **chapter 3**, from which two options follow: battery powered (paragraph 3.3) and hydrogen fuel cell powered (paragraph 3.5). So in both cases an electrical powertrain. Each system has its own main problem: the battery system adds a lot of weight to ship, and hydrogen increases the fuel costs. Electricity is less expensive than diesel fuel, but because the weight of the vessel increases, the resistance increases as well, and thus the energy consumption goes up. This means that both the battery and the hydrogen powered version of the ferry might be more expensive to operate than the diesel driven version.

A larger displacement and/or a higher fuel price is not a problem if the energy consumption is low enough. Therefore, in paragraph 3.6, the financial side of electric propulsion will be discussed. The investment and operational costs of diesel and electric ferry will be compared to each other, in order to determine the targets for a financially feasible concept ferry.

The next step of this project is to implement the electric propulsion systems into the design of the Coastal Cruiser 300. The goal of this step is answering the following question:

*What is the impact on energy consumption,
when implementing the emission free propulsion systems
into the design of the Coastal Cruiser 300,
and how does that impact the costs?*

This question will be answered in **chapter 4**. It turns out that the target energy consumption cannot be reached, and that a battery powered version is not even feasible at all. So the energy consumption has to go down, which raises the question:

*How can the energy consumption of the electric concept ferry be reduced,
and what is the effect on the feasibility?*

Three design related alterations are analysed in this chapter:
- Reducing resistance by increasing the length of the vessel (paragraph 5.1);
- Reducing the displacement by using carbon composite materials instead of aluminium (paragraph 5.2);
- Operating with a better performing electric power and propulsion system, i.e. a future outlook (paragraph 5.3).

An alternative way of affecting the energy consumption is by changing the operational parameters:
- Operating at a lower design speed (paragraph 5.4);
- Operating on a shorter crossing (paragraph 5.5).

From the last paragraph follows that a larger reduction in energy consumption is desirable. This goal can be achieved by a more significant reduction in resistance. Some fast ferries use hydrofoils to reach their high design speed, because such a system has a lower resistance than a comparable ship without hydrofoils. This raises the question:

How much can a hydrofoil system reduce the resistance
and energy consumption of the electric concept ferry?

This question will be discussed in **chapter 6**.

After the analyses of the different concepts, conclusions can be drawn with respect to the feasibility of replacing the CC300 with an emission free ferry. Each chapter has its own conclusion, and an overview can be found in **chapter 7**, which also contains the answer to the main research question, as well as the recommendations that follow from this project.

In this report, a lot of estimations are made, and in order to make these estimations, multiple equations were used, some of which were derived for this thesis. Because the details and derivations of these estimations are not necessarily important for the story of this report, they are included in the appendices:
- **Appendix A** contains an overview of the mass approximations of the ferry:
  - Mass of the components of the electric power and propulsion system (appendix A.1);
  - Structural mass (appendix A.2).
- **Appendix B** describes how the catamaran resistance estimation equations were derived.
- **Appendix C** is about hydrofoils. It contains:
  - The method used for estimating the mass of the hydrofoil system (appendix C.1);
  - The derivations for estimating the lift coefficient and hydrofoil size (appendix C.2);
  - The estimation for the drag of the hydrofoil system (appendix C.3).
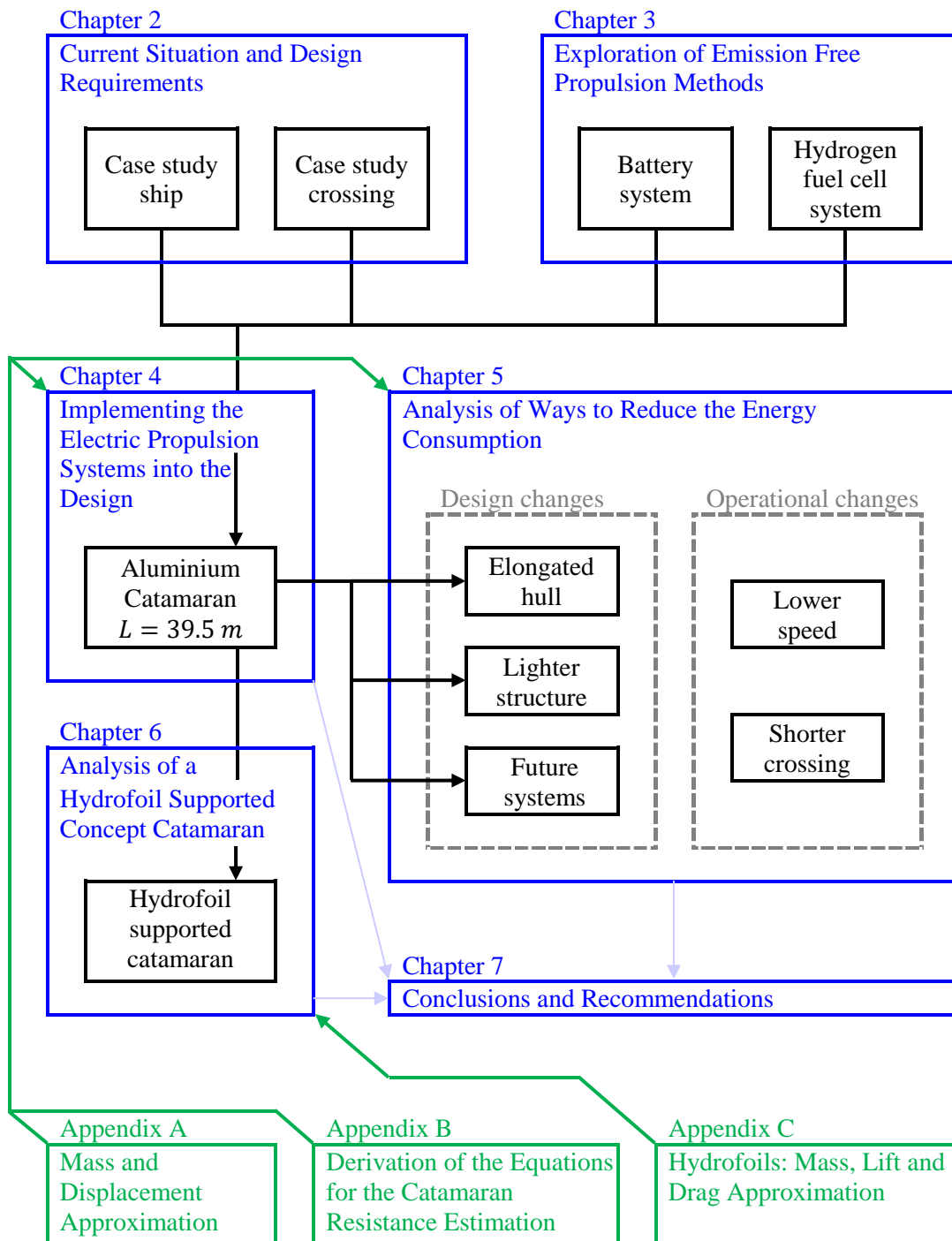
Figure 1.3: project plan of approach. The different topics and their relations are indicated in black, the chapter layout is written in blue, and the appendices and their relation with the main report is indicated in green.

2
Current Situation and Design Requirements

As this project is a case study for an emission free ferry that can replace an existing one, the first thing to discuss is the current vessel and the route on which it operates: the Coastal Cruiser 300 sailing between Shekou and Zhuhai in China. The design requirements for the emission free ferry concept will be based on this.

Structure of this Chapter
Paragraph 2.1 starts with the current Coastal Cruiser 300, followed by the route on which it operates in **paragraph 2.2**. The design requirements that follow from this are presented in **paragraph 2.3**.

2.1 Case Study Ship: Coastal Cruiser 300

Besides the Coastal Cruiser 300 (CC300), seen in figure 2.1, CoCo Yachts has also designed a smaller ferry that is currently operational in Shenzhen, namely the Coastal Cruiser 199 (CC199). The CC300 has a 300 passenger capacity and the CC199 has a 199 passenger capacity [15]. The larger vessel is chosen because of the following two reasons.

It can be expected that a growing city leads to more people using a ferry. Currently over 12 million people live in Shenzhen, and it is estimated that the population will grow with one million people each five years [16]. Hence a larger passenger capacity is desirable rather than a smaller capacity.

A larger vehicle is generally more efficient per passenger-mile than a smaller vehicle, e.g. the CC300 can transport 50% more passengers while it only has 33% more power installed compared to the CC199 [15]. The less energy per passenger, the better it is for the environment.

It must be mentioned here that in absolute terms, the CC300 has a higher energy consumption than the CC199. This increases the challenge, as the energy capacity of an electric vehicle is much smaller than for diesel driven ferries, because the specific energy is much lower: 12 kWh/kg for diesel fuel [17], compared to 1.7 kWh/kg for hydrogen [17] (incl. storage system [18]), and only around 0.1 kWh/kg for batteries [19]. This is one of the reason why up until now only smaller fast electric ferries exist.

Figure 2.1: the Peng Xing 1, CoCo Yachts's Coastal Cruiser 300.   © Barcaferry.com

Ship Type: Catamaran
The Coastal Cruiser 300 is a catamaran, with a waterline length of 39.5 m and an overall beam of 10.3 m [15]. A catamaran is a ship type that consists of two parallel demi-hulls. Looking at comfort, a catamaran has a much higher roll stability than a monohull, because of the separation between the two demi-hulls. Another advantage of this separation is the larger deck area; compared to a monohull, a catamaran with the same displacement has more space for its passengers. A catamaran is also a commonly used ship type for fast vessels, because at higher speeds, two slender demi-hulls have a lower resistance than a single monohull. For these reasons both Coastal Cruisers are catamarans.

The main particulars of the Coastal Cruiser 300 can be seen in table 2.1.

Table 2.1: main particulars of CoCo Yachts' Coastal Cruiser 300.   [15]

Passenger capacity	300	-
Length x beam x draft	39.5 x 10.3 x 1.3	m
Speed (at full load and 95% MCR)	31	knots
Engine power	2 x 1,440	kW
Propulsor	2 x waterjet	

2.2 Case Study Crossing: Shekou – Zhuhai

Shenzhen is a city in south China, near Macau and Hong Kong. The area has a humid subtropical climate; the average temperature ranges from as low as 10°C in the winter, up to 35°C in the summer, and the humidity lies around 70-80% [20]. Around eight days a year the ferries are not operational due to bad weather conditions; above seven Beaufort, they are not allowed to sail [21].

Looking at ferry lines in Shenzhen, there are many different crossings. The distance from quay to quay ranges from 11 NM to 31 NM. The travel times range from 30 minutes to 75 minutes, with the most crossings taking 60 minutes. [22]

The ferry line that is closest to the average is chosen as the subject of this case study, which is the ferry line sailing between Shekou Ferry Terminal and Zhuhai Ferry Terminal, a crossing over the Pearl River Delta between the cities Shenzhen and Zhuhai. This ferry crossing is highlighted in yellow in figure 2.2. According to the timetable, the crossing takes 60 minutes, in which 25 NM is covered. Between each crossing, 30 minutes is available for the passengers to disembark, and for new passengers to get on board. [23]

In case of a battery powered ferry, sufficient time at quay is required in order to have a sufficient time for recharging. For that purpose Shenzhen-Zhuhai is amongst the better suited ferry lines, as the time at quay is 30 minutes, where the time for other crossings is limited to only 15 minutes [23].

Each 'Shekou-Zhuhai-ferry' makes 10 crossing a day, seven days a week. Each year the CC300 is seven days out of service due to maintenance in a dry dock. This leads to 350 operational days a year, including the eight days off due to bad weather conditions. [21]

The final thing to mention is the size limitation. The waterline length of the ferry is limited to 46.5 m, as larger vessels do not fit alongside the quay [21].

Figure 2.2: the ferry lines from and to Shekou Ferry Terminal, Shenzhen, China. The case study crossing 'Shekou – Zhuhai' is highlighted in yellow. [23]

2.3 Design Requirements

Based on the Coastal Cruiser 300 and the Shekou – Zhuhai ferry crossing, the following design requirements are set for the emission free fast ferry concept:

- The ferry must be capable of transporting 300 passengers with at least the same comfort as the Coastal Cruiser 300; the superstructure and the interior arrangement will therefore not be altered;
- The design speed is 30 knots, which is required to keep up with the time table of the ferry line;
- There should be a 15% margin between the required propulsion power and installed propulsion power;
- The ferry makes 10 crossings a day, 350 days a year, and each 25 NM crossing is done in one hour, with 30 minutes in between;
- The ship type is a catamaran, either with or without hydrofoils;
- The desired ship length is 39.5 m, with 46.5 m as the maximum overall length. Besides limitations at quay, another reason not to make the ship longer than this is course stability and maneuverability. [21]

The design of the electric ferry must be as close as possible to the original CC300. The overall beam for example will not change.

3

Exploration of Emission Free Propulsion Methods

Currently most fast ferries operate on internal combustion engines that run on diesel fuel. In order to operate emission free, another propulsion method has to be installed on the vehicle. The question is:

What are suitable methods of emission free propulsion,
and what is the main problem when implementing them into a ferry?

Research is done on internal combustion engines that run on clean fuels such as hydrogen. The only emission that results from a reaction between hydrogen and oxygen is clean water [24]. However, due to the high combustion temperature, some nitrogen in the air is oxidised to harmful NO_X emissions, such as nitrogen dioxide, which is a component of smog [25]. For this reason, the combustion engines on clean fuels will not be considered in this project.

The other method of operating emission free is by means of implementing electric motors instead of diesel engines. Hence the terms 'emission free' and 'electric' are used interchangeably in this thesis. Storing the required energy for electric propulsion can be done in multiple ways. The four most implemented methods are:

- Batteries;
- Supercapacitors;
- Flywheels;
- Hydrogen combined with fuel cells.

Flywheels are mostly known for their application in Formula 1 race cars: break energy is recovered and reused during acceleration. Both the super capacitor and the flywheel are devices that are ideal for short peak loads, such as breaking and accelerating. So they do not seem suitable for a ferry, yet a supercapacitor powered vessel is operational.

The other two methods (batteries and hydrogen fuel cells) are better suited for powering an electric vehicle. Compared to the previous mentioned hydrogen combustion engine, fuel cells do not run on such high temperatures, so this way the use of hydrogen only results in water and not in NO_X.

Structure of this Chapter
Since the emission free ferry has an electric powertrain, an overview of the components of the electric propulsion system will be first presented in **paragraph 3.1**. **Paragraph 3.2** derives an estimation equation for the energy consumption of the ferry, as this is an important parameter for determining the size of the electric power and propulsion system. Batteries will be discussed in **paragraph 3.3**, which also contains an explanation why solar cells will not be applied to the concept. Because a supercapacitor driven ferry does exist, the supercapacitor is discussed in **paragraph 3.4**. The hydrogen fuel cell is discussed in **paragraph 3.5**, followed by the preliminary conclusions in **paragraph 3.7**.

3.1 Overview of the Electric Power and Propulsion System

This paragraph contains an overview of the components of the electric power and propulsion system, as seen in figure 3.1. Different options are available for the 'onboard energy storage'-box in the figure, and these will be discussed in the next three paragraphs.
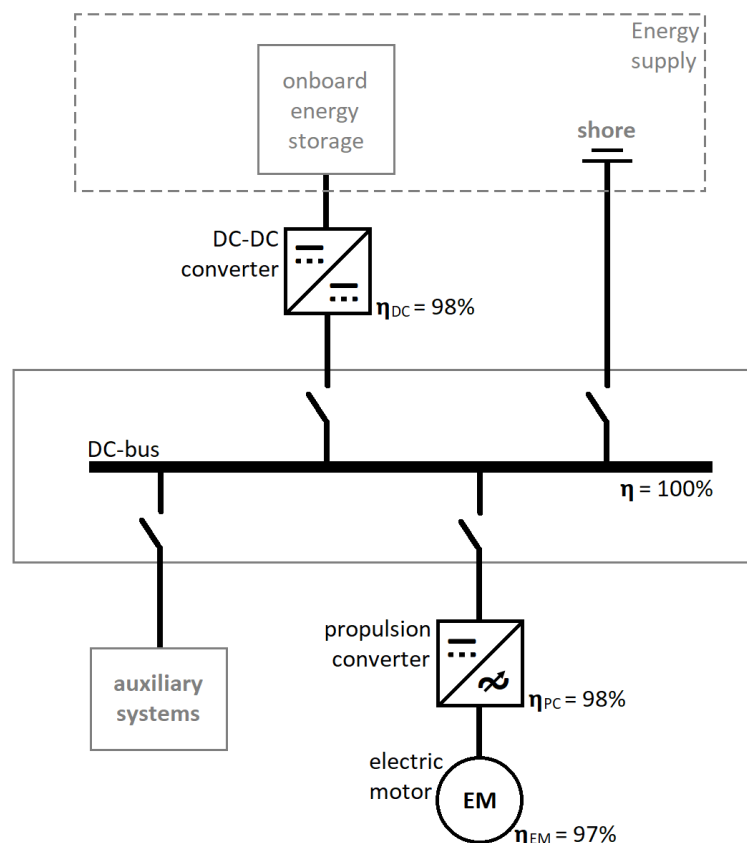
Figure 3.1: line diagram of the electric propulsion system, including the efficiencies of the different components.

Electric Motor

The device that drives the waterjet is the electric motor. Many different types of electric machines exist. These can be separated into two groups: direct current (DC) machines and alternating current (AC) machines. It can be noted that the term 'machine' is used here instead of 'motor', because such a device can be used as a motor as well as a generator.

DC machines require commutators, such as carbon brushes, to supply electric energy to the rotating rotor. This result in wear, and thus in maintenance. Furthermore, DC machines are larger and have a lower efficiency than AC machines [26]. For these reasons they are not used anymore as main propulsion drivers. So only AC machines will be focused on for the electric ferry.

The two main types of AC machines used for propulsion are the Permanent Magnet Synchronous Machine (PMSM) and the Induction Machine (IM), also known as asynchronous machine. Looking at the specifications, these motors are quite similar:

- The speed of both electric motors is controlled by the frequency of the electric current;
- Neither require commutators, so less wear than DC machines;
- Both have very high efficiencies (η_{EM}), in the order of 97% [27] [28];

- Both come in a wide variety of specific powers, while some similar values can be seen, e.g. a 1.4 MW electric motor of 4.4 tonnes in case of both the PMSM [27] and the IM [28].

Propulsion Converter

In order to control the speed of the electric motor, and thus the speed of the vessel, a device is required that can change the frequency of the alternating current that drives the motor. Furthermore, all methods of energy storage that will be discussed in this chapter, work on direct current.

So a propulsion converter is required to change the DC power into AC power with variable frequency. The efficiency of such a device is high: $\eta_{PC} = 98\%$ [29].

Switchboard

All power consumers and energy suppliers are connected to each other via a switchboard, also known as DC-bus, since it only handles direct current in this vessel. Since no conversion takes place within a switchboard (e.g. DC to AC), no significant energy is lost in this device: the efficiency is 100%, the same as for the electric cables.

DC-DC Converter

Between the switchboard and the electric energy supplier is a DC-DC converter, which controls the flow and voltage of the direct current. The efficiency is roughly 98% [29].

Total Electric Powertrain Efficiency

The total efficiency of the electric powertrain is 93%:

$$\eta_{EP} = \eta_{EM} \times \eta_{PC} \times \eta_{DC} = 97\% \times 98\% \times 98\% = 93\%$$

For comaprison, the efficiency of the diesel engines in the Coastal Crusier is only around 40%, based on the fuel consumption [30] and energy content of diesel fuel [17].

3.2 Energy Consumption

The mass of the energy supply systems is related to the energy consumption, therefore a simplified version of the operational profile is analysed in this paragraph. For that purpose, the one hour crossing is divided into three parts: quay, harbour and transit. Table 3.1 shows this simplified operational profile and the corresponding energy consumption.

Quay

Around three minutes of the travel time is lost at quay due to connecting and disconnecting of the ferry [21]. During this stage no propulsion power is required:

$$E_{quay} = 0.0 \ MWh$$

Harbour

Manoeuvring and low speed sailing through the harbour takes around seven minutes each crossing. The required power during this stage is less than 0.1 MW. [21]

Because the power consumption is low and the time short, this part can be neglected, even when including the efficiency of the electric drivetrain ($\eta_{ED} = 93\%$ [paragraph 3.1]):

$$E_{harbour} = \frac{0.1 \ [MW]}{93\%} \times \frac{7}{60} [hour] = 0.0 \ MWh$$

Transit

The largest time is spent at the transit speed of 30 knots. Because the energy consumption in the harbour is negligibly small, the total propulsion energy consumption is roughly equal to the transit energy consumption, which is a function of propulsion power (P_P), electric powertrain efficiency and time at transit (t_t):

$$E_{transit} = \frac{P_P}{\eta_{EP}} \cdot t_t \qquad\qquad (\ 3.1 \ )$$

The transit time is 50 minutes, during which the full installed power is used at most ($P_P \leq P_i = 2.9 \ MW$ [15]). This results in an energy consumption of less than 2.6 MWh:

$$E_{transit} \leq \frac{2.9 \ [MW]}{93\%} \times \frac{50}{60} [hour] = 2.6 \ MWh$$

Auxiliary Power

Auxiliary power (0.1 MW [21]) has to be supplied throughout the entire one hour crossing. Including the efficiency of the DC-DC converter ($\eta_{DC} = 98\%$ [29]) results in the following energy consumption:

$$E_{aux} = \frac{0.1 \ [MW]}{98\%} \times 1 \ [hour] = 0.1 \ MWh$$

Total Energy Consumption

The total energy consumption for one crossing (E_{1c}) is the summation of the propulsion energy during transit and the auxiliary energy consumption:

$$E_{1c} = E_{transit} + E_{aux} = \frac{P_p}{\eta_{EP}} \cdot t_t + E_{aux}, \qquad with \ E_{aux} = 0.1 \ MWh \qquad\qquad (\ 3.2\ )$$

So in case of the Coastal Cruiser 300, the total energy consumption is 2.7 MWh at most, and only around four percent is supplied to auxiliary systems. Also note that the auxiliary energy consumption is constant, as it is not influenced by the way the vessel is powered.

Table 3.1: energy consumption of CoCo Yachts's Coastal Cruiser 300, for one crossing, based on a simplified operational profile.   [15] [21]

Consumer	Power [MW]	Time [minutes]	Energy [MWh]	Percentage of total
Auxiliary	0.1	60	0.1	4%
Propulsion at quay	0.0	3	0.0	0%
Propulsion in harbour	0.1	7	0.0	0%
Propulsion in transit	≤ 2.9	50	≤ 2.6	96%
Total		60	≤ 2.7	100%

3.3 Batteries

One of the most used energy containers is the battery. A battery contains one or more electrochemical cells. Each cell consists of a positive and a negative electrode, with a (liquid) electrolyte between them. The electrolyte allows ions to move between the two electrodes, closing the circuit and allowing electrons, and thus a current, to flow. Energy can be stored inside a battery by running an electrical current through the cell, which results in an electrochemical reaction. This is called charging and discharging is the inverse process.

3.3.1 Battery Powered Ferry: Ampere

The MF Ampere, the first fully electric car ferry in existence, seen in figure 3.2, was taken into service in Norway in 2015, followed by a second vessel in 2017. The 80 meter long vessel can carry up to 360 passengers and 120 cars [31]. The results were better than predicted, with a reduction in operating costs by 80% [11]. This reduction is compared to the old ferry, not to a newer more efficient diesel driven ferry.

Each night, the 1,040 kWh battery system is fully charged. Due to the relatively low specific energy, it is currently not possible to install enough battery capacity to operate a whole day on a single charge, therefore the vessel is recharged at quay, during each stop. According to the timetable, each stop takes 10 minutes. Both mooring and connecting the ferry to the charging station happens with automated systems. Connecting and disconnecting takes around four minutes, so only six minutes is available for transferring the 150 kWh of energy that is required for each crossing battery pack [32]. To achieve fast charging, over one megawatt of power is required. Instead of a significant change to the electric grid of the port, a 410 kWh battery pack is installed on each shore. These are charged when the ferry is on its way, so they can provide the required power when the vessel has arrived and is connected. [31]

Figure 3.2: the electric ferry Ampere.   © Siemens

3.3.2 Energy Storage System

The battery system on board of a vehicle is called the Energy Storage System (ESS). Figure 3.3 shows the components of an ESS, which is in this case the system of the MF Ampere. Table 3.2 contains the specifications of these components, which together lead to the total weight of the system.

The energy is stored in battery cells. The Ampere contains 3,840 battery cells with a specific energy of 163 Wh/kg [33]. The total weight is 6.4 tonnes.

Multiple battery cells are used to create a module, which is basically a box with connectors. A module also contains some equipment, such as sensors to measure the temperature of the battery cells. In the Ampere, 24 cells are packed together in a battery module. Because a module adds material and equipment to the battery cells, the specific energy decreases to 90 Wh/kg [34]. This already almost doubles the weight; the MF Ampere contains 11.5 tonnes of battery modules.

Multiple modules are stacked together in battery packs and arrays, this way forming the complete energy storage system. The ESS has controllers that manages the operation of the modules, combining input data from the vessel and the data from the modules themselves. This again adds material and equipment to the system. In case of water-cooling, the water adds even more weight to the system. As

a result, the weight again almost doubles to 20 tonnes [31], and the effective specific energy is further reduced to 52 Wh/kg. Without water-cooling, the specific energy is 80 Wh/kg [19].

Mass Increase from Battery Cell to Battery System
Battery Manufacturers usually give specifications of battery cells. The mass of the whole battery pack is roughly double the mass of all the battery cells [35]. This can also be calculated from the known specific energies (163 Wh/kg for the battery cell [33] and 80 Wh/kg for the battery pack [19]):

$$\frac{163 \; [Wh/kg_{cell}]}{80 \; [Wh/kg_{pack}]} = 2.0 \; kg_{pack}/kg_{cell}$$

Table 3.2: components of the Corvus ESS of the Ampere, ordered from small to large.   [31] [33] [34]

	Cell	Module	Complete ESS
		Contains 24 cells	Contains 160 modules
Voltage	4.2 V	50.4 V	1,050 V
Energy capacity	271 Wh	6.5 kWh	1,040 kWh
Weight per unit	1.66 kg	72 kg	20 tonnes
Weight of all units	6.4 tonnes	11.5 tonnes	
Specific Energy	163 Wh/kg	90 Wh/kg	52 Wh/kg

| Cell | Module | Pack | Array |
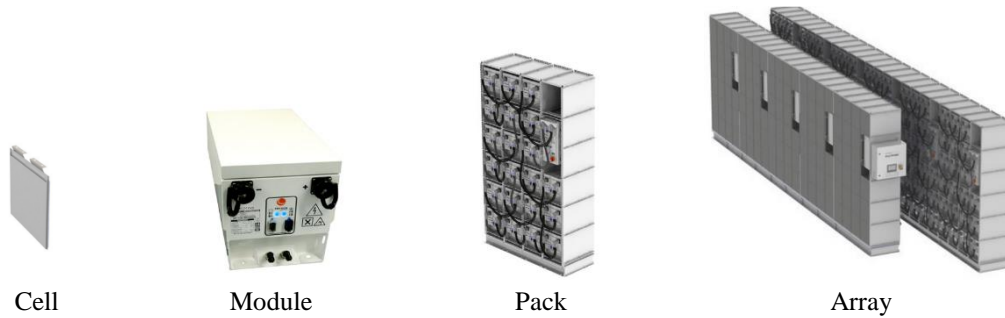
Figure 3.3: components of the Corvus ESS of the Ampere, ordered from small to large.   [34]

3.3.3 Main Battery Properties
There are many different properties that can be specified. The following is an overview of the most important ones.

Battery Type
For this project only current battery technology will be considered, as these are available right away. New battery technology in laboratories might be better on paper, but because it will probably still take several years before they can be implemented in a design, they will not be considered. Only subparagraph 5.3.1 is an exception, which is a future outlook on battery technology.

The most used battery type is the lithium-ion battery. These batteries have lithium (Li) as electrode material, so lithium ions move through the electrolyte, hence the name Li-ion. Instead of a liquid electrolyte, a polymer electrolyte can also be used. This battery type is known as a lithium-ion polymer, or simply as lithium polymer or LiPo.

The main advantages of Li-ion over other battery types is its high specific energy, high energy density, and low self-discharge [36]. The latter means that the stored energy decreases over time, without using the battery. The terms 'specific energy' and 'energy density' are often interchanged with each other, but the first refers to the amount of energy contained per unit of mass, while the second refers to the amount of energy contained per unit of volume.

Specific Energy
A battery driven vehicle has more weight than a comparable fuel driven vehicle, due to the relatively low specific energy. As mentioned above, the ferry Ampere has an ESS with a specific energy of only around 0.1 kWh/kg [19], while diesel fuel has a specific energy of around 5 kWh/kg, when a 40% diesel engine efficiency [30] [17] is included.

Charge C-rate
The electrochemical reaction inside a battery cell also generates heat. The faster a battery is charged or discharged, the more heat is produced, and the larger the risk of a fire or an explosion. Therefore the (dis)charge rate, known as C-rate, is limited.

Charging with a rate of 1C means that the battery is fully charged in one hour. Charging with 2C means that charging happens twice as fast, so a fully charged battery in half an hour.

Depth of Discharge
The percentage of the capacity that is utilized is called the Depth of Discharge (DOD). Suppose the charge rate is 1C and the available charge time is only half an hour, than half the battery can be charged each time, and only half the battery capacity should be used between each charge. In other words: the battery utilizes 50% of its capacity, thus the DOD is 50%.

An example of operating at 50% DOD is to charge the batteries to 80% of their capacity, and then discharge them during operation until 30%, before charging it again to 80%.

Cycle Lifetime
Charging and discharging a battery once is called a cycle. During every cycle the electrodes are a little bit damaged by the electrochemical reaction. As a result, the capacity of the battery deteriorates over time, thus limiting the lifetime of a battery.

The charging rate has an impact on degradation; a higher C-rate decreases the cycle lifetime of the battery. Another major factor is the Depth of Discharge; the lower the DOD, the longer the battery can stay operational.

Lifetime of a battery is generally expressed in the number of cycles that it takes for the capacity of the battery to deteriorate to 80% of its original maximum capacity, specified for a certain C-rate and DOD.

3.3.4 Battery Charging
The most used way of energy transfer to an electric vehicle is by charging via a connection between the ship and the shore. The two main requirements for charging an electric ferry is a fast connection between ship and shore, and sufficient power to transfer enough energy within the available time.

Ship-Shore Connection
Fast and automated systems to connect the charging station to the vessel do already exist. The Ampere in Norway operates with a system from Cavotec SA, and they claim automated mooring and connection in less than 30 seconds [37].

For the electric ferry concept in Shenzhen, this would mean that 29 minutes are available during each 30 minutes stop at quay. Real life conditions might increase the time that it takes to connect and disconnect. Furthermore, some additional time is required to start and stop the charging process itself. For these reasons, 25 minutes is assumed to be available for actually charging.

Charging Power Supply
The energy consumption of the Coastal Cruiser 300 is at most 2.7 MW for each crossing as estimated in subparagraph 3.2. Charging this amount of energy within 25 minutes requires 6.5 MW of power:

$$\frac{2.7\ [MWh\ per\ crossing]}{25/60\ [hour\ charge\ time]} = 6.5\ MW$$

One way of supplying this amount of power is by installing battery packs on shore. This is also done in Norway for the Ampere. The battery packs are charged when the ferry is on its way, so they can provide the required power when the vessel has arrived and is connected.

Another way is with a sufficiently strong power grid. This method is applied to one of the largest battery-driven ships in the world: the MF Tycho Brahe. This vessel is charged via a 10 MW laser guided robot connection, and the required power is supplied by the 10 kV electrical grid, for which new cables had to be laid [38].

Since charging with 10 MW is already possible, it is assumed that an electric ferry in Shenzhen can also be charged with sufficient power, either directly via the grid, or by installing battery packs on shore.

3.3.5 Application of Solar Cells

Solar cells are devices that can transform radiation energy from the sun into electrical energy. Solar cells can be used to charge batteries, but the following explanation will indicate why they are not suitable for fast vehicles, which have a relatively high energy consumption compared to their size.

The average daily energy from the sun that reaches the surface of the earth ranges from 3 kWh/m^2 in Norway to 6.7 kWh/m^2 in the Sahara desert [39]. In Shenzhen, China, the Global Horizontal Irradiance (GHI) is a little over 4 kWh/m^2/day [39].

The efficiency of solar cells ranges from around 15% to 22% [40]. So on average the efficiency (η_{solar}) is 19%.

The Coastal Cruiser 300 is roughly 40 meters long and 10 m wide, so if the entire ferry would be covered with solar cells, the area would be 400 square meter:

$$A_{solar} = L \times B = 40 \ [m \ length] \times 10 \ [m \ beam] = 400 \ m^2 \qquad (\ 3.3\ )$$

The energy production from this area of solar cells is on average 0.3 MWh/day:

$$GHI \times \eta_{solar} \times A_{solar} = 4 \ [\text{kWh/m}^2/day] \times 19\% \times 400 \ [m^2] = 0.3 \ MWh/day \qquad (\ 3.4\ )$$

The energy consumption for each crossing is in the order of 2.7 MWh [subparagraph 3.2], which amounts to 27 MWh/day with ten crossings. This means that the solar cells only supply around 1% of the energy demand:

$$\frac{0.3 \ [MWh/day, energy \ supply \ from \ solar \ panels]}{27 \ [MWh/day, energy \ consumption of \ the \ ferry]} = 0.01$$

This percentage is an average value, during the night-time and on dark cloudy days the energy supply from the solar cells would be much close enough to zero that their contribution can be neglected. Furthermore, this approximation assumed an unrealistically large solar panel; in a real ship the area, and thus the energy production would be even smaller.

From this calculation follows that solar cells are unfit for application on fast electric ferries; they add weight, complexity and extra costs to the vessel, while their contribution to the energy demand is negligibly small.

3.3.6 Application of Battery Swapping

Another way of energy transfer is battery swapping, which means that the empty battery is replaced with a fully charged one. The battery that is taken out is charged on shore, so the charging time is not limited by the ferry's time at quay, and thus the ship can operate on a higher DOD.

Using a larger part of the battery's capacity means less overcapacity is required, i.e. the battery pack is smaller and has less weight. However, a container like structure is required to be able to swap the system to and from the vessel. This might render the savings in weight ineffective.

The Dutch company Port-Liner has a concept where their future inland container vessels are fitted with four 20 foot containers that each contain 1,680 kWh of battery capacity [41]. In case of the concept ferry, there are two problems that did not apply to the concept of Port-Liner.

First, the ferry is not a container vessel; a significant redesign of the structure is required, as it has to withstand the additional weight of the battery units. This further reduces the weight advantage the

battery swap concept. Furthermore, without making the ship longer, it might not even be possible to place the containers on the ship, without sacrificing space for passengers.

The second problem is the swapping itself. Because the ferry's quay is not at a container terminal, there is no crane capacity available. This seems like it can be solved relatively easily, but with passengers walking around, safety is likely to be an issue, as the containers should not be lifted over the passengers.

Another problem is the complexity of the system. Tesla shut down its battery swapping program in favour of fast charging. One of the technical issues was that the car did not recognize the new battery [42].

So it can be concluded that battery swapping is not suited for fast passenger ferries; not only is the expected saving in weight limited, the space and logistics are also problematic, and the complexity makes it susceptible to malfunctions.

3.3.7 Battery Cell Selection

For this project, the size and weight of the battery system is important. Therefore, a battery cell is selected in this subparagraph, which will form the basis for the estimations. The important battery properties of different battery cells are listed in table 3.3. These battery cells are from the Xalt Energy. This company is chosen because they deliver DNVGL type approved products [35].

Table 3.3: Xalt Energy battery cells

Cell type	Charge C-rate [-]	Specific energy [Wh/kg]	Cycle life at 100% DOD [cycles]	Cycle life at 80% DOD [cycles]
60 Ah LTO [43]	6	76	> 60,000[*]	> 90,000[*]
75 Ah HP [44]	3	159	> 5,000[*]	> 14,000[*]
56 Ah HP [45]	2	196	> 4,000[*]	> 5,000[*]
63 Ah UHE [46]	1	221	> 3,000[**]	> 4,000[**]

[*]1C charge-discharge rate
[**]0.3C charge-discharge rate

Battery life is an important factor. The system must last at least long enough to be continuously operational until the maintenance in dry dock. From a financial standpoint, the system must last at least long enough to earn back the investment. Because the battery cells deteriorate over time, it cannot be expected that they last as long as the ship itself. Five to ten years seem like a realistic target for the lifetime of the battery system [47] [48] [49].

According to the operational profile [subparagraph 2.2], the ferry makes 3,500 crossings per year, thus the battery system goes through 3,500 cycles each year. This amounts to 17.5 to 35 thousand cycles over a period of five to ten years.

60 Ah LTO Battery Cells

Only one cell type can last the desired cycle life according to the table: the 60 Ah LTO battery cell, which should last over 60 thousand cycles [43]. However, the specific energy is by far the lowest of the four different battery cells in the table: $76 \, Wh/kg$ [43]. The specific energy of the whole battery system is only half of this [35], so 38 Wh/kg.

Operating at 100% DOD means that there is no margin, while the engines have margin of 15%. So running at 80% DOD would be more realistic, which leads to an effective mass/energy-ratio of $33 \, kg/kWh$:

$$80\% \, [DOD] \times 38 \, [Wh/kg] = 30 \, Wh/kg \rightarrow \frac{1}{30 \, [Wh/kg]} = 33 \, kg/kWh$$

75 Ah HP Battery Cells

The 75 Ah HP batter cell has a much higher specific energy than the 60 Ah LTO battery cell, and a possible lifetime of over 14 thousand cycles [44]. It can be assumed that the cycle life is inversely proportional to the depth of discharge [50] [51]. So the cycle life for 50% DOD is expected to be 41 thousand cycles at 1C charge rate, when extrapolated outside the values of table 3.3 [44]:

$$\frac{(100\%^{-1} - 50\%^{-1}) \cdot 5{,}000 + (50\%^{-1} - 80\%^{-1}) \cdot 14{,}000}{100\%^{-1} - 80\%^{-1}} = 41{,}000 \ cycles$$

The charge rate to reach 50% capacity in the available 25 minutes at quay [subparagraph 3.3.4] is 1.2C:

$$\frac{60 \ [minutes \ per \ hour]}{25 \ [minutes \ charging]} \times 50\% \ capacity = 1.2C \ charge \ rate$$

This is 1.2 times the charge rate for which the cycle life is specified. A third power relation seems a good way to estimate the cycle life with respect to charge rate [52]. The estimated cycle life following from this is 24 thousand:

$$\frac{41{,}000 \ [cycles \ at \ 1C \ charge \ rate]}{(1.2C \ [charge \ rate])^3} \approx 24{,}000 \ cycles$$

This is an acceptable number that falls well within the five to ten years battery lifespan, with 3.5 thousand cycles per year. The effective mass/energy-ratio of the 75 Ah HP battery cell is slightly lower than the previously discussed 60 Ah LTO battery cells:

$$50\% \ [DOD] \times \frac{159 \ [Wh/kg]}{2 \ [kg_{pack}/kg_{cell}]} = 40 \ Wh/kg \rightarrow \frac{1}{40 \ [Wh/kg]} = 25 \ kg/kWh$$

Operating at 45% DOD would be sufficient to reach a lifetime of 35,000 cycles (ten years), when following the same calculation as above. This would however increase the effective mass/capacity-ratio of the system to 28 kg/kWh. This increase of 3 kg/kWh means an increase of seven tonnes for the required energy per crossing. 55% DOD would decrease the expected lifetime to below five years, when using the same calculation as above. Therefore, 50% depth of discharge is deemed to have the best balance between weight of the system and its service life.

56 Ah HP and 63 Ah UHE Battery Cells

The cycle lives of the 56 Ah HP and 63 Ah UHE battery cells are very low in comparison to the other two. This requires a very low DOD. Extrapolating is likely not accurate anymore, but the MF Ampere can be used as an example. This vessel requires around 150 kWh per crossing [32], while the installed battery capacity is 1,040 kWh [31]. This means that the ferry operates at a DOD of 14%:

$$\frac{150 \ [kWh \ per \ crossing]}{1{,}040 \ [kWh \ battery \ capacity]} = 14\% \ DOD \qquad\qquad\qquad (\ 3.5\ )$$

At such a low DOD, the weight of the battery would be much larger than of the other two battery types:

$$14\% \ [DOD] \times \frac{221 \ [Wh/kg]}{2 \ [kg_{pack}/kg_{cell}]} = 15 \ Wh/kg \rightarrow \frac{1}{15 \ [Wh/kg]} = 67 \ kg/kWh$$

Chosen Battery Cells

Based on this analysis, the 75 Ah HP battery cell is chosen to implement in the concept design as it results in the system with the lowest weight. It can be noted that the specific energy of these cells are roughly the same for the system in the MF Ampere [19]. However, the cycle life has improved since 2015, so the new electric vessel can operate at a higher DOD, i.e. operate with a relatively smaller battery system. The mass/capacity-ratio of this system is 12.5 kg/kWh:

$$\frac{159 \left[Wh/kg_{cell}\right]}{2 \left[kg_{pack}/kg_{cell}\right]} = 80 \left[Wh/kg_{pack}\right] \rightarrow \frac{1}{80 \left[Wh/kg\right]} = 12.5 \; kg/kWh$$

3.3.8 System Size

Each battery pack has a weight of 2,000 kg [35], thus their energy capacity is:

$$\frac{2,000 \left[kg\right]}{12.5 \left[kg/kWh\right]} = 0.16 \; MWh/pack$$

Looking at the cross-section of the Coastal Cruiser [53], there is room in each demi-hull for a single battery array in longitudinal direction [35]. The width of each pack is 1.33 m [35], thus the required space to house the batteries is 24 m of the length of the vessel:

$$3 \times \left\lceil \frac{2.7 \left[\frac{MWh}{crossing}\right]/2 \left[demi\text{-}hulls\right]}{3 \left[compartments\right] \times 50\% \left[DOD\right] \times 0.16 \left[\frac{MWh}{pack}\right]} \right\rceil \times 1.33 \left[\frac{m}{pack}\right] = 3 \times 8 \; m$$

Notice in the calculation above that the large brackets are not ordinary square brackets, because they represent 'rounding up'. From this follows that the system does fit within each demi-hull, as seen in figure 3.4, where 'ESS' is the battery system. This figure also explains the '3' in the calculation above, as the spaces in the demi-hulls are divided by bulkheads.

Figure 3.4 shows how the components might fit within each demi-hull. Some tanks, such as the sewage tank, have to be relocated for this arrangement. The size of an electric motor (EM) is similar to the diesel engine [28] [30]. The propulsion converter (PC) required for the electric CC300 would take less than a meter of space [29]. Direct current switchboards are relatively smaller than AC-switchboards, so the switchboard (SB) requires less than two meters [29]. The DC-DC converter (DC) also takes less than a meter of space in each demi-hull [29]. These components are also indicated in figure 3.4.

The illustrated amount of batteries can contain a little over 1.2 times the energy required by the current CC300 for each crossing. This means that the energy consumption per crossing cannot be more than 1.2 times the energy consumption of the current Coastal Cruiser 300.
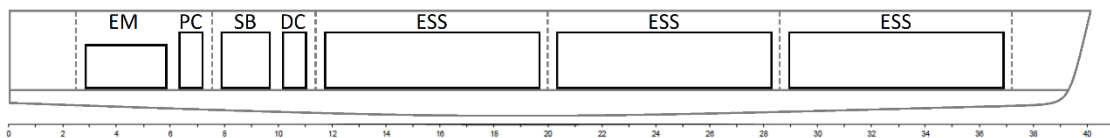
Figure 3.4: side view of a demi-hull with an overview of the battery powered propulsion system: electric motor (EM), propulsion converter (PC), switchboard (SB), DC-DC converter (DC) and energy storage system (ESS).

Longer Version of the Coastal Cruiser 300
An elongated version will also be considered in the next chapter. This vessel is seven meters longer, which means that ten additional battery packs can be installed within the demi-hulls:

$$2 \ [demihulls] \times \left\lfloor \frac{7 \ [m]}{1.33 \ [m/pack]} \right\rfloor = 2 \times 5 \ battery \ packs$$

Note that the large brackets are again no ordinary square brackets; this time indicating 'rounding down'.

With 0.16 MWh per battery pack results in an additional capacity of 0.8 MWh, including the 50% DOD. This is a total overcapacity of close to 1.6 times the required capacity of each crossing. In case of the elongated version, more deck-space is available as well. This means that four more rows of five battery packs can be added to the ship. This brings the total number of battery packs to 66, which can contain 2.2 times the required energy for one crossing.

3.3.9 Environmental Impact of Batteries
Some people claim that the manufacturing an electric car is way more polluting than using a gasoline car. If this is true, it might also apply to ferries. This subparagraph will indicate that a battery driven ferry is more environmentally friendly than a diesel driven ferry, even when taken manufacturing into account.

The mining facilities, which are required to obtain the important materials from the earth, are harmful to the landscape and toxic for the environment. Furthermore, a lot of chemicals are required for the manufacturing process, and this process is also the cause of a lot of pollution. This is true, but the production of fuel is not clean either; refineries are also a major source of (toxic) pollutants to their surroundings. More importantly, oil extraction and transport are risky; many oil spills already happened over the past decades, resulting in major environmental damage. So battery production is harmful, but only during production, while fuel is harmful during both production and usage in a vehicle.

It can be expected that the mining and production processes will improve as technology advances. Scientist are also working on methods for recycling batteries, which would be even more environmentally friendly. So pollution from battery production might decrease in the future, but an argument in favour of battery driven vehicles, regardless of how polluting manufacturing is, is that moving emissions away from the city is healthier for the people in that city.

To indicate that battery driven vehicles are more environmentally friendly than diesel driven vehicles, a comparison must be made between the pollution of battery production with that of combusting fuel. There are many different pollutants (e.g. CO_2, NO_x), and each has its own impact on the environment. Expressing the impact on the climate from the different pollutants can be done by expressing it in the amount of carbon dioxide that would have an equivalent impact. This quantity is called carbon dioxide equivalent (CO_2-eq).

Environmental Impact of a Battery System
According to a 2017 study from the *IVL Swedish Environmental Research Institute*, the greenhouse gas emissions of battery production is 120-250 kg CO_2-eq/kWh [54]. The required energy capacity of the battery is 5.4 MWh, based on the required 2.7 MWh for each crossing [paragraph 3.2] and an operational depth of discharge of 50% [subparagraph 3.3.7]:

$$\frac{2.7 \ [MWh/crossing]}{50\% \ [DOD]} = 5.4 \ MWh$$

From this follows that the total pollution from the production of the battery pack is 0.6 thousand to 1.4 thousand tonnes CO_2-eq.:

$$5.4 \ MWh \times \{120\text{-}250\} \ [kg \ CO_2\text{-}eq/kWh] = \{0.6\text{-}1.4\} \cdot 10^6 \ kg \ CO_2\text{-}eq$$

Possible pollution from recycling the battery at the end of its lifetime is estimated to be no more than 2.5 kg CO_2-eq/kg battery [54]. This is 31 kg CO_2-eq/kWh, based on the 80 Wh/kg specific energy of the battery system:

$$\frac{2.5\ [kg\ CO_2\text{-}eq/kg\ battery]}{0.08\ [kWh/kg\ battery]} = 31\ kg\ CO_2\text{-}eq/kWh$$

From this follows that the total pollution from recycling the battery pack is 0.1 thousand tonnes CO_2-eq.:

$$5.4\ MWh \times 31\ [kg\ CO_2\text{-}eq/kWh] = 0.2 \cdot 10^6\ kg\ CO_2\text{-}eq$$

Environmental Impact of Operating with Green Electricity
The cleanest way of operating an electric ferry is by using green electricity; electricity from renewable resources. While the energy generation itself is clean, manufacturing and installing of the equipment has an impact on the environment. The footprint of solar power is estimated to be below 50 g CO_2-eq/kWh, and the footprint of a windfarm over its entire lifetime is estimated to be below 15 g CO_2-eq/kWh [55]. So the pollution is effectively 17-57 g CO_2-eq/kWh, when including the 93% powertrain efficiency, and 95% charge-discharge efficiency of the batteries [56]:

$$\frac{\{15\text{-}50\}\ [g\ CO_2\text{-}eq/kWh]}{93\% \times 95\%\ [efficiency]} = \{17\text{-}57\}\ g\ CO_2\text{-}eq/kWh$$

The total energy consumption per year is 9.5 GWh, based on 3,500 crossings per year:

$$3{,}500\ [crossings/year] \times 2.7\ [MWh/crossing] = 9.5\ GWh$$

The equivalent pollution following from this is 0.1-0.5 thousand tonnes per year:

$$9.5\ [GWh/year] \times \{17\text{-}57\} \cdot 10^{-3}\ [kg\ CO_2\text{-}eq/kWh] = \{0.2\text{-}0.5\} \cdot 10^6\ kg\ CO_2\text{-}eq/year$$

So the total pollution after the first year is 1.0 to 2.1 thousand tonnes carbon dioxide equivalent:

$$\begin{aligned}
&\{0.6\text{-}1.4\} \cdot 10^6\ [kg\ CO_2\text{-}eq\ from\ battery\ production] \\
+\ &0.2 \cdot 10^6\ [kg\ CO_2\text{-}eq\ from\ battery\ recycling] \\
+\ &\{0.2\text{-}0.5\} \cdot 10^6\ [kg\ CO_2\text{-}eq\ associated\ with\ electricity\ production] \\
=\ &\{1.0\text{-}2.1\} \cdot 10^6\ kg\ CO_2\text{-}eq\ pollution\ after\ the\ first\ year\ of\ operation
\end{aligned}$$

Environmental Impact of Operating with Grey Electricity
Globally, around 90% of the electricity is still generated with fossil fuels [57]. So it is a realistic scenario for an electric vehicle to operate on grey electricity. The corresponding carbon dioxide equivalent pollution is estimated to be 0.53 kg/kWh [58]. The equivalent pollution following from this is 5.7 thousand tonnes per year:

$$9.5\ [GWh/year] \times \frac{0.53\ [kg\ CO_2\text{-}eq/kWh]}{93\% \times 95\%\ [efficiency]} = 5.7 \cdot 10^6\ kg\ CO_2\text{-}eq/year$$

So the total pollution after the first year is around seven thousand tonnes carbon dioxide equivalent:

$$\{0.6\text{-}1.4\} \cdot 10^6 \ [kg \ CO_2\text{-}eq \ from \ battery \ production]$$
$$+0.2 \cdot 10^6 \ [kg \ CO_2\text{-}eq \ from \ battery \ recycling]$$
$$+ 5.7 \cdot 10^6 \ [kg \ CO_2\text{-}eq \ associated \ with \ electricity \ production]$$
$$= \{6.5\text{-}7.3\} \cdot 10^6 \ kg \ CO_2\text{-}eq \ pollution \ after \ the \ first \ year \ of \ operation$$

Environmental Impact of the Diesel Driven Ferry

The emissions from diesel fuel is roughly 0.3 kg CO_2-eq/kWh (83 g CO_2-eq/MJ [59]). This is less than grey energy, but the efficiency of the diesel engine has to be taken into account. As a result the effective pollution is 0.75 kg CO_2-eq/kWh:

$$\frac{0.3 \ [kg \ CO_2\text{-}eq/kWh]}{40\% \ [engine \ efficiency]} = 0.75 \ kg \ CO_2\text{-}eq/kWh$$

This leads to an equivalent pollution of 7.1 thousand tonnes CO_2-eq. per year:

$$9.5 \left[\frac{GWh}{year}\right] \times 0.75 \left[\frac{kg \ CO_2\text{-}eq}{kWh}\right] = 7.1 \cdot 10^6 \ kg \ CO_2\text{-}eq/year$$

This is similar to the battery powered ferry on grey energy after its first year, i.e. after roughly one year, the battery powered ferry is more environmentally friendly than the diesel ferry. When green electricity is used, the break-even point of pollution already falls within the first few months of operation:

$$\frac{\{1.0\text{-}2.1\} \cdot 10^6 \ [kg \ CO_2\text{-}eq/year \ from \ electricity]}{7.1 \cdot 10^6 \ [kg \ CO_2\text{-}eq/year \ from \ diesel \ fuel]} \times 12 \left[\frac{months}{year}\right] = \{2\text{-}4\} \ months$$

This analysis shows that a battery driven ferry is more environmentally friendly than using a diesel driven ferry.

3.3.10 Safety of Batteries

Safety is not expected to be an issue; the chosen battery cells are DNVGL type approved [35], and battery systems are already operational in ferries since 2015. Furthermore, in Shenzhen over 16,000 public busses drive around on batteries [9], so the warm humid climate in Shenzhen also does not seem to pose a problem for battery safety.

3.3.11 Main Problem of a Battery Powered Propulsion System

The main problem of a battery powered propulsion system is its mass. Storing energy in batteries requires a much heavier system than storing energy in the form of diesel fuel. This is due to the lower specific energy.

As a result, the displacement of the ferry increases a lot, which has a huge impact on the resistance. A higher resistance requires a more powerful propulsion system with a larger energy capacity. Thus the displacement will increase even further, and so will the resistance and the energy consumption.

A higher energy consumption is not necessarily a problem as the price for electricity is a lot lower than for diesel fuel. This will be discussed in paragraph 3.6.

3.3.12 Conclusion on Batteries

The battery might be a suitable solution for an electric fast passenger ferry. The technology is already successfully applied to car ferries, charging the batteries should be possible between each crossing, the lifetime is expected to be sufficiently long. The impact on the environment is less than that from the diesel driven ferry, and also safety does not seem to pose a problem.

The main problem however is the large mass of the battery system (0.1 kWh/kg for batteries [19], compared to 12 kWh/kg for diesel fuel [17]). Due to this, the displacement of the ferry will be larger, and thus the resistance and energy consumption will be larger as well. The latter is not necessarily a problem, as the price for electricity is a lot lower than for diesel fuel, which will be discussed in paragraph 3.6.

3.4 Supercapacitors

Another energy container is the supercapacitor, also known as ultracapacitor or double layered capacitor. A supercapacitor is a device that can store energy by means of a static charge. Because there is no electrochemical reaction, there is much less heat generation and degradation, compared to batteries. This means that the lifetime much longer and that (dis)charging can happen much faster, which results in a much higher power output. This can be seen in the comparison in table 3.4, where the top three specifications are in favour of supercapacitors, and the bottom three are in favour of batteries.

The biggest disadvantage of supercapacitors is the much lower specific energy and energy density; a supercapacitor is both heavier and larger than a battery with the same capacity. Furthermore, supercapacitors are still much more expensive than batteries. [48] [49]

As mentioned in the beginning of this chapter, both the supercapacitor and the flywheel are ideal for short power peaks, but not suitable for ferries. Despite this, a ferry in France, the Ar Vag Tredan, runs on supercapacitors. For this reason it is discussed in this paragraph.

Table 3.4: comparison between Li-ion batteries and supercapacitors. [48] [49]

	Li-ion battery	Supercapacitor	
Charge time	< 60 minutes	< 10 s	
Life time	> 500	> 500,000	cycles
	5 - 10	10 - 15	years
Specific power	< 3,000	< 30,000	W/kg
Specific energy	< 200	< 10	Wh/kg
Energy density	< 1,000	< 15	kWh/m^3
Costs	< 1	< 10	€/Wh

3.4.1 Supercapacitor Powered Ferry: Ar Vag Tredan

The Ar Vag Tredan, seen in figure 3.5, is a small supercapacitor powered ferry that was taken into service in France in 2013. The vessel is a 22 meter long catamaran with a 113 passenger capacity and a service speed of 10 knots. The boat has 128 supercapacitors that together weigh of six tonnes, and charging these happens in only four minutes. The boat makes 28 daily roundtrips during the workweek. This means 28 cycles a day, totalling around 7,000 cycles a year. [60]

In case of the Ar Vag Tredan, the choice for supercapacitors can be understood; fast charging and a long lifetime are important factors for this ferry, while the low speed makes the weight of the ESS less important.

Figure 3.5: the Ar Vag Tredan. [60]

3.4.2 Ar Vag Tredan on Batteries

So at first sight, using batteries in the Ar Vag Tredan would not be a wise choice, based on the limited available charging time and the short cycle lifetime as listed in table 3.4. However, when taking a closer look, batteries seem to be the better choice. First of all, fully charging a battery within four minutes is

still impossible, but only charging a small percentage is easily possible. In this case, that the depth of discharge is also a few per cent, meaning that the lifetime gets a lot longer than specified by the battery manufacturer.

The capacity of the MF Ampere is 1,040 kWh [31], and every crossing requires around 150 kWh of energy [32]. This means that the DOD is only 14%, which should be low enough to reach an acceptable lifetime, even though the batteries go through 34 cycles a day, as the ferry has 34 crossings a day [31].

Suppose the same battery modules, as used on the Ampere, would be installed on the Ar Vag Tredan. With a charging rate of 1.5C [34], 10% of the battery capacity can be charged within four minutes. Thus the depth of discharge for operating this ferry is only 10%:

$$1.5 \ [C \ charge \ rate] \times \frac{4 \ [minutes \ charging]}{60 \ [minutes \ per \ hour]} \times 100\% = 10\% \ DOD$$

Each roundtrip requires around 20 kWh [61], so a battery capacity of only 250 kWh would already be sufficient, also taking the limited 80% end-of-life capacity into account:

$$\frac{20 \ [kWh \ per \ roundtrip]}{10\% \ [DOD] \times 80\% \ [end\text{-}of\text{-}life \ capacity]} = 250 \ kWh$$

With a specific energy of 52 Wh/kg [31], the total weight of the ESS would be 4.8 tonnes, which is less than the six tonnes of supercapacitors that are currently installed on the vessel. The DOD, as well as the number of cycles a day (10% and 28 cycles respectively), is lower than what the ESS goes through in the Ampere (14% and 34 cycles respectively [31]). Even though this is favourable for the lifetime of the batteries, the supercapacitors will probably still outlive them. This does however not weight up against the huge price difference, as the battery is around ten times less expensive [49].

It must be mentioned that at the time the Ar Vag Tredan was launched in 2013, battery technology was likely not advanced far enough; at that time the supercapacitor was the right choice. Since that time, battery technology is advanced further than supercapacitors, so even today, the battery is still the better choice for the concept ferry.

3.4.3 Conclusion on Supercapacitors

Based on this paragraph, it can be concluded that choosing supercapacitors over batteries leads to a more expensive ferry with much more weight, while batteries are already a much heavier energy container than diesel fuel. For these reasons, the supercapacitor is not considered as a main energy container in the remainder of this project.

3.5 Hydrogen Fuel Cells

Another way to power a vehicle, without polluting exhaust gasses, is the use of hydrogen fuel cells. A fuel cell is a device in which an electrochemical reaction takes place; hydrogen reacts with oxygen, resulting in electricity and water. This means that energy is converted from chemical straight to electrical. For comparison, diesel-generators use a combustion engine, so the energy conversion goes from chemical to mechanical via heat, and from mechanical to electrical via magnetic energy. As a result, the efficiency of a diesel generator is only 35-45%, while the efficiency of a hydrogen fuel cell is 40-60%. The energy content of hydrogen is also larger than that of diesel fuel, 33 kWh/kg compared to 12 kWh/kg. [17]

Fuel cells on other fuels, such as methanol or ammonia, are also possible, but these can be seen as inferior to hydrogen. First of all, both methanol and ammonia have a lower energy content than hydrogen (5.5 and 5.2 kWh/kg respectively). Furthermore, methanol fuel cells are less efficient, and ammonia is toxic. For these reasons, as well as for the technical advancements of hydrogen fuel cells over the others, only hydrogen fuel cells are considered in this project. [17]

Figure 3.6 shows a render of the SF-BREEZE, a fuel cell powered concept ferry for the San Francisco Bay. The feasibility of this vessel, capable of transporting 150 passengers with 35 knots, was analysed by J.W. Pratt and L.E. Klebanoff [13], and they concluded that such a vessel is feasible if the higher (operational) costs are acceptable.

Figure 3.6: render of the SF-BREEZE, a hydrogen fuel cell [13] powered ferry in the San Francisco Bay.

3.5.1 Hydrogen Production

Today's hydrogen is largely produced from fossil fuels. Heat and pressure is used to break natural gas, oil or coal into hydrogen, but harmful waste products, such as carbon oxides, are also released. Using hydrogen produced from fossil fuels is thus not much cleaner than using diesel engines. [62]

A sustainable way of producing hydrogen is by means of electrolysis. Globally, only 4% of hydrogen is produced this way [63]. This method uses electricity to split water into hydrogen and oxygen. Electrolysis does not result in harmful waste products, but it is 2-5 times as expensive as producing hydrogen from fossil fuels [64].

The efficiency of a hydrogen production plant is 60-70% [63]. So going from renewable electricity to hydrogen via electrolysis, and back to electricity via the fuel cell leads to a loss of 58-76% [17] [63], while the losses in the battery driven ferry can be as low as 9% [56] [65]. On the other hand, hydrogen can be created by renewable energy, at the moments that the energy demand is lower than the supply; currently wind turbines stop operating if the energy demand is low, while they could still subtract energy from the wind to power a hydrogen production plant.

3.5.2 Hydrogen Storage

There are two common ways of storing hydrogen: at low temperature or at high pressure. Hydrogen storage at low temperatures (-253°C [17]) requires a large amount of energy; when using cryogenic

tanks, around 30% of the energy content of hydrogen is required to keep the temperature low enough. Pressurizing hydrogen to 350-700 bar is more efficient, but still requires energy; the efficiency of this storage method is roughly 85-90%. [64]

A high pressure tank can contain around 5 wt% hydrogen [18]. So in practice, the effective specific energy is 1.7 kWh/kg, which is much lower than that of diesel fuel (12 kWh/kg [17]). A cryogenic tank can contain around 25% more hydrogen per unit of system mass [66], but this additional hydrogen is required to cool the tank [64].

Tank Capacity

An overcapacity is required to at least prevent running out of fuel, but it might also be desirable to make two crossings between refuelling, so only one refuelling station is required. In this project 2.5 is chosen as overcapacity factor. This value means that the ferry can make two crossings before refueling, including a margin. This is in line with the hydrogen fuelled ferry concept SF-BREEZE [13].

The amount of hydrogen to store 2.5 times the 2.7 MWh that is required for each crossing is 400 kg, including the efficiencies:

$$\frac{2.5 \times 2.7 \ [MWh/crossing]/93\% \ [powertrain \ efficiency]}{55\% \ [fuel \ cell \ efficiency] \times 33 \ [kWh/kg_{hydrogen}]} = 400 \ kg$$

Refuelling

Industrial gas companies estimate that the transfer flow rate can be high enough that 1,000 kg of hydrogen can be transferred to a ship in 20 to 40 minutes [13]. From this can be concluded that a 400 kg hydrogen tank can be easily filled within the thirty minutes that the vessel is at quay.

3.5.3 Fuel Cell Type

Multiple types of fuel cells exist, but this thesis will only focus on the Proton-Exchange Membrane Fuel Cells (PEMFC), also known as Polymer Electrolyte Membrane Fuel Cells (PEMFC). Other types, such as phosporic acid fuel cells, molten carbonate fuel cells or solid oxide fuel cells, are in a more limited development state, resulting in lower power densities, shorter life times and higher costs as compared to the PEMFC. [17]

The concept ferry will be equiped with Hydrogenics' HyPM-HD 30 Power Modules. These were also used as the basis of the SF-BREEZE study [13]. The HyPM-HD 30 PEMFC have a specific power of 0.43 kW/kg, and they can operate at 55% efficiency [67].

Fuel Cell Life Time

Like batteries, a fuel cell has a limited lifespan. The target life of five years is also applied to the fuel cell system. They are expected to last over 10,000 hours [67], and a service life of over 25,000 hours is achieved with a fuel cell powered bus [68]. This is in average more than 17.5 thousand hours, which leads to an expected lifespan of at least five years:

$$\frac{10,000 + 25,000}{2} = 17,500 \rightarrow \frac{17,500 \ [hours]}{3,500 \ [one \ hour \ crossings \ per \ year]} = 5 \ years$$

3.5.4 Supporting Battery System

During the operation of a vehicle, power demands fluctuate with changes in its speed, as well as with external load conditions (e.g. wind and waves). Fuel cells are not good at handling fluctuating power demands, as their response time is generally not fast enough. For this reason, fuel cell driven vehicles are also equipped with batteries. They can also be equipped with supercapacitors, but this will not be implemented due to the reasons mentioned in the previous paragraph. J. Bauman and M. Kazerani also concluded in their study to hydrogen powered vehicles that the combination fuel-cell-supercapacitor is inferior to the combination fuel-cell-battery [69].

Mass of the Supporting Battery System

Looking at the operational profile, the largest jump in propulsion power is the moment the ferry leaves the harbour and starts its high speed transit. At that point the vessel goes from very low power to almost full power, thus the electric system must be able to provide full power instantly.

In this project, the estimation will be made with the same battery cells as discussed in subparagraph 3.3.7 (the Xalt Energy 75 Ah HP). Looking at the charge and discharge rate of the cells, the battery system can supply twice the power that it can absorb [44]. Thus before transit, the batteries can be charged by the fuel cells with 1/3 of their maximum power. At the beginning of the transit, this 1/3 power of the fuel cells goes to the electric motors, and the other 2/3 is supplied by the batteries. So the power output of the battery system is 2/3 the power output of the fuel cell. This is in line with the fuel-cell-battery system on-board of the Nemo H2 tour boat in Amsterdam [70].

The 3.7 V battery cells have a 75 Ah capacity and continuous discharge rate of 6C [44]. From this follows a power output of 1.7 kW per cell:

$$3.7 \ [V] \times 75 \ [Ah] \times 6 \ [C \ discharge \ rate] = 1.7 \ kVA$$

The cell weight is 1.8 kg [44], thus the mass/power-ratio is 2.1 kg/kW, when also taking into account that the whole battery system is roughly double the weight of only the cells [35]:

$$2 \ [kg_{ESS}/kg_{cell}] \times \frac{1.8 \ [kg]}{1.7 \ [kW]} = 2.1 \ kg/kW$$

From this follows that the required mass, in case of the Coastal Cruiser 300 (2,880 kW installed power [15]), would be 4.1 tonnes:

$$2.1 \ [kg/kW] \times 2/3 \ [kW_{ESS}/kW_{FC}] \times 2.88 \ [MW] = 4.0 \ tonnes$$

The effective mass/energy-ratio was determined to be 25 kg/kWh [subparagraph 3.3.7], thus the usable energy content of the battery system is approximately 0.16 MWh:

$$\frac{4.0 \ [tonnes]}{25 \ [kg/kWh]} = 0.16 \ MWh$$

The energy consumption of one crossing is less than 2.7 MWh [subparagraph 3.2], which means that the supporting battery system can supply at least six percent of the required energy for one crossing:

$$\frac{0.16 \ [MWh]}{2.7 \ [MWh]} \times 100\% = 6\%$$

Six percent seems sufficient for the purpose of handling power fluctuations, especially considering that this not only includes discharging the batteries, but also charging the batteries (if the fuel cell power supply is larger than the energy demand).

3.5.5 System Size

The hydrogen system has three main components: the fuel cell, the hydrogen storage tank and the supporting battery pack.

Fuel Cell

The total fuel cell system consists of multiple Hydrogenics HyPM-HD 30 modules. Six can be placed on top of each other in each demi-hull [67] [71]. The width of such a stack is roughly 0.5 m, and the

total power output 186 kW [67]. Thus the required space in each demi-hull to deliver 2.88 MW of propulsion power is less than five meters:

$$\left\lceil \frac{2.88 \ [MW]/93\% \ [drive \ train \ efficiency]}{2 \ [demi\text{-}hulls] \times 186 \ [kW]} \right\rceil \times 0.5 \ [m] = 4.5 \ m$$

Note that the large square brackets indicate 'rounding up'.

Hydrogen Storage

In subparagraph 3.5.2, the tank capacity was determined to be 400 kg of hydrogen. The design of the SF-BREEZE has a 1,200 kg hydrogen tank on its top deck [13], so it should be no problem to place a 400 kg tank on the top deck of the concept ferry.

Another option might be to place a hydrogen tank in each demi-hull. The volumetric capcity of a hydrogen tank is roughly 0.035 kg_H/L_{system} [18]. So the size of the tank would be around 6 cubic meter, which easily fits within the vessel, as seen in figure 3.7:

$$400 \ [kg_H] \ / \ 0.035 \ [kg_H/L] \ / \ 1,000 \ [L/m^3] \ / \ 2 \ [demi\text{-}hulls] = 13 \ m^3$$

Battery

Only one battery pack is required in each demi-hull to support the fuel cell system:

$$\frac{0.16 \ [MWh]}{50\% \ [DOD] \times 2 \ [demi\text{-}hulls] \times 0.16 \ [MWh/pack]} = 1 \ battery \ pack$$

Total System Size in each Demi-Hull

In total, only 6.5 m is required for the fuel-cell-battery system [35], which easily fits within each demi-hull:

$$5 \ [m \ fuel \ cells] + 1 \ [battery \ pack] \times 1.33 \ [m/battery \ pack] \approx 6.5 \ m$$

This can also be seen in figure 3.7, which shows how the components might fit within each demi-hull. The size of the other components is the same as for the battery powered vessel; the size of an electric motor is similar to the diesel engine [28] [30], and the size of the converters and switchboard is less than one and two meter respectively, in each demi-hull [29]. The hydrogen storage tank (HS) can be placed on the top deck [13], but it is added to the figure to illustrate that it also fits within the demi-hulls. If the energy consumption goes up, the size of the system increases, but as seen in the figure, there is a sufficient margin that it is safe to say that the available space is not a limiting factor.
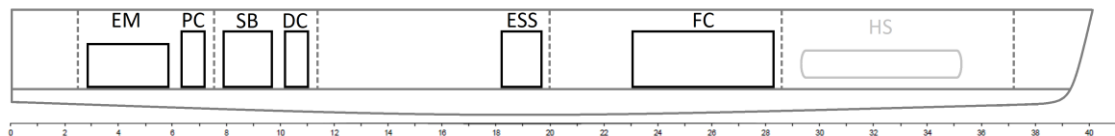
Figure 3.7: side view of a demi-hull with an overview of the hydrogen fuel-cell-battery powered propulsion system: electric motor (EM), propulsion converter (PC), switchboard (SB), DC-DC converter (DC), fuel cell system (FC), battery system (ESS) and hydrogen storage tank (HS).

3.5.6 Safety of Hydrogen

Some concerns exist surrounding the safety of hydrogen, but it is not expected to be a problem. Multiple vehicles already operate on hydrogen, such as the Honda Clarity, a fuel cell powered car that saw its first delivery back in 2008 [72]. So the technology is already successfully applied in vehicles, and also the industry uses hydrogen for decades; ways to safely handle hydrogen are therefore well developed [73].

A well-known disaster is the Hindenburg in 1937. In case of that fatal accident, the skin of the airship ignited due to an electrical discharge. This caused the incident, not the hydrogen within the ship. The diesel fuel kept burning for multiple hours after the ignition, while the hydrogen in the ship burned quickly and relatively safe, as it produces much less radiant heat and hot ash than diesel fuel. [73]

Refuelling hydrogen is also expected to be safer than diesel fuel. In case of a leakage, hydrogen will disperse quickly, as it is the lightest known element. Diesel fuel, on the other hand, will get into the water in case of a leakage, with the risk of fire and environmental damage.

The humid climate of Shenzhen also does not seem to be a problem. High relative humidity might even have a positive effect on the efficiency of the fuel cell [74]. So it can be assumed that safe operation on hydrogen is possible.

So it can be concluded that it is possible to operate safely with a hydrogen powered passenger ferry. The same conclusion was drawn for the feasibility study of the SF-BREEZE concept [13].

3.5.7 Main Problem of a Hydrogen Powered Propulsion System

The main problem of a hydrogen fuel cell powered system is the high price of the fuel, which will be discussed in the next paragraph. A higher fuel price is not necessarily a problem, as long as the fuel consumption is low enough. So like the battery powered concept, the main problem is related to the energy consumption.

3.5.8 Conclusion on Hydrogen Fuel Cells

The hydrogen fuel cell might be another suitable emission free propulsion method. In such a fuel cell, electricity is generated by combining hydrogen and oxygen, and the only waste product is water. Because the specific energy of hydrogen is much higher than of battery systems (1.7 kWh/kg [17] including its storage tank [18], and around 0.1 kWh/kg for batteries [19]), it does not have the same problem as the battery powered vessel: a hydrogen system is neither too heavy nor too large to fit within the vessel. Furthermore, safely operating with hydrogen should also be possible.

Instead of a large increase in weight, a hydrogen powered ferry suffers from a large increase in fuel costs, as hydrogen is much more expensive than diesel fuel (21 c€/kWh compared to 12 c€/kWh on average, which will be discussed in the next paragraph).

3.6 Financial Side of electric Propulsion: Cost Exploration and Design Target

First of all, costs is not the most important aspect for renewable energy projects and emission free vehicles. Money is only one way of valuing something, emission is another way of valuing something. Furthermore, a lot of indirect costs are related to pollution, e.g. related to deaths and hospitalizations due to bad air quality. The costs of global pollution are estimated to be well over four trillion euro per year [7] [75]. So the indirect costs are high, but they are difficult to estimate, especially when related to only a single vessel.

It must be mentioned that this analysis compares a new electric vessel with a new diesel powered vessel. If a currently operating diesel powered ferry would be replaced by a new electric ferry, before the end of its lifetime, the investment costs are much higher, as it would also include the vessel as a whole, not only the components that are related to propulsion. Furthermore, this thesis is focused on the ship itself, so only direct costs of the vessel are taken into account, not the additional costs of changes to quay. These changes are also difficult to estimate, primarily because they heavily depend on the existing infrastructure of the harbour.

This thesis will only present an indication of the difference in costs, which can be used to compare the different concepts. Ideally, an emission free ferry is not more expensive than a diesel powered ferry. This will be the target for the concept, and it can be achieved if the energy consumption is sufficiently low. In that case, the operational costs are lower than the diesel ferry's operational costs, and the additional investment can be earned back.

3.6.1 Investment Costs for the Propulsion System

In this initial estimation, the investment costs are limited to the main components of the powertrain, for which the price ratios of table 3.5 are used. This table is based on a five year period, which is the minimal life expectancy of the electric systems [subparagraph 3.3.7 and 3.5.3]. The real investment costs might deviate from the values in the table, but this is not taken into account. A range will be used for the operational costs, so a range is also included in the total costs, i.e. the end results do include margins.

Since come other systems have a longer life expectancy, the investment costs have to be corrected for this. Based on 3,500 one hour crossings a year, a lifetime of ten years is assumed for the diesel engine [76]. Because this is twice the target lifetime, the investment costs are divided by two. The electric motor is expected to last at least 15 years under the same operational conditions [77]. The same lifespan is assumed for the power electronics. So the investment costs for electric motor and power electronics is divided by three to take their expected lifespan into account.

Another remark has to be made on the investment costs of the fuel cell system. The indicated price of 400 euro per kW might be an optimistic value, as the estimations range from 200 euro [78] to above 1,800 euro [79] [80] per kW.

Investment costs of the powertrain are estimated as a function of installed power and energy consumption per crossing. An expression for the energy consumption per crossing (E_{1c}) as a function of installed power (P_i) was derived in appendix B.4.4:

$$E_{1c} \approx 0.8 \, [kWh/kW] \times P_i \qquad\qquad \text{Ref. (B.39)}$$

Diesel Powered Ferry
The only main component in the diesel powered ferry's powertrain is the diesel engine, which results in the following expression for the investment costs:

$$\mathcal{C}_{i_D} = 0.3 \, [\text{k€/kW}] \times P_i \qquad\qquad \text{(3.6)}$$

Table 3.5: overview of price ratios of different components of the powertrain,
based on an expected minimum of five operational years.

Diesel engine	0.3[*]	k€/kW	[29] [81]
Electric motor	0.1[**]	k€/kW	[29] [76]
Power electronics	0.3[**]	k€/kW	[29] [80]
Fuel cell system	0.4	k€/kW	[29] [82]
Battery system	0.5	k€/kWh	[82] [78]
Hydrogen storage system	0.0[***]	k€/kWh	[13] [78]

[*] 10 year lifespan [76], so investement cost is devided by 2.
[**] 15 year lifespan [77], so investement cost is devided by 3.
[***] based on 33 kWh/kg$_H$, the estimated value is only
20 €/kWh [13] [78], which is neglectably small.

Battery Powered Ferry

The main components of the battery powered ferry's powertrain are the electric motor (0.1 k€/kW), the power electronics (0.3 k€/kW), and the battery system (0.5 k€/kWh). The depth of discharge of the battery system was detemined to be 50% [subparagraph 3.3.7]. From this follows the following expression for the investment costs:

$$\mathcal{C}_{i_{ESS}} = (0.1 + 0.3)\,[\text{k€/kW}] \times P_i + 0.5\,[\text{k€/kWh}] \times \frac{E_{1c}}{50\%\,[DOD]} \qquad (\ 3.7\ )$$

$$= 1.2\,[k\text{€/kW}] \times P_i$$

Hydrogen Powered Ferry

The main components in case of the hydrogen fuel-cell-battery powered ferry are the electric motor (0.1 k€/kW), the power electronics (0.3 k€/kW), the fuel cell system (0.4 k€/kW), and hydrogen and energy storage system (0.0 k€/kWh). From this follows the following expression for the investment costs:

$$\mathcal{C}_{i_{FC}} = (0.1 + 0.3 + 0.4)\,[\text{k€/kW}] \times P_i + (0.0)\,[\text{k€/kWh}] \times E_{1c} \qquad (\ 3.8\ )$$

$$= 0.8\,[k\text{€/kW}] \times P_i$$

3.6.2 Operational Costs Related to the Propulsion System

The operation costs are limited to fuel costs and electricity costs; both are a function of total energy consumption over the period of five years, which can be expressed as follows, with 3,500 crossings per year [21]:

$$E_{total} = 5\,[years] \times 3{,}500\,[crossings/year] \times E_{1c} \qquad (\ 3.9\ )$$

$$\approx 14 \cdot 10^3\,[kWh/kW] \times P_i$$

Maintenance is not taken into account, as it is expected that this does not severely change the outcome. The maintenance costs of diesel engines is estimated to be less than 5 euro per kW per year [76]. This amounts to less than 0.03 k€ per kW of installed power over a five year period, which is small enough that it can be neglected. Furthermore, it is not expected that the maintenance of electric propulsion is significantly higher, and also the maintenance costs of fuel cells can be comparable to diesel engines [83].

Diesel Powered Ferry

Diesel fuel has an energy content of 12 kWh/kg [17], and the price over the past year ranges between 44 and 66 c€/kg (~490-740 USD/tonne [84]). From this follows an average price of 12 euro cent per kWh, including the efficiency of the engine (40% [30] [17]):

$$\frac{\{0.44\text{-}0.66\}\ [\text{€/kg}]}{12\ [kWh/kg] \times 40\%\ [engine\ efficiency]} = \{0.09\text{-}0.14\}\ \text{€/kWh}_{\text{effective}}$$

Combining this with equation 3.9 leads to the following expression for the total operational costs:

$$\mathcal{C}_{o_D} = \{0.09\text{-}0.14\}\ [\text{€/kWh}] \times E_{total} \tag{3.10}$$
$$= \{1.3\text{-}2.0\}\ [k\text{€/kW}] \times P_i$$

Battery Powered Ferry

The price for electricity from renewable resources ranges from around 2 c€/kWh [85] to 5 c€/kWh (0.06 USD/kWh [86]). The charge-discharge efficiency of a battery system is approximately 95% [56]. From this follows an average effective price of 4 c€/kWh, which is 1/3 the average price of diesel fuel:

$$\frac{\{0.02\text{-}0.05\}\ [\text{€/kWh}]}{95\%\ [charge\text{-}discharge\ efficiency]} = \{0.02\text{-}0.05\}\ \text{€/kWh}_{\text{effective}}$$

The corresponding expression for the operational costs is the following:

$$\mathcal{C}_{o_{ESS}} = \{0.02\text{-}0.05\}\ [\text{€/kWh}] \times E_{total} \tag{3.11}$$
$$= \{0.3\text{-}0.7\}\ [k\text{€/kW}] \times P_i$$

Hydrogen Powered Ferry

The price for hydrogen from renewable recourses ranges from around 2 €/kg [85] to 5 €/kg (6 USD/kg [63]). The energy content of hydrogen is 33 kWh/kg, and the efficiency of a fuel cell is roughly 55% [67]. The power train is efficiency is 93% [paragraph 3.1]. This results in an average effective price of 21 c€/kWh, almost twice the average price for diesel fuel:

$$\frac{\{2\text{-}5\}\ [\text{€/kg}]}{33\ [kWh/kg] \times 55\%\ [fuel\ cell\ efficiency]} = \{0.12\text{-}0.30\}\ \text{€/kWh}_{\text{effective}}$$

The following expression follows from this:

$$\mathcal{C}_{o_{FC}} = \{0.12\text{-}0.30\}\ [\text{€/kWh}] \times E_{total} \tag{3.12}$$
$$= \{1.7\text{-}4.2\}\ [k\text{€/kW}] \times P_i$$

3.6.3 Total Propulsion Costs and Target Energy Consumption

The total propulsion costs is simply the sum of the investment costs ($\mathcal{C}_i$) and the operational costs ($\mathcal{C}_o$). This results in the following expressions, for respectively the diesel, battery and hydrogen powered ferry:

$$\mathcal{C}_D = \mathcal{C}_{i_D} + \mathcal{C}_{o_D} = (0.3 + \{1.3\text{-}2.0\}) \, [k€/\text{kW}] \times P_i = \{1.6\text{-}2.3\} \, [k€/\text{kW}] \times P_i \qquad (\;3.13\;)$$

$$\mathcal{C}_{ESS} = \mathcal{C}_{i_{ESS}} + \mathcal{C}_{o_{ESS}} = (1.2 + \{0.3\text{-}0.7\}) \, [k€/\text{kW}] \times P_i = \{1.5\text{-}1.9\} \, [k€/\text{kW}] \times P_i \quad (\;3.14\;)$$

$$\mathcal{C}_{FC} = \mathcal{C}_{i_{FC}} + \mathcal{C}_{o_{FC}} = (0.8 + \{1.7\text{-}4.2\}) \, [k€/\text{kW}] \times P_i = \{2.5\text{-}5.0\} \, [k€/\text{kW}] \times P_i \qquad (\;3.15\;)$$

The target is a concept ferry with a sufficiently low energy consumption that the total costs over the five year period is not higher than that of the diesel driven ferry, i.e. lower than around 5.3 M€:

$$\mathcal{C}_D = \{1.5\text{-}2.2\} \, [k€/\text{kW}] \times 2,880 \, [kW] = \{4.3\text{-}6.3\} \, M€ \qquad (\;3.16\;)$$

The energy consumption of the ferry is roughly proportional to the installed power and resistance of the ferry ($E \sim P_i \sim R$). This results in the following ratios, for respectively the battery and hydrogen powered ferry:

$$\frac{\mathcal{C}_{ESS}}{\mathcal{C}_D} < 1.0 \rightarrow \frac{E_{ESS}}{E_{CC300}} \approx \frac{P_{i,ESS}}{P_{i,CC300}} < \frac{\{1.6\text{-}2.3\} \, [k€/\text{kW}]}{\{1.5\text{-}1.9\} \, [k€/\text{kW}]} = \{0.8\text{-}1.5\} \qquad (\;3.17\;)$$

$$\frac{\mathcal{C}_{FC}}{\mathcal{C}_D} < 1.0 \rightarrow \frac{E_{FC}}{E_{CC300}} \approx \frac{P_{i,FC}}{P_{i,CC300}} < \frac{\{1.6\text{-}2.3\} \, [k€/\text{kW}]}{\{2.5\text{-}5.0\} \, [k€/\text{kW}]} = \{0.3\text{-}0.9\} \qquad (\;3.18\;)$$

These ratios mean the following for the concept ferry in order to be financially feasible:
- the battery powered ferry should have a resistance that is below 0.8-1.5 times the resistance of the Coastal Cruiser 300;
- the hydrogen powered ferry should have a resistance that is at most 30% to 90% that of the Coastal Cruiser 300.

A remark must be made that these ratios are purely based on costs. In case of the battery powered ferry, without making the ferry longer, the upper limit is 1.2 instead of 1.5, because a larger energy capacity does not fit within the ship. This was discussed in subparagraph 3.3.8. For the hydrogen powered ferry, no limitation is applied to the ratio, as size does not pose a problem.

The ratios also depend on fuel and electricity prices, e.g. if the diesel price is low and electricity price high, than a 20% reduction in energy consumption is desirable, but if the diesel price is high and the electricity price low, than the energy consumption can be 50% higher than the current Coastal Cruiser 300.

3.7 Conclusions on Emission Free Propulsion Systems

Because there is a desire to replace polluting diesel engines with a propulsion method that is emission free, the following question was written at the beginning of this chapter:

What are suitable methods of emission free propulsion,
and what is the main problem when implementing them into a ferry?

Two suitable methods follow from this chapter, so there are two answers:

A battery powered system might be a suitable method for emission free propulsion,
but the main problem is its much larger weight.

A hydrogen fuel cell powered system might be a suitable method for emission free propulsion,
but the main problem is the higher (operational) costs.

3.7.1 Electric Powertrain

Using an internal combustion engine with a clean fuel is a possibility, but because that still results in harmful exhaust gasses, this option is not further considered. Therefore the emission free ferry will be an electric ferry, where the energy is supplied by batteries or by hydrogen fuel cells.

An overview of the components of the electric propulsion system can be seen in figure 3.8 on the next page. The two most important quantities are the mass of the system, which is discussed in appendix A.1, and the efficiency of the system, which is 93% for the electric motor, propulsion converter and DC-DC converter together. In case of a hydrogen powered ferry, a 55% fuel cell efficiency must also be taken into account.

Operating on supercapacitors is similar to operating on batteries, but because they lead to a larger and more expensive ferry, supercapacitors are not chosen as an option. Solar cells will also not be implemented in the concept design, as their contribution is negligibly small.

The cost estimations in this thesis is used for determining the target, as well as to compare the different concepts. It is important to keep in mind that an increase in costs should not necessarily be a deal breaker, as it must be weighed against the improvements for society. Furthermore, sailing emission free results in a reduction of indirect costs, e.g. less health problems occur related to pollution.

3.7.2 Battery Powered Catamaran

Paragraph 3.3 indicated that the battery might be a suitable solution for an electric fast passenger ferry. The technology is already successfully applied to car ferries, charging the batteries should be possible between each crossing, the lifetime is expected to be sufficiently long, and the impact on the environment is less than that from the diesel driven ferry. Furthermore, safety should also no be a problem, as multiple battery powered vessels are already operational, and also the public busses in Shenzhen operate safely on batteries.

The main problem however is the large mass of the battery system (0.1 kWh/kg for batteries [19], compared to 12 kWh/kg for diesel fuel [17]). Due to this, the displacement of the ferry will be larger, and so will the resistance and energy consumption. The latter is not necessarily a problem, as the price for electricity is a lot lower than for diesel fuel, which is roughly three times more expensive per unit of energy. Based on the difference in costs, the following energy consumption target ratio was determined in paragraph 3.6:

$$\frac{E_{ESS}}{E_{CC300}} < \{0.8\text{-}1.5\}$$
Ref. (3.17)

This means that a battery powered system is financially feasible if the energy consumption is below 80%-150% of that of the current Coastal Cruiser 300, depending on the price difference between electricity and diesel fuel.

Besides this target ratio, there is also a maximum ratio, which is determined by the limited space that is available onboard of the vessel. In case of 39.5 m long vessel it is 1.2, and for the elongated version it is 2.2.
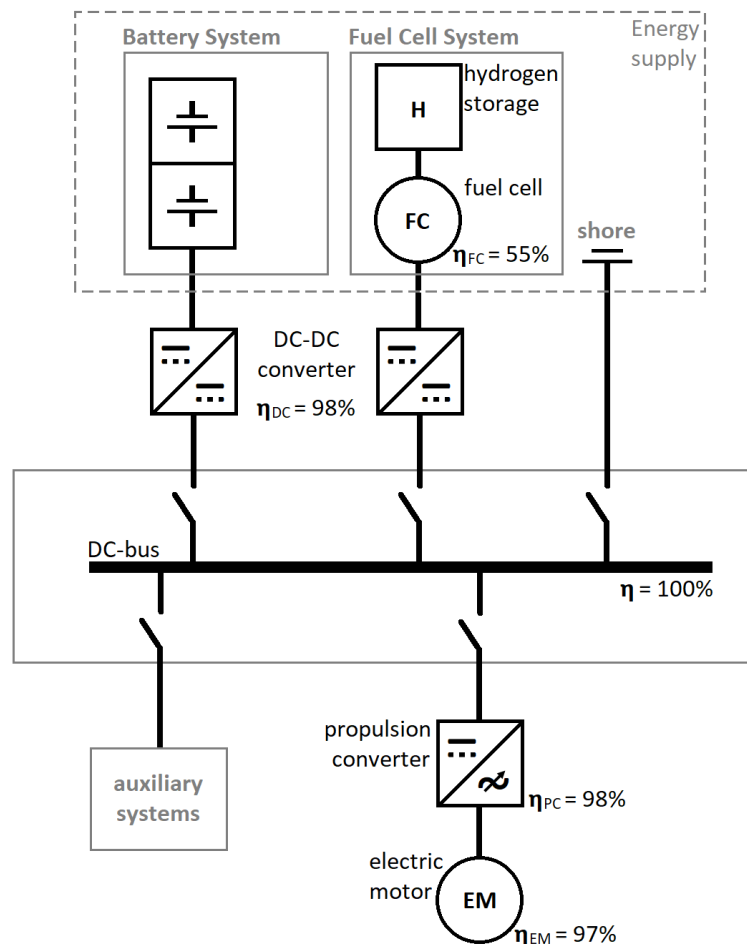
Figure 3.8: line diagram of the electric propulsion system, both
battery powered and fuel-cell-battery powered,
including the efficiencies of the different components.

3.7.3 Hydrogen Fuel Cell Powered Catamaran

The other emission free propulsion method that might be suitable is the hydrogen fuel cell, which was discussed in paragraph 3.5. In such a fuel cell, electricity is generated by combining hydrogen and oxygen, and the only by-product is water. Because the specific energy of hydrogen is much higher than of battery systems (1.7 kWh/kg [17] including its storage tank [18], and 0.1 kWh/kg for batteries [19]), it does not have the same problem as the battery powered vessel: a hydrogen fuel cell system is neither too heavy nor too large to fit within the vessel. Also safety does not seem to pose a problem, based on the properties of hydrogen and the already existing vehicles that are powered by hydrogen.

Instead of a large increase in weight, a hydrogen powered ferry suffers from a large increase in costs, as hydrogen is much more expensive than diesel fuel (21 c€/kWh compared to 12 c€/kWh on average [subparagraph 3.6.2]). Based on the difference in costs, the following energy consumption target ratio was determined in paragraph 3.6:

$$\frac{E_{FC}}{E_{CC300}} < \{0.3\text{-}0.9\} \qquad\qquad \text{Ref. (3.18)}$$

This ratio means that the energy consumption must be reduced to 30% to 90% of that of the current Coastal Cruiser 300, in order to be financially feasible. But again the remainder: it should not all be about money.

4

Implementing the Electric Propulsion Systems into the Design

As mentioned in the introduction, this project will be a case study for a fast ferry line in Shenzhen, China. The current diesel driven passenger ferry is an aluminium catamaran, so this chapter presents the analysis on the feasibility of an electric version of such an aluminium catamaran.

The previous chapter indicated that the energy consumption has to be sufficiently low, for the electric ferry to be (financially) feasible. So the question is:

What is the impact on energy consumption,
when implementing the emission free propulsion systems
into the design of the Coastal Cruiser 300,
and how does that impact the costs?

Structure of this Chapter
Paragraph 4.1 starts with an overview of the resistance estimation method. Implementing the battery and fuel cell powered powertrain in the current design is done in **paragraph 4.2**. The preliminary conclusions can be found in **paragraph 4.3**.

4.1 Overview of the Estimation Method

The main focus point is energy consumption, as this is related to the size of the system, as well as to the operational costs. It is mainly determined by the resistance of the ferry, which is largely influenced by the displacement of the vessel.

4.1.1 Mass and Displacement

The displacement of a ship can be split into lightship and deadweight. Lightship is constant for a vessel, and deadweight varies with different load conditions. This thesis looks at the ship in design condition, which means that the deadweight is constant as well in this analysis. Therefore, the displacement of the catamaran (Δ_{cat}) is not split into lightship and deadweight, but instead into the following three components:

$$\Delta_{cat} = M_S + M_{PP} + M_{add} \hspace{4cm} \text{Ref. (A.1)}$$

With:
- M_S, structural mass (hull and superstructure);
- M_{PP}, mass of the power and propulsion system;
- M_{add}, additional mass.

Additional Mass

The additional mass contains everything that is not related to the way the ship is powered. It is partly lightship (e.g. interior arrangement and radar equipment) and partly deadweight (e.g. passengers and luggage). Since these components are not related to the way the ship is powered, nor to the displacement of the vessel, the additional mass is held constant in this analysis; it is the same as for the Coastal Cruiser 300.

Mass of the Power and Propulsion System

The components within the power and propulsion system are also partly lightship (e.g. diesel engines or electric motors) and partly deadweight (e.g. diesel fuel or hydrogen). The mass of the different components in this system are mainly depend on the propulsion power that they have to provide, and the energy capacity that is required to make each crossing. The following components were taken into account, most of them seen in figure 3.8 on page 40:
- Waterjet;
- Electric motor;
- Propulsion converter;
- Switchboard;
- DC-DC converter;
- Energy storage system;
- Fuel cell system;
- Hydrogen storage system;
- Electric cable and shore supply.

How the mass of these components are estimated is explained in appendix A.1. From this estimation follows that the electric power and propulsion system is heavier that the diesel powered system. Thus the initial displacement of the electric ferry will be larger.

Structural Mass

The structural mass (hull and superstructure) is purely lightship and it is mainly dependent on the size of the vessel. The displacement of the vessel influences the size, and thus the mass of the structure. This is indicated in figure 4.1 with a red arrow. So an increase in displacement results in an increase in structural mass, which means an increase in displacement. In other words: it is an iterative process. Because the influence on each other is relatively small, a break-even point can be easily found, especially with the use of a computer.

Estimating the structural mass is done with equation A.31. The derivation of this equation can be found in appendix A.2.

$$M_S = L \cdot B_{oa} \cdot \left(\left(H + \frac{\nabla}{L} \cdot \left[\frac{L \cdot T}{\nabla} \right] \right) \cdot \left[\frac{M_{hull}}{L \cdot B_{oa} \cdot D} \right] + \left[\frac{M_{ss}}{L \cdot B_{oa}} \right] \right)$$ Ref. (A.31)

This equation contains the following constants:
- $L = 39.5\ m$ [15];
- $B_{oa} = 10.3\ m$ [15];
- $H = 2.10\ m$ [15];
- $\left[\frac{L \cdot T}{\nabla} \right] = \mathbf{X}\ m^{-1}$;
- $\left[\frac{M_{hull}}{L \cdot B_{oa} \cdot D} \right] = \mathbf{X}\ kg/m^3$;
- $\left[\frac{M_{ss}}{L \cdot B_{oa}} \right] = \mathbf{X}\ kg/m^2$.

The only variable in this equation is the displacement of the catamaran ($\nabla = \Delta_{cat}/\rho/2$).
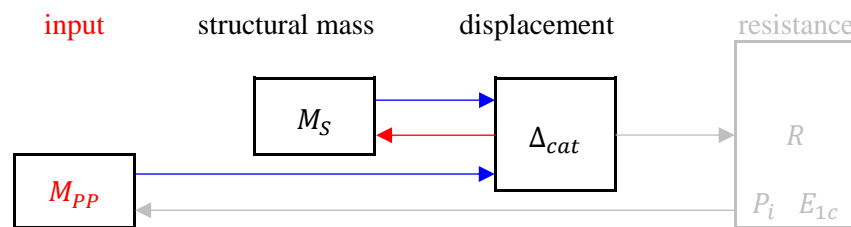
Figure 4.1: overview of the components that influence the displacement.

Displacement Error Margin
Because this method is an estimation, error margins should be included. The displacement in this estimation is a function of three components (as seen in equation A.1). The first two components are approximations, thus subjected to errors. The last is assumed to be constant, but it might as well deviate from the assumed value. Therefore a $\pm 5\%$ margin is included in the calculations. Five percent is chosen as the error margin, as the estimation is deemed accurate enough that a larger margin is not required.

4.1.2 Resistance and Energy Consumption
Because the main dimensions of the ship, as well as the design velocity remain constant (30 knots), the resistance is only influenced by the displacement, as illustrated in figure 4.2.
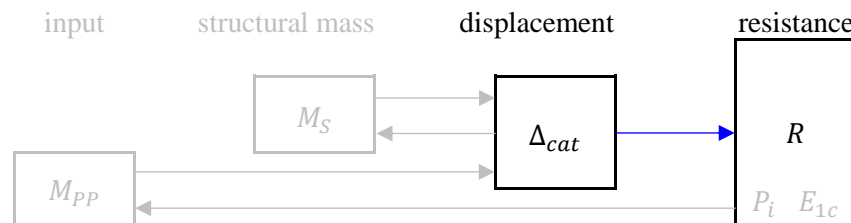
Figure 4.2: overview of the components that influence the resistance.

In this thesis, the following equations are used for estimating the resistance of the catamaran ferry:

$$R = (C_F + C_R) \cdot \tfrac{1}{2}\rho V^2 \cdot S + R_{air}$$ Ref. (B.34)

With:

- $$C_F = \frac{0.075}{\left(\log_{10}\left(\frac{V}{v}\cdot L\right)-2\right)^2} \qquad\qquad \text{Ref. (B.4)}$$

- $$C_R = \frac{(L_{0.8}-L)\cdot C_{R.7} + (L-L_{0.7})\cdot C_{R.8}}{L_{0.8}-L_{0.7}} \qquad\qquad \text{Ref. (B.27)}$$

  - $$C_{R.7}\cdot 1{,}000 = 0.43 + 115\cdot\exp\left(-0.48\cdot L/\nabla^{1/3}\right) \qquad \text{Ref. (B.23)}$$

  - $$C_{R.8}\cdot 1{,}000 = 0.26 + 90\cdot\exp\left(-0.47\cdot L/\nabla^{1/3}\right) \qquad \text{Ref. (B.24)}$$

- $$S = 0.78\cdot L\cdot\nabla^{1/3} + 8.2\cdot\nabla^{2/3} \qquad\qquad \text{Ref. (B.33)}$$

- $$R_{air} = R_{air_{30\,knots}}\cdot\left(\frac{V\,[knots]}{30\,[knots]}\right)^2 \qquad\qquad \text{Ref. (B.35)}$$

These equations contain the following constants:
- $L = 39.5\ m$ [15];
- $\rho = 1{,}025\ kg/m^3$;
- $V = 30\cdot 1{,}852/3{,}600\ m/s$;
- $v = 1.2\cdot 10^{-6}\ m^2/s$;
- $L_{0.7} = 49.6\ m$;
- $L_{0.8} = 37.9\ m$;
- $R_{air_{30\,knots}} = \mathbf{X}\ kN$.

The only variable in these equations is the displacement of the catamaran ($\nabla = \Delta_{cat}/\rho/2$).

The estimation of the residual resistance coefficient (C_R) is based on Froude number (Fn, equation B.5). Because the velocity is fixed at 30 knots, the Froude number is only a function of the length of the vessel. This means that the residual resistance coefficient can be estimated for $L_{0.7} = 49.6\ m$ when $Fn = 0.7$, and $L_{0.8} = 37.9\ m$ when $Fn = 0.8$. In order to estimate the C_R-value for $L = 39.5\ m$, linear interpolation is used (equation B.27).

$$Fn = \frac{V}{\sqrt{g\cdot L}} \qquad\qquad \text{Ref. (B.5)}$$

The derivations of the estimation equations can be found in appendix B, in which also is explained how the required propulsion power (P_P) and installed propulsion power (P_i) is related to the resistance:

$$P_P = \mathbf{X}\cdot R - \mathbf{X} \qquad\qquad \text{Ref. (B.37)}$$

$$P_i = 1.15 \times P_P \qquad\qquad \text{Ref. (B.38)}$$

The energy consumption of the ferry was discussed in subparagraph 3.2, where the following relation was derived for the energy consumption of one crossing (E_{1c}):

$$E_{1c} = \frac{P_p}{\eta_{EP}}\cdot t_t + E_{aux} \qquad\qquad \text{Ref. (3.2)}$$

With:
- $\eta_{EP} = 93\%$, efficiency of the electric drivetrain [paragraph 3.1];

- $t_t = 50/60\ hour$, time at transit speed [21];
- $E_{aux} = 0.1\ MWh$, auxiliary energy consumption [21].

Resistance Error Margin

The estimation method is based on curves that are fitted through the three lowest data points. Assuming that the real resistance is lower than this is therefore considered to be too optimistic. It can however be expected that the real resistance might be a bit higher. Therefore only a positive margin is added to the estimation. The resistance estimation is also deemed accurate enough that an error margin of five percent is sufficient.

4.1.3 Complete Overview of the Estimation Method

Combining figures 4.1 and 4.2 results in figure 4.3. The large red arrow at the bottom indicates the large iterative process: the installed power and energy consumption determine the mass of the power and propulsion system, which ultimately determines the installed power and energy consumption, as explained above.
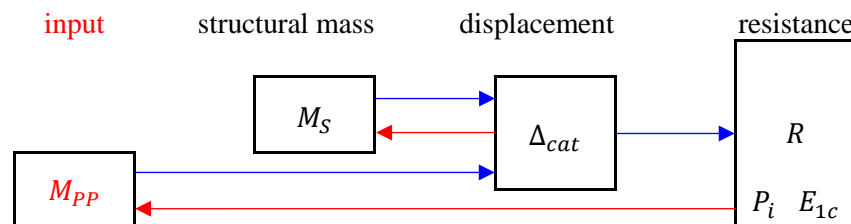
Figure 4.3: overview of the resistance estimation method. The arrows indicate how the components are related to each other.

4.1.4 Target Energy Consumption

The target energy consumption was determined in the previous chapter:

$$\frac{E_{ESS}}{E_{CC300}} < \{0.8\text{-}1.5\} \qquad\qquad \text{Ref. (3.17)}$$

$$\frac{E_{FC}}{E_{CC300}} < \{0.3\text{-}0.9\} \qquad\qquad \text{Ref. (3.18)}$$

The limited space onboard the ship results in the following limitation for the battery powered ferry [subparagraph 3.3.8]:

$$\frac{E_{ESS}}{E_{CC300}} \leq 1.2$$

4.2 Estimation Results

This paragraph presents an analysis of converting the design of the Coastal Cruiser 300 into a battery powered concept ferry, without changing any other major characteristic. The only input variable is the mass of the power and propulsion system (M_{PP}).

4.2.1 Battery Powered Coastal Cruiser 300

In case of the battery powered concept, the mass of the power and propulsion system results in an initial increase of the displacement of around 40%, when the error margins are not included. As a result, the resistance without error margins increases with roughly 50%. This means that the concept requires a more powerful propulsion system, in order to cope with the higher resistance. As a result, M_{PP} is larger, thus Δ_{cat} is larger, and thus the resistance increases even further. Because the weight increase is so large, the process diverges and no feasible break-even point is found.

So in case of the battery powered ferry, a reduction in energy consumption is required to make the ship even technically feasible.

4.2.2 Hydrogen Powered Coastal Cruiser 300

The weight increase of the hydrogen fuel cell powered ferry is smaller. The initial displacement increases with a little over 10%, and as a result, the resistance also increases with a little over 10%, when the error margins are not included.

This time a break-even point does exist, with the results as seen in table 4.1. At the top of the table, the error margins can be seen. The main part of the table has three rows: displacement ratio, resistance of energy consumption ratio, and the cost ratio.

In the middle column, it can be seen that the initial displacement and resistance increase of around 10%, has grown to 20% over multiple iterations.

The current hydrogen energy consumption ratio ranges from 1.1 to 1.5, while the target is 0.3-0.9. Because the energy consumption is higher than the target, the costs are also higher. Thus the hydrogen powered concept is feasible, but a reduction in energy consumption is desirable in order to reduce the costs.

Table 4.1: comparison between the Coastal Cruiser 300 and the hydrogen fuel-cell-battery powered ferry ($L = L_{CC300} = 39.5\ m$).

	-5%	0%	+5%
Displacement margin	-5%	0%	+5%
Resistance margin	0%	0%	+5%
$\dfrac{\Delta_{cat,FC}}{\Delta_{cat,CC300}}$	1.1	1.2	1.4
$\dfrac{R_{FC}}{R_{CC300}} \approx \dfrac{E_{FC}}{E_{CC300}}$	1.1	1.2	1.5
Costs ratio $\left(\dfrac{\mathcal{C}_{FC}}{\mathcal{C}_{D}}\right)$	1.2-3.7	1.4-4.1	1.7-5.1

4.3 Preliminary Conclusions

This chapter analysed the effect of implementing the electric propulsion systems into the design of the Coastal Cruiser 300. This way the following question can be answered:

What is the impact on energy consumption,
when implementing the emission free propulsion systems
into the design of the Coastal Cruiser 300,
and how does that impact the costs?

The short answers are:

A battery powered version is not feasible.

The hydrogen powered version is feasible, but much more expensive.

4.3.1 Battery Powered Catamaran

The required amount of batteries is simply too large for the concept to be feasible. So a reduction in energy consumption is required to make the concept even feasible.

4.3.2 Hydrogen Powered Catamaran

A hydrogen version of the Coastal Cruiser is feasible, but energy consumption will go up with around 10% to 50%. This means a significant increase in costs, making a reduction in energy consumption desirable.

5

Analysis of Ways to Reduce the Energy Consumption

From the previous chapter follows that a battery powered Coastal Cruiser 300 is not feasible, if the energy consumption is not reduced. A hydrogen powered version is feasible, but much more expensive. So a reduction in energy consumption is required in order to reduce the costs. Thus the question is:

How can the energy consumption of the electric concept ferry be reduced,
and what is the effect on the feasibility?

One way of reducing energy consumption is by reducing the resistance of the ferry. This can be done be elongating the hull. Another way of reducing the resistance is by making the ship lighter, which can be done by replacing the aluminium structure with a carbon composite structure. A more extreme reduction in resistance is possible with hydrofoils, but because that would change the ship type, it will be discussed in chapter 6. The final design related topic that will be discussed in this chapter is the future outlook: the energy consumption will go down as a result of improved performance of the electric power and propulsion system in the future.

Besides changes to the design, operational changes can also result in a lower energy consumption. Reducing the design speed leads to a reduction in resistance, and operating on a shorter crossing has a positive effect on the energy consumption.

Structure of this Chapter
The first three paragraphs of this chapter are related to the design of the ferry. An analysing of the effect of elongating the hull can be found in **paragraph 5.1**. The effect of replacing the aluminium structure with a carbon composite structure is analysed in **paragraph 5.2**. The future outlook can be found in **paragraph 5.3**.

The next two paragraphs are related to operational profile of the ferry. Sailing at lower velocities is discussed in **paragraph 5.4**, followed by an analysis of operating on a shorter crossing in **paragraph 5.5**.

Paragraph 5.6 contains the preliminary conclusions on these emission free concept ferries.

5.1 Electric Catamaran with an Elongated Hull

Reducing the resistance of the ferry can be done by making the vessel longer. The longer the ship, the higher the slenderness ratio, but also the heavier the structure. The first is positive for resistance, the second negative. This can be seen in figure 5.1, where the optimum lies well beyond the 50 m. The red dash-dotted line indicates the length at Froude number 0.7, the upper limit in this analysis. The total resistance for longer ship lengths (the dotted part of the black curve) is the result of extrapolation, and thus subjected to larger errors. Due to operational limitations, the maximum overall length is 46.5 m, as discussed in paragraph 2.3, which is indicated with a blue dashed line in figure 5.1. A final remark on this figure is that the black curve is the first iteration, meaning that the mass of the power and propulsion system is constant, and thus it is not adjusted to the resistance of the concept.
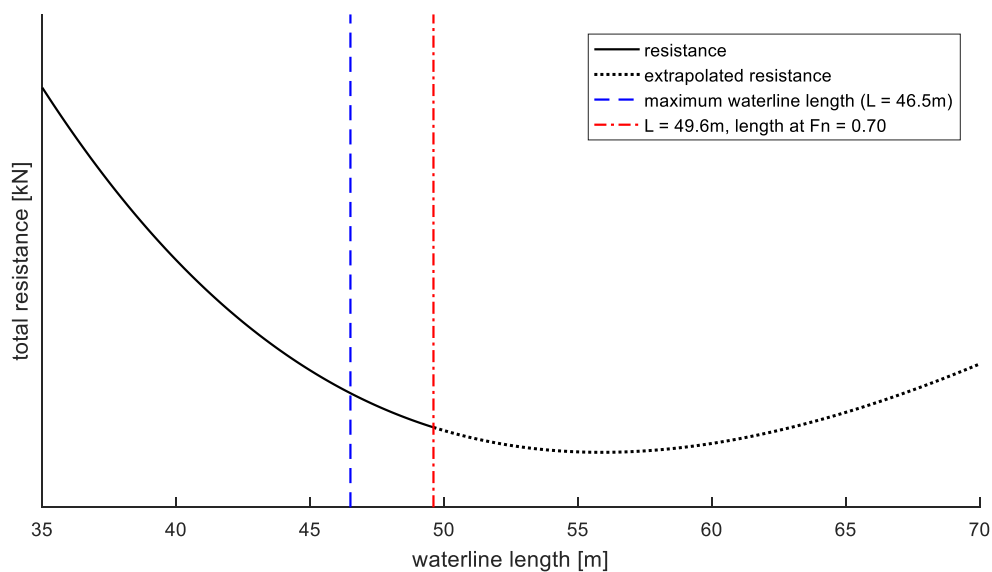
Figure 5.1: resistance plotted against ship length (first iteration). The blue dashed line indicates the maximum operational length ($L = 46.5\ m$), and the red dash-dotted line indicates the length at Froude number 0.70 ($L = 49.6\ m$).

5.1.1 Estimation Method

The estimation method used for this paragraph is similar to the one as explained in paragraph 4.1. The only addition is the inclusion of waterline length (L, blue in paragraph 4.1). An overview of the complete estimation method is seen in figure 5.2.
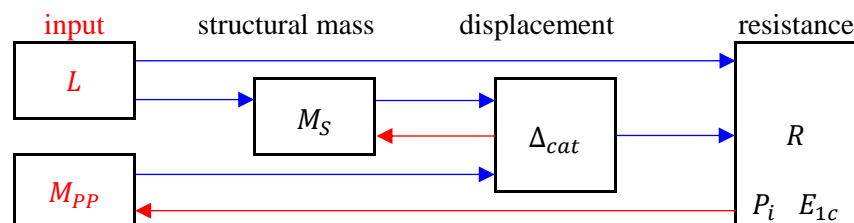
Figure 5.2: overview of the resistance estimation method. The arrows indicate how the components are related to each other.

There are now two input variables, waterline length (L) and the mass of the power and propulsion system (M_{PP}, appendix A.1). The structural mass (M_S) is influenced by the length of the vessel, as well

as by the displacement of the vessel (Δ_{cat}), as explained in appendix A.2. The displacement is determined by the structural mass and the mass of the power and propulsion system.

Together with the length of the vessel, the displacement leads to the resistance of the ferry (R), from which the installed power (P_i) and energy consumption per crossing (E_{1c}) follow. This is explained in appendix B.

The residual resistance coefficient (C_R) can be estimated for $L_{0.7} = 49.6\ m$ when the Froude number is 0.7, and $L_{0.8} = 37.9\ m$ when the Froude number is 0.8. Linear interpolation was used (equation B.27) to estimate the C_R-value for $L = 39.5\ m$. Because the elongated hull length of 46.5 m also falls between $L_{0.7}$ and $L_{0.8}$, the same linear interpolation method can be used here as well.

$$C_R = \frac{(L_{0.8} - L) \cdot C_{R.7} + (L - L_{0.7}) \cdot C_{R.8}}{L_{0.8} - L_{0.7}} \qquad\qquad \text{Ref. (B.27)}$$

5.1.2 Additional Cost Estimation and Target Energy Consumption

With the use of the method from appendix A.2, the structural mass increase is estimated to be six tonnes, when the ship is elongated from 39.5 to 46.5 m. Based on the aluminium price (13 \$/kg [87]), the labour costs (38 \$/man-hour in Europe [88] and 0.5 man-hour/kg [87]), and the exchange rate (0.89 €/\$ [89]), the aluminium price is approximately 28 €/kg:

$$0.89\ [\text{€/\$}] \times (13\ [\text{\$/}kg] + 38\ [\text{\$/}h] \times 0.5\ [h/kg]) = 28\ \text{€/}kg$$

The lifetime of the vessel is at least 20 years, four times longer than the minimal target lifetime of the electric propulsion system. So the relative additional investment is only 42 thousand euro:

$$\frac{28\ [\text{€/}kg] \times 6\ [tonnes\ weight\ increase]}{4\ [ship\text{-}life/electric\text{-}system\text{-}life]} = 42\ k\text{€}$$

This is negligibly small compared to the total costs of around 5.3 million euro that is the target for electric ferry, as calculated in subparagraph 3.6.3. Thus the target ratios remain the same:

$$\frac{E_{ESS}}{E_{CC300}} < \{0.8\text{-}1.5\} \qquad\qquad \text{Ref. (3.17)}$$

$$\frac{E_{FC}}{E_{CC300}} < \{0.3\text{-}0.9\} \qquad\qquad \text{Ref. (3.18)}$$

The hard limit for the battery powered elongated ferry, based on the available space on board, is the following [subparagraph 3.3.8]:

$$\frac{E_{ESS}}{E_{CC300}} \leq 2.2$$

5.1.3 Battery Powered Catamaran

Making the battery powered concept longer results in an increase in displacement of around 3%, but a reduction in resistance of around 11%, when the margins are not included. However, compared to the Coastal Cruiser 300, it is still an increase of around 50% and 30% respectively. This resistance increase is small enough that the iterative process converges and a break-even point can be found, as seen in table 5.1.

However, the break-even point is not a certainty, as including positive margins does not lead to a feasible concept. This can be seen by the infinity symbols (∞) in the table, which indicate that the process diverges. Furthermore, without margins, the result is an energy consumption that is close to the limit ($E_{ESS}/E_{CC300} = 2.2$), meaning that fitting the system onboard might become an issue.

Table 5.1: comparison between the Coastal Cruiser 300 and the battery powered ferry with a longer hull ($L = 46.5\ m$). For financial feasibility, the cost ratio should be smaller than 1.0.

Displacement margin	-5%	0%	+5%
Resistance margin	0%	0%	+5%
$\dfrac{\Delta_{cat,ESS}}{\Delta_{cat,CC300}}$	1.9	2.3	∞
$\dfrac{R_{ESS}}{R_{CC300}} \approx \dfrac{E_{ESS}}{E_{CC300}}$	1.7	2.2	∞
Costs ratio $\left(\dfrac{\mathcal{C}_{ESS}}{\mathcal{C}_{D}}\right)$	1.1-2.1	1.4-2.7	∞

5.1.4 Hydrogen Powered Catamaran

In case of the hydrogen fuel-cell-battery powered catamaran, without margins, a resistance reduction of 8% can be achieved by stretching the length of the ferry to 46.5 m, which is only 4% more than the CC300, while the displacement is 16% higher.

Because the resistance is only four percent higher, the propulsion system only requires a few percent more power. After multiple iterations, the resistance converges to 6% more than the Coastal Cruiser 300, when the margins are not included.

The result of the elongated hydrogen powered ferry can be seen in table 5.2, which also contains the result of the previous chapter. The estimation again shows that a hydrogen powered ferry is feasible, but more expensive than the diesel powered ferry. It can also be seen that the difference in cost ratios is relatively small, when comparing the two lengths with each other.

Table 5.2: comparison between the Coastal Cruiser 300 and the hydrogen fuel-cell-battery powered ferry with equal hull length and a longer hull. For financial feasibility, the cost ratio should be smaller than 1.0.

	$L = L_{CC300} = 39.5\ m$			$L = 46.5\ m$		
Displacement margin	-5%	0%	+5%	-5%	0%	+5%
Resistance margin	0%	0%	+5%	0%	0%	+5%
$\dfrac{\Delta_{cat,FC}}{\Delta_{cat,CC300}}$	1.1	1.2	1.4	1.1	1.2	1.3
$\dfrac{R_{FC}}{R_{CC300}} \approx \dfrac{E_{FC}}{E_{CC300}}$	1.1	1.2	1.5	1.0	1.1	1.2
Costs ratio $\left(\dfrac{\mathcal{C}_{FC}}{\mathcal{C}_{D}}\right)$	1.2-3.7	1.4-4.1	1.7-5.1	1.1-3.3	1.2-3.5	1.4-4.2

5.1.5 Conclusion of the Elongated Hull Concepts

This analysis shows that the reduction for the battery powered concept is quite significant, changing the infeasible concept into a possibly feasible concept. The effect for the hydrogen powered ferry is less severe, the only effect is a small reduction in energy consumption.

When comparing both elongated concepts, it can be seen that the costs are similar (a cost ratio of 1.1-3.5 compared to 1.1-2.7, without positive margins). So if the electricity price is high and hydrogen price low, it might be less expensive to operate on hydrogen, while it was previously expected that hydrogen would be more expensive.

5.2 Reducing Weight by Implementing a Carbon Composite Structure

Reducing the weight of the vessel is another way of reducing the resistance. Using carbon composite materials for the structure instead of aluminium is a way of saving weight. Already in 2003, a composite ferry was launched in Norway, which had a 70 passenger capacity [90]. Since then larger vessels were made from composite materials, such as the Zhong Shan 6, seen in figure 5.3, a 44 m long catamaran that can transport 300 passengers with a speed of 40 knots [91]. This example shows that a composite version of the Coastal Cruiser 300 is possible.

Figure 5.3: the Zhong Shan 6, a 44 m long carbon composite catamaran that can   [91]
transport 300 passengers with a speed of 40 knots.

5.2.1 Basics of Composites and the Reduction in Weight

A composite material is a material that is composed of two or more significantly different base materials. A well-known example is reinforced concrete, a combination of steel and concrete. Generally when people talk about composite materials, they mean fibre reinforced polymers, such as Carbon Fibre Reinforced Polymers (CFRB).

Two other fibres that are often used in composite materials are glass and aramid (e.g. Kevlar). The first has a lower strength/weight-ratio and a lower stiffness than CFRP. The second is generally less strong than carbon composites, but it is tougher, which means it can absorb more energy without breaking. This makes Kevlar especially good with impact forces, therefore suited for bulletproof armour. In this thesis, the application of composite materials will be limited to CFRP, as this material has the best suited properties, e.g. relatively high strength/weight-ratio, high stiffness, and high corrosion resistance. [92]

Fibre reinforced polymers consist of two main components: fibres and a resin. The main strength of the material comes from the fibres, and the main function of the resin is to keep the fibres in their place. The strength of the fibres in longitudinal direction is much higher than the strength in transverse direction. This means that composite materials are nonhomogeneous. Metals on the other hand are homogeneous materials, which means that they have the same material properties in every direction. The fibre orientation in each structural component can be optimized for the load in that component, which is an advantage of the nonhomogeneous property of the material. This also means that the strength/weight-ratio for each component is different. Due to this, estimating the reduction in weight based on only the material properties is very difficult for composite materials.

In order to determine the savings in weight, the structure must be analysed as a whole. This is done in multiple studies, such as the one of J. Kuzjatkin, who investigated the weight reduction of a fast ferry with similar particulars as the Coastal Cruiser 300, e.g. 40 length, 10 m beam, 160 tonnes displacement and 30 knots service speed [93]. This study, amongst others, indicate that if the structure of a ship is built with CFRP instead of aluminium, a weight reduction of 35% can be achieved [93] [94]. It must be mentioned here that the 35% weight reduction applies to only the structural mass. Looking at the total displacement, the weight reduction is close to only 10%.

5.2.2 Estimation Method

The 35% weight reduction can be easily implemented in the previously used estimation method, by adding the following calculation step to the structural mass estimation:

$$M_{S,CFRP} = (100\% - 35\% \, [weight \; reduction]) \times M_{S,aluminium} \qquad (\; 5.1 \;)$$

In this equation, $M_{S,aluminium}$ is the structural mass as calculated in appendix A.2. The new structural mass ($M_{S,CFRP}$) is used to estimate the displacement:

$$\Delta_{cat} = M_{PP} + M_{S,CFRP} + M_{add} \qquad (\; 5.2 \;)$$

5.2.3 Additional Cost Estimation and Revised Target Energy Consumption

Based on the material price (61 \$/kg [87]), the labour costs (38 \$/man-hour in Europe [88] and 1.1 man-hour/kg [87]), and the exchange rate (0.89 €/\$ [89]), the carbon composite price is estimated to be 91 €/kg:

$$0.89 \, [€/\$] \times (61 \, [\$/kg] + 38 \, [\$/h] \times 1.1 \, [h/kg]) = 91 \, €/kg$$

Looking at price per kilogram, CFRP is 51 euro more expensive than aluminium ($28 \, €/kg_{alu}$). However, the mass of the structure is 35% lower, so effectively, the price difference is 31 €/kg, an increase of 150%:

$$(100\% - 35\% \, [weight \; reduction]) \times 91 \, [€/kg] - 28 \, [€/kg_{alu}] = 31 \, €/kg_{alu.ferry}$$

For the total vessel, this amounts to 1.3 M€ for the original length, and 1.5 M€ for the elongated vessel. The design lifetime of the vessel is four times longer than the target lifetime of the electrical system, so the effective additional investment for CFRP is little less than 0.4 M€ in for both vessel lengths. The total target costs for the electric ferry is roughly 5.3 M€, as calculated in subparagraph 3.6.3. This slightly affects the target ratios of the battery powered and hydrogen powered ferry respectively:

$$\frac{E_{ESS}}{E_{CC300}} < \left(\frac{5.3 \, [M€]}{5.3 \, [M€] + 0.4 \, [M€]} \right) \times \{0.8\text{-}1.5\} = \{0.7\text{-}1.4\} \qquad (\; 5.3 \;)$$

$$\frac{E_{FC}}{E_{CC300}} < \left(\frac{5.3 \, [M€]}{5.3 \, [M€] + 0.4 \, [M€]} \right) \times \{0.3\text{-}0.9\} = \{0.3\text{-}0.8\} \qquad (\; 5.4 \;)$$

The hard limits for the battery powered ferry are not affected. Based on the available space onboard, they are, for the "normal" and elongated version respectively [subparagraph 3.3.8]:

$$\left(\frac{E_{ESS}}{E_{CC300}} \right)_{39.5m} \leq 1.2$$

$$\left(\frac{E_{ESS}}{E_{CC300}} \right)_{46.5m} \leq 2.2$$

5.2.4 Battery Powered Catamaran

The results of all four battery powered concepts can be seen in table 5.3. Due to the diverging iterative process, not all concepts result in a feasible solution, as indicated by the infinity symbols (∞).

Without an elongated hull, no break-even point exists, not for the aluminium version, nor for the carbon composite version. In case of the CFRP elongated version, a break-even point is found, this time also when including positive margins. However, the energy consumption ratio is 2.7, which is higher than the limit of 2.2, i.e. the required battery capacity does not fit within the hull. This is indicated in the table by the crossed-out values.

Though the total reduction in displacement due to the lighter structure is only around 10%, the effect can be quite large. Without margins, the reduction in energy consumption is close to 30%.

The most optimistic estimation shows that the CFRP elongated version of the battery powered ferry might be cost competitive with the diesel powered ferry ($\cancel{C}_{ESS}/\cancel{C}_D = $ **1.0**). When comparing both structural materials, it can be seen that the impact of CFRP is small, in case of the battery powered concept.

A larger reduction in energy consumption is still required in order to increase feasibility and further reduce the costs.

Table 5.3: comparison between the Coastal Cruiser 300 and the battery powered ferry with an aluminium structure, a CFRP structure, equal hull length and a longer hull length. For technical feasibility, the energy consumption ratio must be below 2.2, and for financial feasibility, the cost ratio should be smaller than 1.0.

	$L = L_{CC300} = 39.5\,m$ Aluminium structure			$L = 46.5\,m$ Aluminium structure		
Displacement margin	-5%	0%	+5%	-5%	0%	+5%
Resistance margin	0%	0%	+5%	0%	0%	+5%
$\dfrac{\Delta_{cat,ESS}}{\Delta_{cat,CC300}}$	∞	∞	∞	1.9	2.3	∞
$\dfrac{R_{ESS}}{R_{CC300}} \approx \dfrac{E_{ESS}}{E_{CC300}}$	∞	∞	∞	1.7	2.2	∞
Costs ratio $\left(\dfrac{\cancel{C}_{ESS}}{\cancel{C}_D}\right)$	∞	∞	∞	1.1-2.1	1.4-2.7	∞

	$L = L_{CC300} = 39.5\,m$ CFRP structure			$L = 46.5\,m$ CFRP structure		
Displacement margin	-5%	0%	+5%	-5%	0%	+5%
Resistance margin	0%	0%	+5%	0%	0%	+5%
$\dfrac{\Delta_{cat,ESS}}{\Delta_{cat,CC300}}$	∞	∞	∞	1.5	1.8	~~2.7~~
$\dfrac{R_{ESS}}{R_{CC300}} \approx \dfrac{E_{ESS}}{E_{CC300}}$	∞	∞	∞	1.3	1.6	~~2.7~~
Costs ratio $\left(\dfrac{\cancel{C}_{ESS}}{\cancel{C}_D}\right)$	∞	∞	∞	**1.0**-1.7	1.1-2.0	~~2.0-3.4~~

5.2.5 Hydrogen Powered Catamaran

Table 5.4 contains the results for a carbon composite hydrogen powered catamaran, for 39.5 and 46.5 m ship length respectively. The table also contains the previous results for the aluminium structure. The table clearly shows that, in case of the hydrogen powered concept, the effect of CFRP is larger than the effect of elongating the hull.

Because the displacement of the hydrogen powered ferry is lower than that of the battery powered ferry, the effect of the lighter structure is also smaller. The reduction in energy consumption is roughly twice the reduction in displacement due to the CFRP structure.

Three optimistic estimations result in a costs-ratio of **1.0**, meaning that the total costs are equal to that of the Coastal Cruiser 300 over the five year period. But because this is only the case for the most optimistic estimations, a further reduction in energy consumption is still desirable.

Table 5.4: comparison between the Coastal Cruiser 300 and the hydrogen fuel-cell-battery powered ferry with an aluminium structure, a CFRP structure, equal hull length and a longer hull length. For financial feasibility, the cost ratio should be smaller than 1.0.

	$L = L_{CC300} = 39.5\,m$ Aluminium structure			$L = 46.5\,m$ Aluminium structure		
Displacement margin	-5%	0%	+5%	-5%	0%	+5%
Resistance margin	0%	0%	+5%	0%	0%	+5%
$\dfrac{\Delta_{cat,FC}}{\Delta_{cat,CC300}}$	1.1	1.2	1.4	1.1	1.2	1.3
$\dfrac{R_{FC}}{R_{CC300}} \approx \dfrac{E_{FC}}{E_{CC300}}$	1.1	1.2	1.5	1.0	1.1	1.2
Costs ratio $\left(\dfrac{\cent_{FC}}{\cent_{D}}\right)$	1.2-3.7	1.4-4.1	1.7-5.1	1.1-3.3	1.2-3.5	1.4-4.2

	$L = L_{CC300} = 39.5\,m$ CFRP structure			$L = 46.5\,m$ CFRP structure		
Displacement margin	-5%	0%	+5%	-5%	0%	+5%
Resistance margin	0%	0%	+5%	0%	0%	+5%
$\dfrac{\Delta_{cat,FC}}{\Delta_{cat,CC300}}$	0.9	1.0	1.2	0.9	1.0	1.1
$\dfrac{R_{FC}}{R_{CC300}} \approx \dfrac{E_{FC}}{E_{CC300}}$	0.9	1.0	1.3	0.9	0.9	1.1
Costs ratio $\left(\dfrac{\cent_{FC}}{\cent_{D}}\right)$	**1.0**-3.1	1.2-3.5	1.4-4.2	**1.0**-2.9	**1.0**-3.1	1.2-3.5

5.2.6 Conclusion of the Carbon Composite Concepts

This paragraph shows that a lighter structure can result in a large reduction in energy consumption in case of the battery powered concept. It does however not result in a fully feasible concept, as the inclusion of positive margins results in a concept where the batteries do not fit within the vessel anymore.

The hydrogen powered ferry was already feasible, but a carbon composite structure can reduce the operational costs; in three optimistic cases, the hydrogen ferry is even cost competitive with the diesel powered ferry.

So the battery powered concept requires a larger reduction in energy consumption to lead to a fully feasible concept, and the hydrogen powered concept would also benefits from a further reduction in energy consumption.

5.3 Future Outlook: Effect of Improved Performance of the Electric Propulsion System

In the future, the energy consumption will go down as a result of improved performance of the electric power and propulsion system. This will increase the feasibility of the concept ferry.

5.3.1 Battery Powered Catamaran

Up until now, a specific energy of 159 Wh/kg was used for the battery cells, which was based on an existing cell from XALT [44]. It can be expected that in the future, the energy capacity of batteries increases.

Innolith, the Switzerland-based company with labs in Germany, claims that it is on a path to 1,000 Wh/kg. They already achieved a few breakthroughs and expect that the new batteries could be ready within 3-5 years. [95]

Another development in battery technology is the solid-state battery. As the name suggests, this battery type has no liquid electrolyte, as is the case with Li-ion batteries. Because there is no electro chemical reaction, there is less degradation, i.e. the cycle life is much longer than that of current Li-ion batteries. Therefore, a higher depth of discharge can be used. Currently, the energy density is 200 Wh/L [96], with a recent (June 2019) breakthrough of 400 Wh/L and a charge rate of 0.5 C [97]. For comparison, the battery cells used in this thesis (XALT 75 Ah HP) have an energy density of around 300 Wh/L and a continuous charge rate of 3.0 C [44]. Imec's target for 2024 is Solid-state batteries with a 1,000 Wh/L energy density and a charge rate of 3C [97]. The corresponding specific energy is around 400 Wh/kg [98], which is lower than the effective specific energy of the future Li-ion batteries:

$$1,000 \ [Wh/kg] \times 50\% \ [DOD] = 500 \ Wh/kg$$

If the battery cells would have a specific energy of 1,000 Wh/kg, the weight of the battery system would be reduced with 84%:

$$1 - \frac{159 \ [Wh/kg]}{1,000 \ [Wh/kg]} = 0.84$$

This improved battery performance not only means that the system has less weight, but also that it is smaller, i.e. the available space is no longer a limiting factor.

Discussion of the Results

If the same estimation method is used as before, the result is a feasible concept in all cases, as seen in table 5.5. It is even fully financially feasible in the most optimistic estimation, which is indicated in green. The range of all other price ratios also lie around 1.0. This suggest that a battery powered ferry is cost competitive with the diesel powered version in the future.

The most optimistic estimation for the 39.5 m aluminium catamaran concept, indicated in blue, has a similar displacement as the current Coastal Cruiser 300. This suggest that in the future, it might be possible to convert existing vessels into battery powered ferries.

For comparison, the previous results (table 5.3) are presented below table 5.5.

5.3.2 Hydrogen Powered Catamaran

The effect of two changes is analysed in this subparagraph:
- Decrease in weight, by:
    - Operating without batteries;
    - Fuel cells with a higher specific power.
- Increase in efficiency.

Operating Without Batteries

In the first four paragraphs of this chapter, the fuel cell system also contained multiple battery packs, which were required to handle fluctuating powers. This need might disappear in the future as the response time of fuel cells improve. Hydrogenics already claims a response time from idle to full power in less than three seconds [67].

In the feasibility study of the fuel cell powered ferry for the San Francisco Bay, it was also assumed that the fuel cells can operate without support from a large battery system. Only some batteries are present for the stability of the electrical system, and as a back-up for the navigational and emergency systems. They are not capable of providing enough energy to drive the motors for a significant length of time. Furthermore, the report states a fuel cell response time of less than a second to go from low power to full power, which is superior to the response time of a diesel engine. [13]

In this subparagraph, it is assumed that the supporting battery system is small enough that its weight can be neglected. As a result the mass/power-ratio goes from 4.2 kg/kW for the fuel-cell-battery system to 2.6 kg/kW for the fully fuel cell system [appendix A.1.7].

Higher Specific Power

For the fuel cell modules, a specific power of 431 W/kg was used [67]. A specific power of 650 W/kg expected to be possible [99], which is a weight reduction of 34%:

$$1 - \frac{431 \ [W/kg]}{650 \ [W/kg]} = 0.34$$

Thus the mass/power-ratio decreases further, from 2.6 to 1.7 kg/kW:

$$(1 - 0.34) \times 2.6 \ [kg/kW] = 1.7 \ kg/kW$$

Operating at a Higher Efficiency

Up until now, a 55% efficiency was assumed, as this is a representative value [67]. Efficiencies of fuel cells can go up to 60% [17], and it is expected that in the future, 70% will be reached [99].

Discussion of the Results

Using the lighter weight system with 70% efficiency results in the values as seen in table 5.6, which is estimated with the previously used methods. Indicated in the orange box is the only result where the costs might be lower than that of the current diesel powered ferry. All other results are at least equally expensive as the diesel powered ferry ($\text{\textcent}_{FC}/\text{\textcent}_{D} \geq 1.0$).

When compared to the battery powered concept (table 5.5), it can be seen that the cost ratios are much higher, while the previous results (table 5.3 and 5.4) were more similar. From this can be concluded that the technical improvements of battery technology will be more significant than that of hydrogen fuel cells.

The result that is indicated in blue in table 5.6 suggests that in the future, it might also be possible to convert existing vessels into hydrogen fuel cell powered ferries. This is because the displacement is similar to that of the current Coastal Cruiser 300.

Table 5.5: comparison between the Coastal Cruiser 300 and the battery powered ferry with an aluminium structure, a CFRP structure, equal hull length and a longer hull length. For financial feasibility, the cost ratio should be smaller than 1.0. These results are for a battery system with 1,000 W/kg specific energy.

	$L = L_{CC300} = 39.5\ m$ Aluminium structure			$L = 46.5\ m$ Aluminium structure		
Displacement margin	-5%	0%	+5%	-5%	0%	+5%
Resistance margin	0%	0%	+5%	0%	0%	+5%
$\dfrac{\Delta_{cat,ESS}}{\Delta_{cat,CC300}}$	1.0	1.1	1.3	1.0	1.1	1.2
$\dfrac{R_{ESS}}{R_{CC300}} \approx \dfrac{E_{ESS}}{E_{CC300}}$	1.0	1.1	1.4	0.9	1.0	1.2
Costs ratio $\left(\dfrac{\textcent_{ESS}}{\textcent_{D}}\right)$	0.7-1.3	0.7-1.4	0.9-1.7	0.6-1.2	0.7-1.3	0.8-1.4

	$L = L_{CC300} = 39.5\ m$ CFRP structure			$L = 46.5\ m$ CFRP structure		
Displacement margin	-5%	0%	+5%	-5%	0%	+5%
Resistance margin	0%	0%	+5%	0%	0%	+5%
$\dfrac{\Delta_{cat,ESS}}{\Delta_{cat,CC300}}$	0.9	1.0	1.1	0.9	1.0	1.0
$\dfrac{R_{ESS}}{R_{CC300}} \approx \dfrac{E_{ESS}}{E_{CC300}}$	0.9	1.0	1.1	0.8	0.9	1.0
Costs ratio $\left(\dfrac{\textcent_{ESS}}{\textcent_{D}}\right)$	0.6-1.1	0.7-1.2	0.8-1.4	0.6-1.0	0.6-1.1	0.7-1.2

Ref. table 5.3

	$L = L_{CC300} = 39.5\ m$ Aluminium structure			$L = 46.5\ m$ Aluminium structure		
Displacement margin	-5%	0%	+5%	-5%	0%	+5%
Resistance margin	0%	0%	+5%	0%	0%	+5%
$\dfrac{\Delta_{cat,ESS}}{\Delta_{cat,CC300}}$	∞	∞	∞	1.9	2.3	∞
$\dfrac{R_{ESS}}{R_{CC300}} \approx \dfrac{E_{ESS}}{E_{CC300}}$	∞	∞	∞	1.7	2.2	∞
Costs ratio $\left(\dfrac{\textcent_{ESS}}{\textcent_{D}}\right)$	∞	∞	∞	1.1-2.1	1.4-2.7	∞

	$L = L_{CC300} = 39.5\ m$ CFRP structure			$L = 46.5\ m$ CFRP structure		
Displacement margin	-5%	0%	+5%	-5%	0%	+5%
Resistance margin	0%	0%	+5%	0%	0%	+5%
$\dfrac{\Delta_{cat,ESS}}{\Delta_{cat,CC300}}$	∞	∞	∞	1.5	1.8	~~2.7~~
$\dfrac{R_{ESS}}{R_{CC300}} \approx \dfrac{E_{ESS}}{E_{CC300}}$	∞	∞	∞	1.3	1.6	~~2.7~~
Costs ratio $\left(\dfrac{\textcent_{ESS}}{\textcent_{D}}\right)$	∞	∞	∞	**1.0**-1.7	1.1-2.0	~~2.0-3.4~~

Table 5.6: comparison between the Coastal Cruiser 300 and the hydrogen fuel-cell-battery powered ferry with an aluminium structure, a CFRP structure, equal hull length and a longer hull length. For financial feasibility, the cost ratio should be smaller than 1.0. These results are for a fuel cell system with a higher efficiency and a higher specific power that operates without batteries.

	$L = L_{CC300} = 39.5\ m$ Aluminium structure			$L = 46.5\ m$ Aluminium structure		
Displacement margin	-5%	0%	+5%	-5%	0%	+5%
Resistance margin	0%	0%	+5%	0%	0%	+5%
$\dfrac{\Delta_{cat,FC}}{\Delta_{cat,CC300}}$	1.0	1.1	1.2	1.0	1.1	1.2
$\dfrac{R_{FC}}{R_{CC300}} \approx \dfrac{E_{FC}}{E_{CC300}}$	1.0	1.1	1.3	0.9	1.0	1.1
Costs ratio $\left(\dfrac{\text{¢}_{FC}}{\text{¢}_{D}}\right)$	1.1-3.3	1.2-3.6	1.4-4.3	1.0-3.1	1.1-3.3	1.2-3.7

	$L = L_{CC300} = 39.5\ m$ CFRP structure			$L = 46.5\ m$ CFRP structure		
Displacement margin	-5%	0%	+5%	-5%	0%	+5%
Resistance margin	0%	0%	+5%	0%	0%	+5%
$\dfrac{\Delta_{cat,FC}}{\Delta_{cat,CC300}}$	0.9	0.9	1.0	0.9	0.9	1.0
$\dfrac{R_{FC}}{R_{CC300}} \approx \dfrac{E_{FC}}{E_{CC300}}$	0.9	0.9	1.1	0.8	0.9	1.0
Costs ratio $\left(\dfrac{\text{¢}_{FC}}{\text{¢}_{D}}\right)$	1.0-2.9	1.0-3.1	1.2-3.6	0.9-2.7	1.0-2.9	1.1-3.2

Ref. table 5.4

	$L = L_{CC300} = 39.5\ m$ Aluminium structure			$L = 46.5\ m$ Aluminium structure		
Displacement margin	-5%	0%	+5%	-5%	0%	+5%
Resistance margin	0%	0%	+5%	0%	0%	+5%
$\dfrac{\Delta_{cat,FC}}{\Delta_{cat,CC300}}$	1.1	1.2	1.4	1.1	1.2	1.3
$\dfrac{R_{FC}}{R_{CC300}} \approx \dfrac{E_{FC}}{E_{CC300}}$	1.1	1.2	1.5	1.0	1.1	1.2
Costs ratio $\left(\dfrac{\text{¢}_{FC}}{\text{¢}_{D}}\right)$	1.2-3.7	1.4-4.1	1.7-5.1	1.1-3.3	1.2-3.5	1.4-4.2

	$L = L_{CC300} = 39.5\ m$ CFRP structure			$L = 46.5\ m$ CFRP structure		
Displacement margin	-5%	0%	+5%	-5%	0%	+5%
Resistance margin	0%	0%	+5%	0%	0%	+5%
$\dfrac{\Delta_{cat,FC}}{\Delta_{cat,CC300}}$	0.9	1.0	1.2	0.9	1.0	1.1
$\dfrac{R_{FC}}{R_{CC300}} \approx \dfrac{E_{FC}}{E_{CC300}}$	0.9	1.0	1.3	0.9	0.9	1.1
Costs ratio $\left(\dfrac{\text{¢}_{FC}}{\text{¢}_{D}}\right)$	1.0-3.1	1.2-3.5	1.4-4.2	1.0-2.9	1.0-3.1	1.2-3.5

5.3.3 Conclusion on Expected Future Improvements

In the four tables on page 62 and 63, it can be seen that the expected future improvements of battery systems has much more impact on the feasibility of the electric ferry, than future improvements of fuel cell systems have on the hydrogen powered concept. It is expected that in the future, a battery powered ferry will be cost competitive with a diesel powered ferry. Future fuel cell technology also reduces the energy consumption, but the effect is smaller and the hydrogen powered concept is still not cost competitive with the diesel powered version.

In the future, it might be possible to convert existing ferries into electric versions. In that case, both the battery and the fuel system might be feasible.

So future technology drastically improves feasibility, but since it is not yet available, some other measures are analysed in the next two chapters.

5.4 Effect of Lowering the Design Speed

Sailing at a lower speed might be an alternative solution for lowering the energy consumption, as a lower velocity leads to a lower resistance.

5.4.1 Estimation Method

In order to analyse the effect of varying speed, the estimation method from subparagraph 5.1.1 is slightly altered, as seen in figure 5.4. The main difference is that this time the length of the vessel is fixed (at 39.5 and 46.5 m) and the speed is a variable (V). So instead of linear interpolation over length, extrapolation over speed is used:

$$C_R = \frac{(V_{0.8}^{-2.8} - V^{-2.8}) \cdot C_{R.7} + (V^{-2.8} - V_{0.7}^{-2.8}) \cdot C_{R.8}}{V_{0.8}^{-2.8} - V_{0.7}^{-2.8}} \qquad \text{Ref. (B.29)}$$

The velocity values ($V_{0.7}$ and $V_{0.8}$) are listed in table B.8. It can be noted that equation B.29 is not linear extrapolation, but to the power '-2.8'. This value is chosen as it results in the best fit for the Coastal Cruiser 300, as explained in appendix B.2.7. The negative power indicates that the residual resistance coefficient goes down if the speed goes up. This is valid for velocities above the "hump speed", roughly above Froude number 0.5, which corresponds to a speed of around 20 knots. This can also be seen in figure B.18 on the next page.

Ref. table B.8: speed of the vessel as a function of waterline length (L) and Froude number (Fn).

		L	39.5	46.5	m
$Fn = 0.7$	$V_{0.7}$		26.8	29.1	knots
$Fn = 0.8$	$V_{0.8}$		30.6	33.2	knots
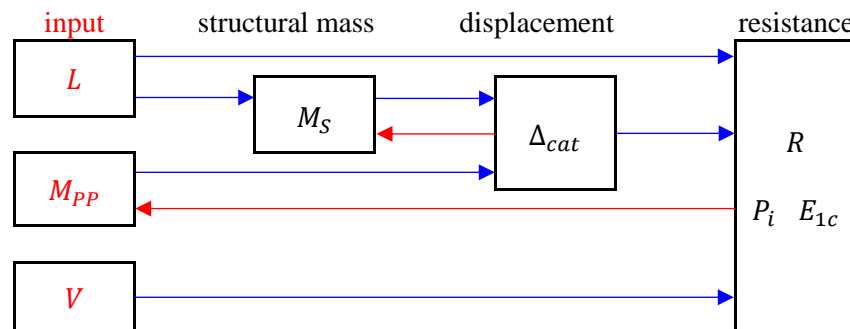
Figure 5.4: overview of the resistance estimation method for varying speed. The arrows indicate how the components are related to each other.

Because the ferry operates well above the "hump speed", the residual resistance coefficient only goes up if the speed decreases, and thus the total resistance only slightly goes down if the speed is decreased. At the same time, the travel time gets longer, so the energy consumption does not go down much by decreasing the velocity.

The energy consumption can be calculated in the same way as before (equation 3.2, see next page), but the travel time at transit speed (t_t) is no longer a constant, as it changes with the velocity of the vessel:

$$t_t = \frac{25\,[NM]}{V\,[knots]} \qquad \text{Ref. (B.40)}$$

$$E_{1c} = \frac{P_p}{\eta_{EP}} \cdot t_t + E_{aux}$$
<div align="right">Ref. (3.2)</div>
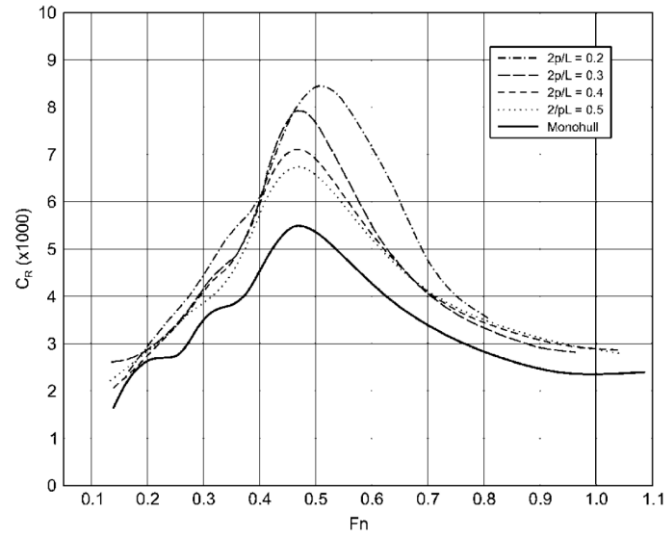
Ref. figure B.18: residual resistance coefficient of model 4b of   [100]
the systematic demi-hull series of Molland et al.

5.4.2 Battery Powered Concept

From estimating the energy consumption of the 39.5 m long battery powered ferry follows that not the high speed, but the distance is the problem. This true for both the aluminium version and the CFRP version. Even if the design speed is decreased to 20 knots, a feasible option does not exist.

The lowest resistance can be achieved in case of an elongated hull with a carbon composite structure. The result for that concept can be seen in figure 5.5 and 5.6. The first figure shows that the resistance goes only slightly down, up to a little over 30% for velocities close to 20 knots. At this speed however, the travel time is 50% longer. So the overall reduction in energy consumption is small, as illustrated in the latter figure.

The figures also clearly show that a small change can have a large effect. Compared to the optimistic estimation (dash-dotted curve), if the displacement and the resistance estimation is 5% higher, the result is a total resistance and energy consumption that is over 30% higher (dashed curve). If another 5% is added to the displacement and the resistance estimation, the effect is another increase of over 50% (solid curve).

The largest reduction in energy consumption is roughly 10%, at a transit speed of 24 knots. This might seem like much, but it is not a feasible concept, as the lower speeds impacts the available charging time, if the departure times are not altered in the timetable. The travel time is increased by 12.5 minutes:

$$\frac{25 \, [NM]}{24 \, [knots]} \times 60 \left[\frac{minutes}{hour} \right] = 62.5 \, minutes$$

This means that the time at quay, and thus the available time for charging, is also reduced by 12.5 minutes. In subparagraph 3.3.4, it was assumed that 25 minutes is available for charging. Thus the energy consumption goes down with 10%, while the available charging time goes down with 50%. This means that there is not enough time available to properly charge the batteries.

It can be concluded that sailing at lower speeds is not the solution for the battery powered concept.
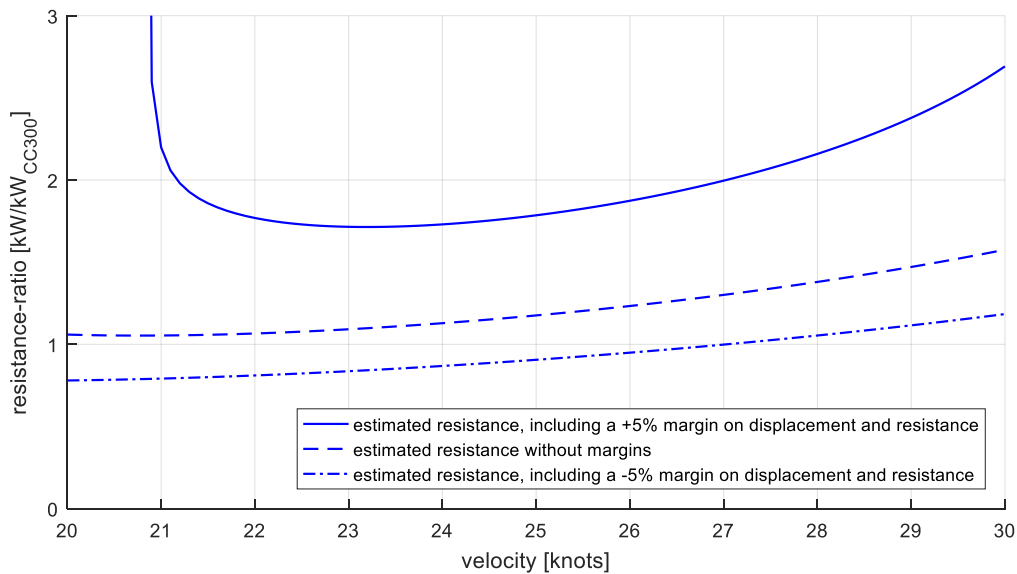
Figure 5.5: estimated resistance of the 46.5 m long carbon composite battery powered concept ferry plotted against design velocity. The resistance is normalized with the resistance of the CC300 at 30 knots.

Figure 5.6: estimated energy consumption of the 46.5 m long carbon composite battery powered concept ferry plotted against design velocity. The energy consumption is normalized with the energy consumption of the CC300 at 30 knots.

5.4.3 Hydrogen Powered Concept

The result for the hydrogen powered ferry is similar to the battery powered ferry: nothing large is won by decreasing the speed of the ferry. This can be seen in figure 5.7 and 5.8. The first figure shows that the resistance at 30 knots is roughly 60% higher than the resistance at 20 knots. But the travel time at 20 knots is 50% higher than at 30 knots. So the combined result, the energy consumption, is not so much lower, as seen in the latter figure.

By decreasing the speed, the energy consumption can be lowered from around 8% lower than that the current CC300 to 18% lower. Based on the difference in costs, a reduction of 10% to 70% is required, so even at a lower speed, the costs might still be higher. Charging this to the passengers would not be welcome, because in this case the higher price would be accompanied with a significantly longer travel time.

So this analysis also shows that the speed is not the real problem, as the impact on energy consumption is only minor.
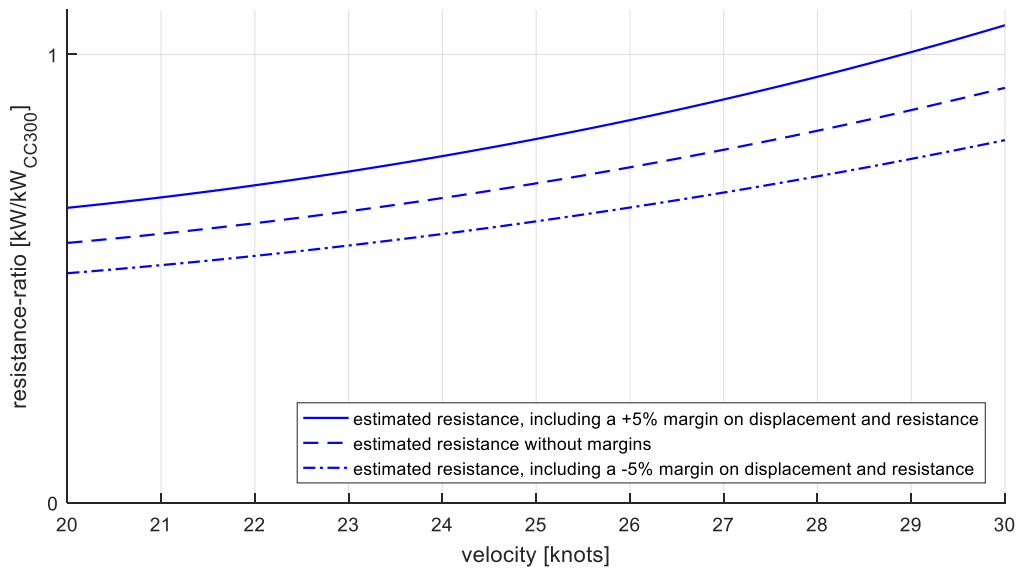
Figure 5.7: estimated resistance of the 46.5 m long carbon composite hydrogen powered concept ferry plotted against design velocity. The resistance is normalized with the resistance of the CC300 at 30 knots.

Figure 5.8: estimated energy consumption of the 46.5 m long carbon composite hydrogen powered concept ferry plotted against design velocity. The energy consumption is normalized with the energy consumption of the CC300 at 30 knots.

5.4.4 Conclusion on a Lower Design Speed

If the design transit speed is lowered, the reduction in resistance in roughly proportional to the increase in travel time. Therefore, sailing at a lower speed is not the solution.

5.5 Effect of Operating on a Shorter Crossing

The previous paragraph showed that a lower velocity does not improve the feasibility much, but a shorter crossing might be an improvement. This paragraph will therefore analyse the effect of the crossing distance on the feasibility of the battery powered ferry.

The hydrogen concept will not be analysed in this paragraph, because it is already feasible. It is still desirable to lower the costs of this concept, but because these are mainly related to the difference in fuel price, it does not change much with a varying crossing distance.

Up until now, the analyses were focused on the 25 NM crossing that is highlighted yellow in figure 5.9. A shorter crossing, Shekou – Hong Kong Airport, is indicated in green. It is a 30 minute crossing over a distance of 11 NM, which the ferry makes 14 times per day [101]. Assuming the same time in the harbour (10 minutes [subparagraph 3.2]), leaves 20 minutes to make the crossing, which requires a speed of 33 knots:

$$\frac{11\ [NM]}{20\ [minutes]}/60\left[\frac{minutes}{hour}\right] = 33\ knots$$

Figure 5.9: the ferry lines from and to Shekou Ferry Terminal, Shenzhen, China. [23]
The case study route 'Shekou – Zhuhai' is highlighted in yellow, and
the shorter route 'Shekou – Hong Kong Airport' is indicated in Green.

5.5.1 Estimation Method

Because the speed is slightly higher, the resistance will be slightly higher as well. Estimating this can be done in the same way as was done in the previous paragraph, but instead of varying the speed between 20 and 30 knots, it is fixed at 33 knots. The travel time is also constant (20 minutes: $t_t = 1/3$ hour).

5.5.2 Target Energy Consumption Ratio

The target energy consumption ratio might change, as the way it is determined in paragraph 3.6 is valid for the 50 minute crossing, for which the following relation was used:

$$E_{1c} \approx \frac{P_i}{1.15 \times 93\%} \times \left(\frac{50\,[minutes]}{60\,[minutes/hour]} \right) = 0.8\,[kWh/kW] \times P_i \qquad \text{Ref. (B.39)}$$

In the expression above, it can be seen that energy consumption is directly proportional to travel time, thus the following expression can be used:

$$E_{1c} \approx \frac{P_i}{1.15 \times 93\%} \times \left(\frac{20\,[minutes]}{60\,[minutes/hour]} \right) = 0.3\,[kWh/kW] \times P_i \qquad (5.5)$$

This means that the investment costs of the battery powered vessel ($\mathcal{C}_{i_{ESS}}$) is lower, while the cost for the diesel powered vessel ($\mathcal{C}_{i_D}$) remain the same:

$$\mathcal{C}_{i_D} = 0.2\,[\text{k€/kW}] \times P_i \qquad \text{Ref. (3.6)}$$

$$\mathcal{C}_{i_{ESS}} = (0.1 + 0.3)\,[\text{k€/kW}] \times P_i + 0.5\,[\text{k€/kWh}] \times \frac{E_{1c}}{50\%\,[DOD]} \qquad \text{Ref. (3.7)}$$

$$= 0.7\,[k€/kW] \times P_i$$

It also means that the operational costs are different, because the total energy consumption over the five year period is different (it was '$14 \cdot 10^3\,[kWh/kW] \times P_i$' in paragraph 3.6):

$$E_{total} = 5\,[years] \times 14\,[crossings/day] \times 350\,[day/year] \times E_{1c} \qquad (5.6)$$

$$\approx 7.4 \cdot 10^3\,[kWh/kW] \times P_i$$

The total energy consumption changes the operational costs over the five year period, for diesel powered and battery powered vessel respectively:

$$\mathcal{C}_{o_D} = \{0.09\text{-}0.14\}\,[\text{€/kWh}] \times E_{total} \qquad \text{Ref. (3.10)}$$

$$= \{0.7\text{-}1.0\}\,[k€/kW] \times P_i$$

$$\mathcal{C}_{o_{ESS}} = \{0.02\text{-}0.06\}\,[\text{€/kWh}] \times E_{total} \qquad \text{Ref. (3.11)}$$

$$= \{0.1\text{-}0.4\}\,[k€/kW] \times P_i$$

As a result the total costs are different as well, for diesel powered and battery powered vessel respectively:

$$\mathcal{C}_D = \mathcal{C}_{i_D} + \mathcal{C}_{o_D} = (0.2 + \{0.7\text{-}1.0\})\,[k€/kW] \times P_i = \{0.9\text{-}1.2\}\,[k€/kW] \times P_i \qquad (5.7)$$

$$\mathcal{C}_{ESS} = \mathcal{C}_{i_{ESS}} + \mathcal{C}_{o_{ESS}} = (0.7 + \{0.1\text{-}0.4\})\,[k€/kW] \times P_i = \{0.8\text{-}1.1\}\,[k€/kW] \times P_i \qquad (5.8)$$

The new target ratio turns out to be the same as the original ratio:

$$\frac{\mathcal{C}_{ESS}}{\mathcal{C}_D} < 1.0 \rightarrow \frac{E_{ESS}}{E_{CC300}} \approx \frac{P_{i,ESS}}{P_{i,CC300}} < \frac{\{0.9\text{-}1.2\}\,[k€/kW]}{\{0.8\text{-}1.1\}\,[k€/kW]} = \{0.8\text{-}1.5\} \qquad (5.9)$$

For the 25 NM crossing, the maximum energy consumption ratio was determined to be 1.2, based on available space in the hull of the 39.5 m version of the concept. At the shorter distance, the energy consumption is lower, thus the ratio is higher:

$$\frac{E_{ESS}}{E_{CC300}} < 2.5$$

5.5.3 Analysis of the Battery Powered Ferry on the Crossing Shekou – Hong Kong Airport

The result of the estimation for the 'Shekou – Hong Kong Airport'-crossing can be seen in table 5.7. The largest difference with the estimation for the 25 NM crossing is that this time, all estimations did converge to a result. Furthermore, there are now multiple possible financially feasible solutions, as indicated in the table in orange.

One option, the aluminium version with 39.5 m length, has crossed-out values. This is because the energy consumption is slightly too high, i.e. the battery system does not fit within the hull of the vessel.

So in case of the battery powered concept, an 11 NM crossing at a 33 knots speed has a higher feasibility than a 25 NM crossing at a 30 knots speed. This shows that not the speed, but the distance is the main problem for a battery powered fast ferry.

Table 5.7: comparison between the Coastal Cruiser 300 and the battery powered ferry with an aluminium structure, a CFRP structure, equal hull length and a longer hull. For financial feasibility, the cost ratio should be smaller than 1.0. The results are for the shorter route (Shekou – Hong Kong Airport, 30 minutes, 11 NM [101]).

	$L = L_{CC300} = 39.5\ m$ Aluminium structure			$L = 46.5\ m$ Aluminium structure		
Displacement margin	-5%	0%	+5%	-5%	0%	+5%
Resistance margin	0%	0%	+5%	0%	0%	+5%
$\dfrac{\Delta_{cat,ESS}}{\Delta_{cat,CC300}}$	1.4	1.6	~~2.1~~	1.3	1.4	1.7
$\dfrac{R_{ESS}}{R_{CC300}} \approx \dfrac{E_{ESS}}{E_{CC300}}$	1.6	1.8	~~2.5~~	1.3	1.4	1.7
Costs ratio $\left(\dfrac{\cent_{ESS}}{\cent_D}\right)$	1.1-1.9	1.3-2.3	~~1.8-3.2~~	0.9-1.6	1.0-1.7	1.2-2.1

	$L = L_{CC300} = 39.5\ m$ CFRP structure			$L = 46.5\ m$ CFRP structure		
Displacement margin	-5%	0%	+5%	-5%	0%	+5%
Resistance margin	0%	0%	+5%	0%	0%	+5%
$\dfrac{\Delta_{cat,ESS}}{\Delta_{cat,CC300}}$	1.2	1.3	1.6	1.1	1.2	1.4
$\dfrac{R_{ESS}}{R_{CC300}} \approx \dfrac{E_{ESS}}{E_{CC300}}$	1.3	1.5	1.9	1.1	1.2	1.4
Costs ratio $\left(\dfrac{\cent_{ESS}}{\cent_D}\right)$	0.9-1.6	1.0-1.8	1.3-2.4	0.7-1.4	0.8-1.5	0.9-1.8

5.5.4 Analysing Varying Distance at the Design Speed

Energy consumption can be plotted against crossing distance, which is done in figures 5.10 to 5.13 for the design speed of 30 knots. The graphs are created using the previously discussed estimation methods.

The blue energy consumption curves are in line with what is expected. A shorter distance requires less energy, thus a smaller battery system, which results in a lighter ship with less resistance, which further reduces the energy consumption.

The blue curves also clearly show where the process diverges, as the energy consumption goes up almost vertically at some point. For the 39.5 m long aluminium catamaran, the maximum distance that the vessel can operate on is somewhere between 16 and 23 NM. Using CFRP as construction material shifts this limit to somewhere between 18 and 25 NM. The figures also show that elongating the hull has more effect than making the structure lighter, as the divergence distance of the 46.5 m long aluminium catamaran lies beyond 23 NM.

The available space onboard of the vessel limits the available energy capacity of the battery system. This is indicated by the red dotted curve in the figures. Note that the y-axis of the figures is a ratio: the energy consumption of the electric ferry is normalized with the energy consumption of the diesel powered ferry sailing the same distance. The available energy capacity of the vessel is thus also normalized with the diesel energy consumption. Therefore the red dotted curve goes down if the crossing distance increases, e.g. at 31 NM distance, the battery capacity equals the diesel energy consumption, thus the red dotted curve is 1.0 at that point. In case of the elongated version, more space is available, thus the red dotted curve is shifted upwards. The available space limits the crossing distance on which the battery powered ferry can operate. This can be seen in the figures at the locations where the red dotted curve intersects a blue curve.

The figures also show that for crossings shorter than 13 NM, every concept is feasible when the design speed is 30 knots. In case of the carbon composite ferry with elongated hull, every crossing shorter than 24 NM is possible at 30 knots. Comparing the blue curves with the black dotted lines also gives an indication if the electric version is cost competitive with the diesel powered version.

The figures also explain the previous results. The 25 NM crossing can only be reached with the elongated hull, as the resistance of the "normal" version increases too fast with a growing design distance. In case of the elongated carbon composite version, it can be seen in figure 5.13 that with positive margins (the solid blue curve), the required energy at 25 NM is larger than what fits in the vessel (red dotted curve). This was already seen in table 5.3 (page 58, subparagraph 5.2.4), where the values where crossed-out.
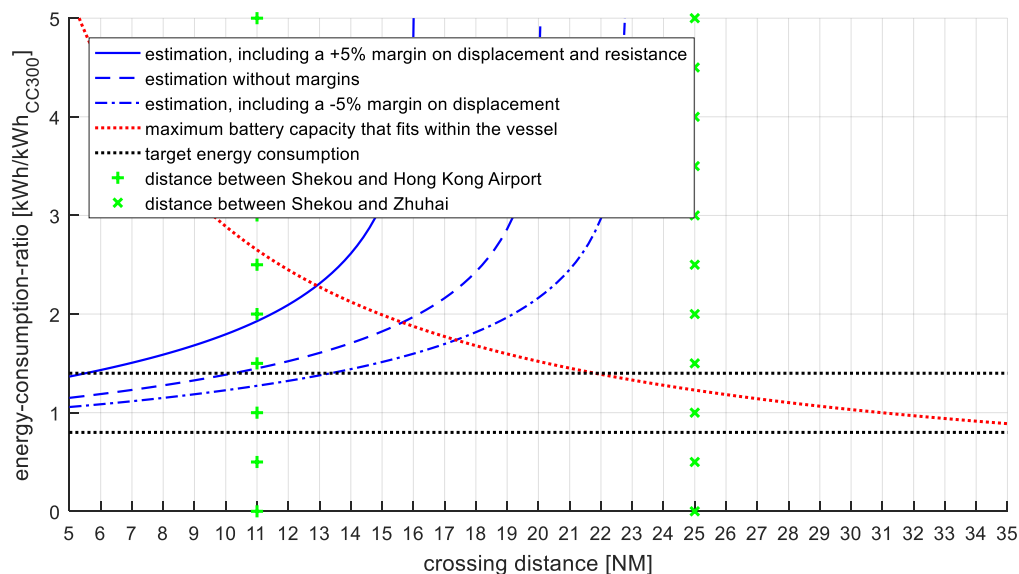
Figure 5.10: estimated energy consumption of the 39.5 m long aluminium battery powered concept ferry plotted against design crossing distance. The energy consumption is normalized with the energy consumption of the CC300 sailing that same distance. The design speed is 30 knots.
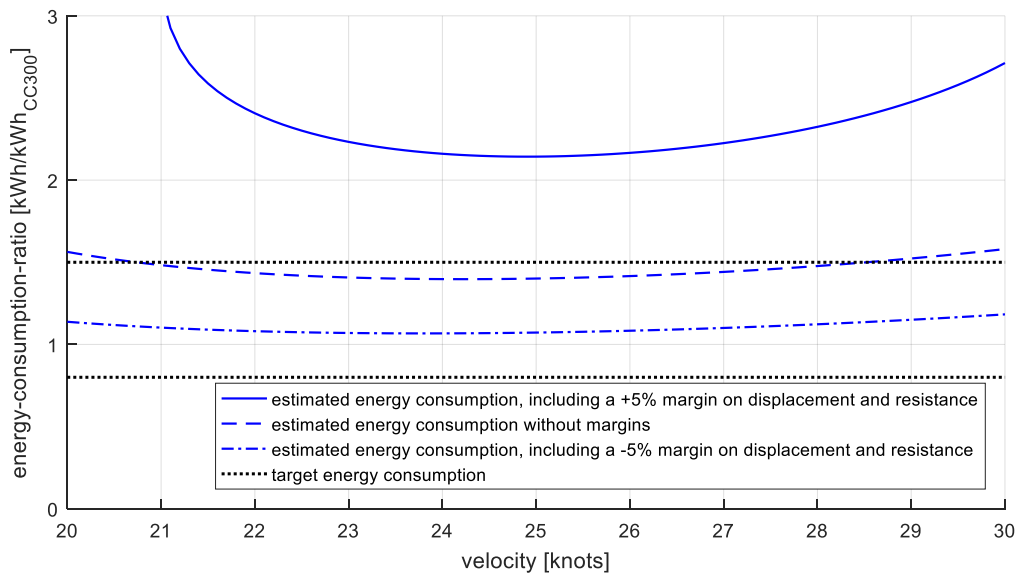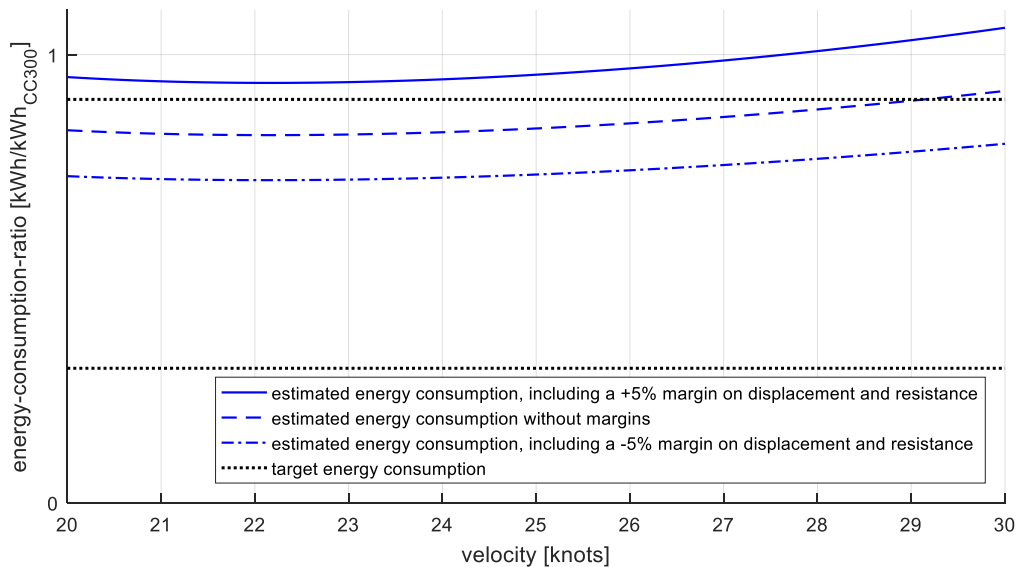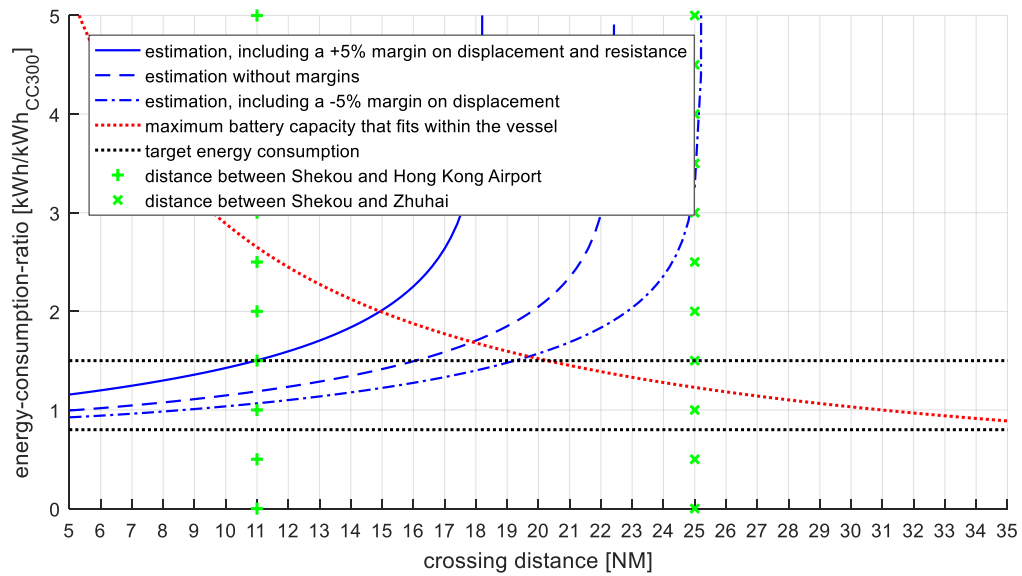
Figure 5.11: estimated energy consumption of the 39.5 m long carbon composite battery powered concept ferry plotted against design crossing distance. The energy consumption is normalized with the energy consumption of the CC300 sailing that same distance. The design speed is 30 knots.
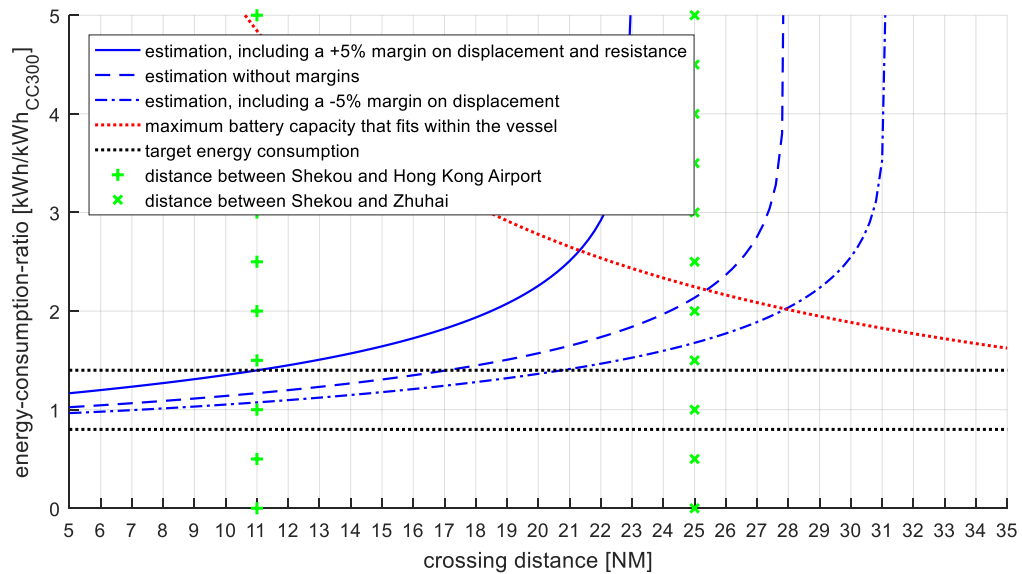
Figure 5.12: estimated energy consumption of the 46.5 m long aluminium battery powered concept ferry plotted against design crossing distance. The energy consumption is normalized with the energy consumption of the CC300 sailing that same distance. The design speed is 30 knots.
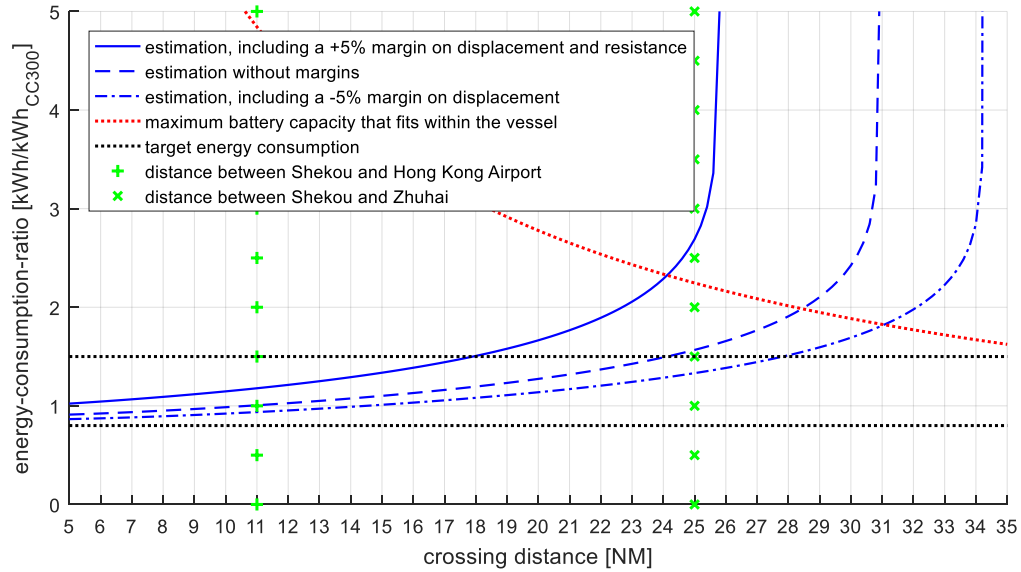
Figure 5.13: estimated energy consumption of the 46.5 m long carbon composite battery powered concept ferry plotted against design crossing distance. The energy consumption is normalized with the energy consumption of the CC300 sailing that same distance. The design speed is 30 knots.

5.5.5 Conclusion on Operation on a Shorter Crossing

The shorter the crossing, the higher the feasibility of the battery powered ferry, as a shorter distance requires less energy, thus a smaller battery system, which results in a lighter ship with less resistance, which further reduces the energy consumption.

The available space onboard limits the operational distance, but because of the uncertainties, there is no hard limit, as seen by the three blue curves with different margins. It can be said that the 25 NM crossing is on the edge of feasibility in case of the battery powered concept, in other words: for short crossings, roughly below 25 NM, the battery powered ferry can be a feasible concept.

5.6 Preliminary Conclusions

In this chapter, different ways of reducing the energy consumption where analysed, in order to answer the following question:

How can the energy consumption of the electric concept ferry be reduced,
and what is the effect on the feasibility?

The short answer is, when looking at changes to the design:

Feasibility can be increased by elongating the concept vessel and by reducing the structural weight.
In case of the battery powered concept, feasibility can only be achieved with an elongated hull, and
future improvements will significantly improve its feasibility.

The short answer is, when looking at changes to the operational profile:

Reducing the design speed has little effect on the energy consumption,
but reducing the crossing's distance significantly increases the feasibility.

5.6.1 Battery Powered Catamaran

Reaching the other side of the 25 NM crossing is only possible with an elongated hull, in case of the battery powered catamaran. For the original hull length, the iteration process diverges and no feasible solution exists, independent of the structural material. Looking at costs, the battery powered ferry is likely to be more expensive than the diesel powered ferry, but this depends on the electricity price and diesel fuel price.

If the battery performance improves in the future, the feasibility increases. If battery cells would have a specific energy of 1,000 Wh/kg, feasibility exists for all estimations, with a strong indication that operating on batteries is cost competitive with operating on diesel fuel. Furthermore, it might even be possible to convert existing vessels to battery powered ferries in the future.

Decreasing the design speed does not significantly reduce energy consumption, as the reduction in resistance is roughly proportional to the increase in travel time. Furthermore, without changing the timetable, the charging time at quay gets smaller if the travel time increases, making this option not feasible.

Operating on a shorter distance increases the feasibility. It can be advised to consider a battery powered ferry for short crossings, roughly shorter than 25 NM.

5.6.2 Hydrogen Powered Catamaran

For the hydrogen powered ferry, all analysed concepts are feasible, but all are more expensive than the diesel powered ferry. The same is true in the future, when the fuel cell performance has improved.

Lowering the design speed also has little effect on the costs of the hydrogen powered ferry, for the same reason as it has little effect for the battery powered ferry.

Changing the design crossing's distance also does not have any significant impact on the total costs of the hydrogen powered ferry in comparison to the diesel powered ferry.

For the case study crossing of 25 NM, the hydrogen powered version is likely to be the better choice, as the battery powered version is on the edge of feasibility. So it can be advised to consider a hydrogen fuel cell powered ferry for long crossings, roughly longer than 25 NM.

As mentioned before, costs is not the most important aspect of this analysis. The reduction in pollution, and all other negative effects of emissions, might be worth the extra costs. Because the costs of the hydrogen powered ferry are likely to be higher than that of the battery powered version, it makes sense to only consider hydrogen for distances beyond 25 NM, which cannot be reached by the battery powered version.

6

Analysis of a Hydrofoil Supported Concept Catamaran

From the previous chapter follows that on the 25 NM crossing, a battery powered catamaran is on the edge of feasibility, i.e. it might not be feasible. So a more extreme reduction in resistance is required. The hydrogen powered ferry is feasible, but due to the cost increase, it would also benefit from a more severe resistance reduction.

Looking at fast ferries, multiple vessels operate on hydrofoils, because these underwater wings can result in a significantly lower resistance. The Norwegian start-up company Flying Foil also plans to have its first battery powered ferry operational in 2022, and it will be a hydrofoil supported catamaran that can reach 35 knots [14]. This raises the following question:

How much can a hydrofoil system reduce the resistance
and energy consumption of the electric concept ferry?

Structure of this Chapter
Paragraph 6.1 will first explain the basics of hydrofoils. The concept design of the hydrofoil system can be found in **paragraph 6.2**. The estimated resistance and energy consumption is discussed in **paragraph 6.3**, in which the estimation method is explained first. **Paragraph 6.4** contains the conclusions on hydrofoils.

6.1 Basics of Hydrofoils

A hydrofoil is an underwater wing that generates lift when it moves through the water. The faster it goes, the higher the lift, and a larger part of the vessel rises above the water. If the hull of the vessel is completely out of the water, the vessel is fully foilborne. If the hull is no longer in the water, the resistance is much lower. Besides lowering the resistance, foilborne vessels can also have better seakeeping characteristics, create a smaller wash, and experience less speed variations due to incident waves [100].

An example of a hydrofoil catamaran is the Foilcat, which is seen in fully foilborne condition in figure 6.1. The 35 m long Foilcat has a 378 passenger capacity and a maximum speed of 45 knots [102]. One of the advantages of a catamaran over a monohull, in case of hydrofoil vessels, is the absence of the resistance hump [100], which is illustrated by Van Walree in figure 6.2.

An important reason hydrofoil vessels are not dominating the maritime world, are the higher costs associated with these ships. The complexity of the system increases the initial investment. Furthermore, frequent maintenance is required, in order to keep the hydrofoil surfaces smooth enough, which is important when looking at lift, drag and cavitation [100].

Figure 6.1: Foilcat, a hydrofoil catamaran, in fully foilborne [102] condition.
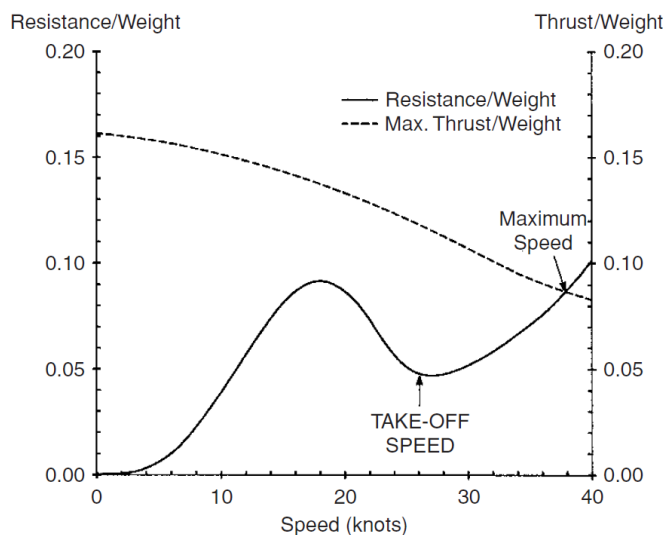
Figure 6.2: illustration of the resistance hump of a [100] monohull hydrofoil vessel.

6.1.1 Hydrofoil System Configuration

In general, a hydrofoil system consists of two or more hydrofoils, each connected to the hull by one or more struts. The hydrofoils can be either free-surface piercing or fully submerged. This is illustrated in figure 6.3.

Free-surface piercing systems are self-stabilizing with respect to vertical position, heel and trim [100]. A fully submerged hydrofoil systems require active control mechanisms to keep the vessel in balance, but they are more efficient. Controlling fully submerged hydrofoils is possible with flaps, similar to how airplanes are controlled. The Foilcat is also equipped with fully submerged hydrofoils, as seen in figure 6.1.
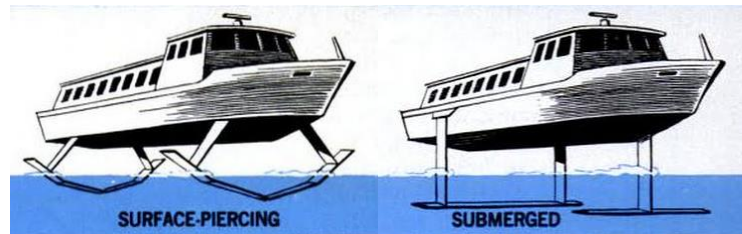
Figure 6.3: illustration of the two main hydrofoil types, free-surface piercing (on the left) and fully submerged (on the right).

© R. Pioch, *Popular Science*, vol. 202, nr. 4, 1973

6.1.2 Main Particulars of a Hydrofoil

A rectangular foil has three main dimensions: span (s), chord length (c) and thickness (t). These dimensions can be seen in figure 6.4. The planform area (A) is the projected area of a wing, which is the span times the chord length, in case of a rectangular shaped foil:

$$A = s \cdot c \qquad\qquad\qquad (\ 6.1 \ )$$

The aspect ratio (AR) can be seen as the slenderness ratio of a foil. It is in this case the span divided by the chord length:

$$AR = \frac{s}{c} \qquad\qquad\qquad (\ 6.2 \ )$$
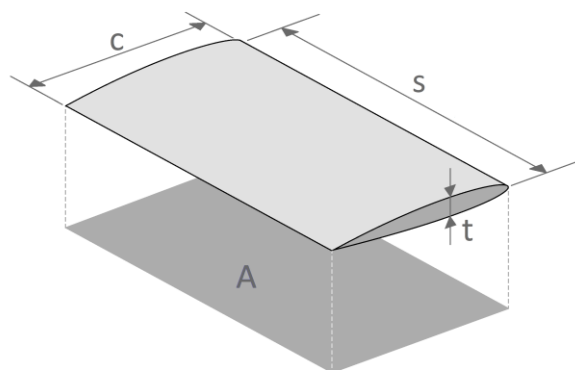
Figure 6.4: illustration of the main dimensions of a hydrofoil. Indicated are the chord length (c), span (s), thickness (t) and planform area (A).

6.1.3 Lift and Drag Characteristics of a Hydrofoil

A hydrofoil generates a force when it is subjected to a fluid flow. This force can be split into lift (perpendicular to the free-stream flow), and drag (parallel to the flow). This is illustrated in figure 6.5. The letters L and D are used to indicate lift and drag respectively, but because these letters are also used

to indicate the length and draft of the ship, F_L and F_D will be used in the remainder of this thesis to indicate lift and drag.

The equations for lift and drag are similar to each other; both are a function of a coefficient (C_L and C_D respectively), the fluid density (ρ), the velocity of the vessel (V), and the planform area of the foil or wing (A):

$$F_L = C_L \cdot \tfrac{1}{2}\rho V^2 \cdot A \qquad\qquad (\;6.3\;)$$

$$F_D = C_D \cdot \tfrac{1}{2}\rho V^2 \cdot A \qquad\qquad (\;6.4\;)$$
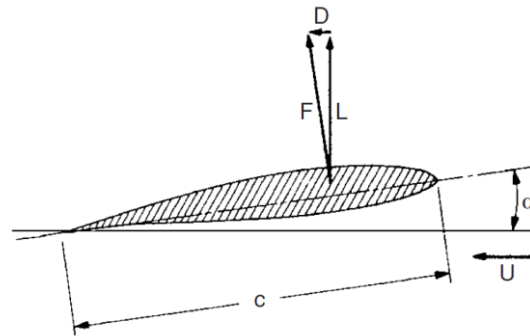
Figure 6.5: foil-profile with chord length c, positioned   [100]
in a fluid flow with velocity U, under an
angle of attack α. As a result, a force (F) is
generated, which can be split into lift (L)
and drag (D).

Figure 6.6 shows the typical characterises of a wing: lift coefficient (C_L), drag coefficient (C_D) and their ratio (L/D), as function of angle of attack (α, indicated in figure 6.5).

It is desirable to have a lift coefficient that is as high as possible, while at the same time the drag coefficient should be as low as possible. In other words: the lift/drag-ratio should be as high as possible, e.g. in figure 6.6, the optimum is $L/D = 32$, at an angle of attack close to zero degrees.

The highest achievable lift for the wing of figure 6.6 is more than 1.6, for an angle of attack of slightly above 16 degrees. This is however the start of stalling and this point should be avoided. Stalling is a condition where separation occurs in the flow around the foil. As a result the lift drops and the resistance increases.

Cavitation
Cavitation can occur because the working of a foil is based on a pressure difference, similar to the blades of a propeller. Water vapor is created in a region where the pressure is lower than the vapor pressure. If these vapor bubbles get into a region with a higher pressure, they collapse. The creation and collapsing of these vapor bubbles is called cavitation. The negative effects of this phenomenon are noise, vibrations and damage, as well as a lower efficiency of the hydrofoil.

Cavitation limits the speed of a hydrofoil vessel to around 50 knots, and above this speed supercavitating hydrofoils must be used to prevent cavitation damage [100]. According to Hoerner et al., cavitation becomes a problem for speeds in excess of 35 knots [103]. Because the design speed of the electric ferry is lower (30 knots), it is assumed that cavitation is not a problem.

3D and Interference Effects
Each foil-profile has its own characteristics, similar to the one as seen in figure 6.6. These coefficients are the free-stream characteristics of a two-dimensional foil, meaning: a foil with an infinite span placed in an empty infinite fluid. These values are not representative for a real hydrofoil. This is due to 3D and interference effects. In general, the larger the hydrofoil, the larger these effects. The three main factors that influence lift are the following:
  - Finite aspect ratio;

- Presence of the water surface;
- Disturbance to the inflow of the aft foil, due to the presence forward foil.

The specified drag coefficient is only the parasitic drag coefficient, which is related to the pressure distribution over the foil. There are more components that have to be take into account:

- Friction drag;
- Induced drag;
- Wave making drag;
- Interference drag;
- Spray drag.

Appendix C.2 describes how the magnitude of the lift is determined, and appendix C.3 contains information on the determination of the drag of the hydrofoil system.
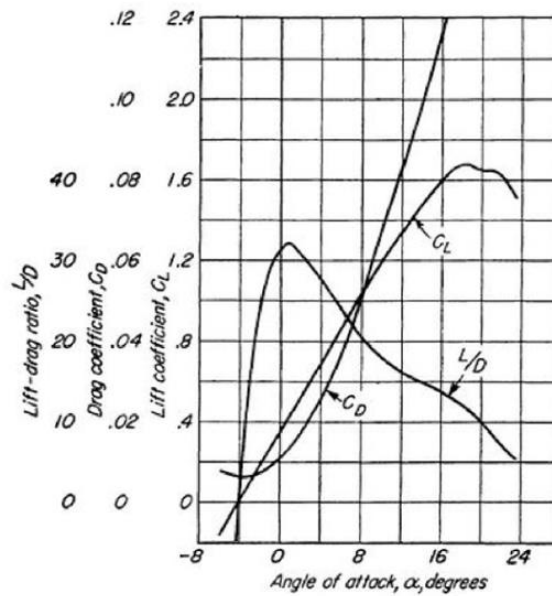
Figure 6.6: typical characteristics of a wing.   [104]

6.2 Concept Design of the Hydrofoil System

Before estimating the resistance of the electric hydrofoil vessel, a concept design has to be made. Especially the size of the system is important for determining the resistance.

6.2.1 Hydrofoil Type, Foil Submergence and Strut Height

The concept will be equipped with fully submerged hydrofoils, because they have a higher efficiency than surface piercing foils. The system consists of two foils, a forward foil and aft foil, and each carries 50% of the weight.

For a higher efficiency, the foil submergence should be as large as possible. However, a larger submergence does require larger struts, which has a negative effect on the resistance, as well as on the weight of the system. Furthermore, the submergence might be limited by other factors, such as the water depth. For the concept ferry, a hydrofoil submergence in fully foilborne condition of 2.5 m is chosen, which is based on the Foilcat [102].

The hull of the vessel will be lifted to 0.9 m above the waterline, which leads to a total hydrofoil system height of 3.4 m. The hull draft of the Coastal Cruiser 300 is 1.3 m [15], so the total hull borne draft would be 4.7 m, the same hull borne draft as the Foilcat [102]:

$$1.3 \ [m \ hull \ draft] + 3.4 \ [m \ hydrofoil \ system \ height] = 4.7 \ m$$

6.2.2 Hydrofoil Span, Chord Length and Thickness

Because a higher aspect ratio leads to a higher efficiency, the span must be as large as possible, but not wider than the overall beam of the vessel: $s \leq B_{oa} = 10 \ m$. The effective span is lower, as no lift is generated at the strut-foil connection points. Therefore a span of 9 m is assumed. Because the span is fixed, the chord length can be directly related to the planform area:

$$c = \frac{A}{s}, \qquad with \ s = 9 \ m \hspace{4cm} \text{Ref. (C.16)}$$

The chord length cannot be determined beforehand, as the required planform area is determined by the lift that the foils have to generate, the speed at which they operate, and the lift coefficient, as seen in equation C.4.

$$A = \frac{F_L}{C_L \cdot \frac{1}{2}\rho V^2} \hspace{5cm} \text{Ref. (C.4)}$$

The free-stream lift coefficient is a property of the foil profile. NACA profiles are commonly used for hydrofoils [100], as these profiles are extensively tested. Looking at the characteristics of different profiles [105], a lift and drag coefficient of respectively 0.8 and 0.01 are common numbers. A lift coefficient of 1.0 is achievable, but around 20% has to be reserved in order to control trim for example [100].

According to Faltinsen [100], the pressure distribution over a hydrofoil should be relatively flat, as large suction peaks increase the risk of cavitation. An example of such a foil is the NACA 64 series [100]. The NACA 64_1-212 is one of the profiles in this series, and it has, at an angle of attack of around 6°, the same characteristics as mentioned above: a lift and drag coefficient of respectively 0.8 and 0.01 [105].

The thickness of the hydrofoil has a fixed ratio with its chord length. The ratio is determined by the foil profile, and in case of the NACA 64_1-212 the thickness is 12% of the chord length: $t/c = 0.12$.

6.2.3 Propulsion System

Many hydrofoil vessels use waterjet propulsion. Like the Coastal Cruiser 300, the Foilcat is a catamaran with waterjet propulsion. Operating on hydrofoils has an impact on the performance of the propulsion system. This subparagraph discusses how that is taken into account.

Waterjet

When the vessel is fully foilborne, the hull is no longer in contact with the water. This means that the inlet duct of the waterjet has to be altered. In general, the inlet is located at the same depth as the hydrofoils, and the inlet duct goes through a strut. This means that the waterjet system becomes less efficient, as more energy is required to get water into the pump section of the waterjet. An illustration of the situation can be seen in figure 6.7.
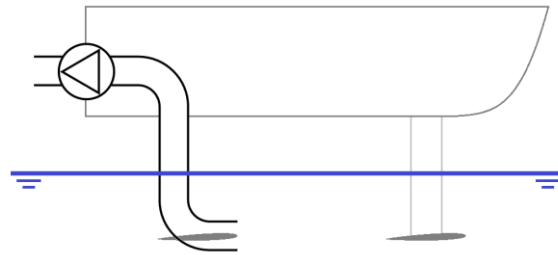
Figure 6.7: illustration of a waterjet system in a hydrofoil vessel. The inlet duct now consists of two 90° bends and a vertical part in between.

The required amount of additional power can be estimated by looking at the theory for pipe flow systems, where the required pump power is a function of pressure difference and volume flow [106]:

$$P = \Delta p \cdot Q \tag{6.5}$$

Pressure difference (Δp) is in this case is the loss in the intake of the waterjet. The two main components of the pressure difference are the height difference (Δz) and the two 90 degree bends:

$$\Delta p_{loss} = \Delta p_{loss,height} + 2 \times \Delta p_{loss,bend} \tag{6.6}$$

The pressure difference due to the height can be calculated with the following formula [106]:

$$\Delta p_{loss,height} = \rho g \Delta z \tag{6.7}$$

As mentioned in subparagraph 6.2.1, the foil system height is 3.4 m, so the pressure difference due to height is 34 kPa:

$$\Delta p_{loss,heigth} = \rho g \Delta z = 1{,}025 \cdot 9.81 \cdot 3.4 = 34 \, kPa$$

The pressure loss in a bend can be calculated with the following formula [106]:

$$\Delta p_{loss,bend} = \zeta \cdot \tfrac{1}{2}\rho V^2 \tag{6.8}$$

The resistance factor (ζ) of a 90 degree bend is roughly 0.4 [106]. Based on the available data [107], the volume flow (Q) is estimated to be 5 m³/s. Combined with an inlet duct diameter of 0.75 m [108] results in a flow velocity (V) of 11 m/s:

$$V = \frac{Q}{A} = \frac{Q}{\frac{\pi}{4}D^2} = \frac{5}{\frac{\pi}{4} \cdot 0.75^2} = 11 \, m/s \qquad\qquad (6.9)$$

The pressure loss that follows from this is 25 kPa:

$$\Delta p_{loss,bend} = \zeta \cdot \tfrac{1}{2}\rho V^2 = 0.4 \times \tfrac{1}{2} \cdot 1{,}025 \cdot 11^2 = 25 \, kPa$$

So the total pressure loss is estimated to be 84 kPa (as calculated with equation 6.6):

$$\Delta p_{loss} = \Delta p_{loss,height} + 2 \times \Delta p_{loss,bend} = 34 \, [kPa] + 2 \times 25 \, [kPa] = 84 \, kPa$$

The additional required power that follows from this pressure loss is 420 kW (as calculated with equation 6.5):

$$P_{loss} = \Delta p_{loss} \cdot Q = 84 \, [kPa] \cdot 5 \, [m^3/s] = 420 \, kW$$

This means that the engines need to deliver roughly 30% more power to overcome the losses [15]:

$$\frac{1{,}440 + 420 \, [kW]}{1{,}440 \, [kW]} = 1.3$$

The efficiency of the waterjet is in the order of 70% [107]. This efficiency drops to around 54% in case of a fully foilborne ship:

$$\eta_{waterjet} = \frac{70\% \, [hull \, borne \, efficiency]}{1.3 \, ["power \, ratio"]} = 54\%$$

This low propulsion efficiency makes the waterjet not the best option for the hydrofoil powered catamaran. Another drawback related to this is the strut size; in order to house the inlet duct, larger struts are required, which also increase the resistance.

For higher speeds, e.g. 45 knots instead of 30 knots, the required propulsion power is much higher, while the required power to move the water through the suction line is not significantly higher [107]. Thus the efficiency goes up if the speed increases. At these higher speeds, a waterjet is generally also more efficient than a propeller. Therefore a waterjet is suitable for faster hydrofoil vessels such as the Foilcat, but not for the electric version of the Coastal Cruiser 300.

Propeller

In this thesis, the hydrofoil concept will be propelled by propellers instead of waterjets. Their efficiency at 30 knots is in the order of 65% [103], which is much higher than that of the waterjet. Johnston also states that below 40 knots, the sub-cavitating propeller is by far the most efficient device for producing thrust, with efficiencies up to 0.8 [109]. An example of a hydrofoil propelled catamaran is the Foilcat 2900, a vessel with a 140 passenger capacity and a service speed of 45 knots [110]. Be aware that this Foilcat 2900 is a different vessel than the Foilcat (without '2900') as mentioned before.

The high propeller efficiency applies to hydrofoil vessels, where propellers operate close to open water conditions, as they are not located in the wake of the ship. Furthermore, because the hydrofoil struts act as rudders, no additional appendages are required that would decrease the overall efficiency of a propeller propelled ship. Compared to a waterjet propelled hydrofoil vessel, the struts can even be smaller, because the propeller drive shaft diameter is a lot smaller than the waterjet inlet duct diameter.

This means that the resistance is also slightly lower, when comparing the propeller vessel with the waterjet vessel.

The shaft will go vertical through the strut, while the propeller shaft is orientated horizontally. So a gear is required, which means some additional losses have to be taken into account. Therefore, 60% propulsion efficiency can be assumed, which is still higher than the efficiency of the waterjet.

A disadvantage of propeller propulsion in a hydrofoil system, is the risk it brings with it. Both hydrofoil system and propulsion system are susceptible for critical failure due to a collision, for example with debris.

6.2.4 Number of Struts and Strut Dimensions

When looking at resistance, the number of struts should be as small as possible. When looking at struts from a structural point of view, the number might be higher. Taking both into account has led to three struts per foil. A similar design can be seen in figure 6.8, which shows the aft hydrofoil system of the Jetfoil, a hydrofoil supported monohull from the airplane manufacturer Boeing. This figure shows that the outward struts have a similar size as the hydrofoil, but the middle strut is a lot larger to support the waterjet intake.
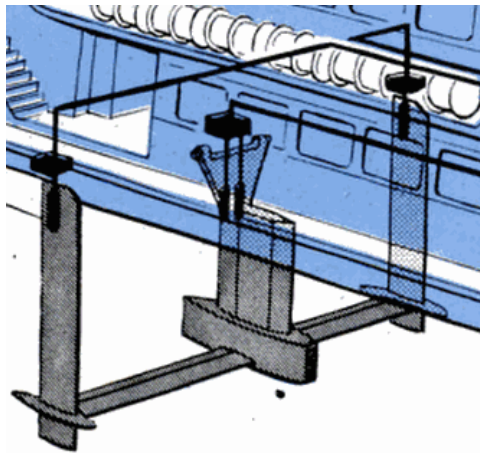
© R. Pioch, *Popular Science*,
Figure 6.8: aft hydrofoil system of the Boeing Jetfoil.   vol. 202, nr. 4, 1973

For the concept ferry, the chord length and thickness of the struts is equal to the hydrofoil that they support, as this is in line with existing hydrofoil vessels such as the Boeing Jetfoil from figure 6.8.

The two struts that also support the propulsion system might be larger, because their thickness should at least be thick enough to support the drive shaft of the propeller. The shaft that drives the waterjet in the Coastal Cruiser 300 has a diameter of 130 mm [108]. Doubling this value, to take the shaft bearings into account, as well as a margin, results in 0.3 m. Thus the strut thickness of the propeller supporting aft struts ($t_{strut_{aft}}$) is equal to the foil thickness (t), but not smaller than 0.3 m:

$$t_{strut_{aft}} = \max\{t, \quad 0.3\ [m]\} \qquad\qquad (\ 6.10\ )$$

The propulsor supporting struts not only have a minimum thickness, but also a minimum chord length. In this thesis it is 1.2 m, which is four times the minimum thickness. This ratio of four is based on the NACA 2424 airfoil, which has a chord length of four times the thickness, while the parasitic drag coefficient is still similar to that of the hydrofoil and other struts ($C_{D,0} = 0.01$) [104]. Thus the chord length of the propeller supporting aft struts ($c_{strut_{aft}}$) is equal to the foil chord length (c), but not smaller than 1.2 m:

$$c_{strut_{aft}} = \max\{c, \quad 1.2\ [m]\} \qquad\qquad (\ 6.11\ )$$

If instead the same t/c-ratio of 0.12 is used as for the hydrofoil and the other struts, the minimal chord length would be 2.5 m, which is the same as the hydrofoil submergence:

$$\frac{0.3}{0.12} = 2.5 \ m$$

6.2.5 Overview of the Concept Hydrofoil System
Figure 6.9 shows an illustration of the hydrofoil system. The two main components are the (horizontal) hydrofoils and the (vertical) struts.

Hydrofoils
The concept has two hydrofoils in tandem configuration, each carrying half the weight of the vessel. The main parameters of each hydrofoil are the following:
- $C_{L_0} = 0.8$, free stream lift coefficient;
- $C_{D_0} = 0.01$, parasitic drag coefficient;
- $h = 2.5 \ m$, hydrofoil submergence;
- $s = 9 \ m$, span;
- c, chord length;
- $t = [t/c] \cdot c$, thickness ($t/c = 0.12$);

Struts
Each hydrofoil is supported by three struts. Each strut has the same chord length and thickness as the hydrofoil, except for the two propulsor supporting struts, which have a minimum chord length and thickness of 1.2 m and 0.3 m respectively.
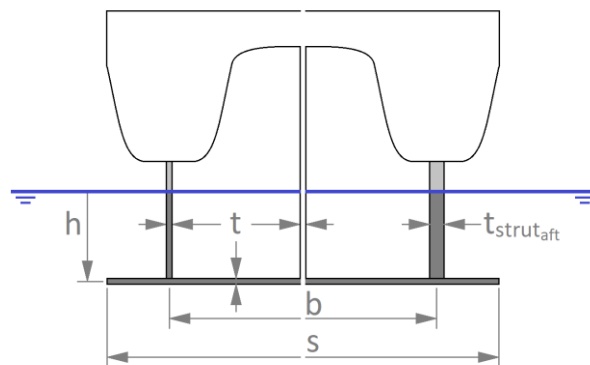
Figure 6.9: front view of the concept hydrofoil system, with
the forward foil on the left and aft foil on the right.

6.3 Resistance Estimation of the Hydrofoil Supported Electric Concept Ferry

Compared to existing hydrofoil vessels, two major differences can be mentioned for the hydrofoil supported version of the electric ferry concept:

- Relatively larger weight;
- Relatively lower speed.

Both these differences require a larger hydrofoil system, which follows from the equation for the lift (equation 6.3):

$$A = \frac{F_L}{C_L \cdot \frac{1}{2}\rho V^2} \sim \frac{\Delta_{\text{cat}}}{V^2} \qquad\qquad (\ 6.12\ )$$

So the hydrofoil system is relatively large, and a larger hydrofoil system has two consequences:

- Larger 3D and interference effects;
- Larger resistance [equation 6.6].

$$F_D = C_D \cdot \frac{1}{2}\rho V^2 \cdot A \qquad\qquad \text{Ref. (\ 6.6\ )}$$

Especially the larger 3D and interference effects pose a problem, because they decrease the effective lift coefficient. This means that an even larger hydrofoil is required which also increases the magnitude of the interference effects. This cycle can be repeated until a break-even point is found, but when the mass is too larger, the process diverges and no feasible solution exists.

6.3.1 Estimation Method

Figure 6.10 presents an overview of the estimation method for determining the drag of the hydrofoil system.
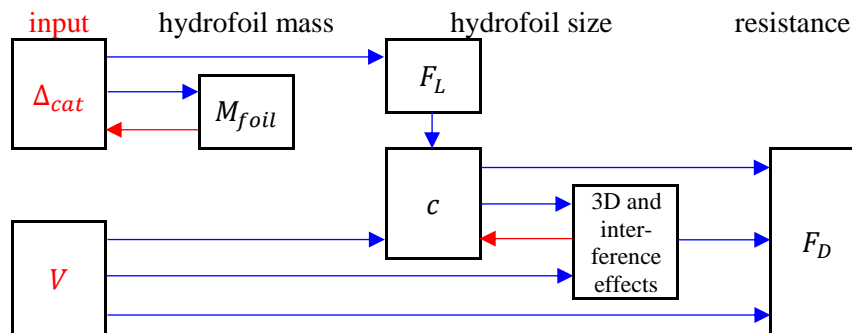
Figure 6.10: overview of the resistance estimation method for the hydrofoil supported
ferry. The arrows indicate how the components are related to each other.

Hydrofoil Mass and Displacement

The first step is estimating the mass of the hydrofoil system (M_{foil}). In this thesis it is estimated based on the displacement of the catamaran (Δ_{cat}), according to equation C.1 [111] from appendix C.1. This is an iterative process, as the mass of the foil system increases the displacement of the vessel.

$$M_{foil} = \left(0.020 + 0.031 \sqrt{\frac{\Delta_{\text{cat}}}{100}} \right) \cdot \Delta_{\text{cat}} \qquad\qquad \text{Ref. (\ C.1\ )}$$

Hydrofoil Size and Effective Lift Coefficient

The weight of the ferry is in balance with the lift (F_L) of the hydrofoil system. This required lift, combined with the velocity of the ship (V) determines the size of the hydrofoil system, which is only determined by the chord length (c), as the span (s) is fixed:

$$c = \frac{A}{s}, \qquad with \ s = 9 \ m \hspace{4cm} \text{Ref. (C.16)}$$

With:

$$A = \frac{F_L}{C_L \cdot ½\rho V^2}, \qquad with: F_L = \frac{\Delta_{cat}}{2} \cdot g \hspace{2.5cm} \text{Ref. (C.4)}$$

Note in equation C.4 that the displacement of the catamaran is divided by two, as each foil carries half the weight.

3D and interference effects influence the lift coefficient of the hydrofoil, and thus the size of the hydrofoil system. The size of the hydrofoil determines the magnitude of the effective lift coefficient, and the effective lift coefficient determines the size of the hydrofoil. Thus determining the size of the hydrofoil system is also an iterative process, as indicated by the red arrow in figure 6.10.

The following equations, derived in appendix C.2, are used to estimate the effective lift coefficient:

$$C_{L,forward} = \min\left\{\left(C_{L_0} \cdot \left[\frac{C_L}{C_{L_0}}\right]_{water\text{-}surface}\right), \quad C_{L,max,forward}\right\} \hspace{1.5cm} \text{Ref. (C.17)}$$

$$C_{L,aft} = \min\left\{\left(C_{L_0} \cdot \left[\frac{C_L}{C_{L_0}}\right]_{water\text{-}surface} \cdot \left[\frac{C_L}{C_{L_0}}\right]_{foil\text{-}foil}\right), \quad C_{L,max,aft}\right\} \hspace{0.8cm} \text{Ref. (C.18)}$$

With:

- $C_{L_0} = 0.8$

- $\left[\dfrac{C_L}{C_{L_0}}\right]_{water\text{-}surface} = \exp(-0.2 \cdot c) \cdot \left(\dfrac{Fn_h}{2}\right)^{c/8}$ \hspace{2cm} Ref. (C.9)

- $\left[\dfrac{C_L}{C_{L_0}}\right]_{foil\text{-}foil} = 0.75$ \hspace{5cm} Ref. (C.7)

- $C_{L,max} = \dfrac{F_L}{½\rho V^2 \cdot A_{min}}$ \hspace{5cm} Ref. (C.15)

  - $A_{min} = s \cdot c_{min}$ \hspace{5.5cm} Ref. (C.14)

  - $c_{min} = \left(\dfrac{1.92}{b} \cdot \sqrt{\dfrac{\sigma}{f}} \cdot \dfrac{t/c}{\sqrt{F_L/s}}\right)^{-3/2}$ \hspace{2.5cm} Ref. (C.13)

It can be noted that the result of equation C.17 and C.18 is the minimum value of two options. That is because the maximum lift coefficient is limited: if it would be too large, the foil size would be too small,

and a too small hydrofoil is not strong enough to carry the weight of the vessel. This is explained in Appendix C.2.4.

Resistance of the Hydrofoil System

The final step is determining the total resistance of the hydrofoil system (F_D), which consists of the following components:

- Friction drag ($F_{D,friction}$);
- Parasitic drag ($F_{D,parasitic}$);
- Induced drag ($F_{D,induced}$);
- Wave making drag ($F_{D,waves}$);
- Interference drag ($F_{D,interference}$);
- Spray drag ($F_{D,spray}$).

The total drag (F_D) can be calculated with the following equations, which follow from appendix C.3:

$$F_D = \left(F_{D_{foil}}\right)_{forward} + \left(F_{D_{foil}}\right)_{aft} + F_{D,interference} + F_{D,spray} \qquad \text{Ref. (C.35)}$$

With:

- $$F_{D_{foil}} = F_{D,friction} + F_{D,parasitic} + F_{D,induced} + F_{D,waves} \qquad \text{Ref. (C.36)}$$

   With:

   ○ $$F_{D,friction} = C_F \cdot \tfrac{1}{2}\rho V^2 \cdot A_{total} \qquad \text{Ref. (C.22)}$$

      ▪ $$C_F = \frac{0.075}{(\log_{10} Rn - 2)^2} \qquad \text{Ref. (B.2)}$$

         * $$Rn = \frac{V \cdot c}{\nu} \qquad \text{Ref. (C.21)}$$

      ▪ $$A_{total_{forward}} = (s + 3 \times h) \cdot c_{forward} \qquad \text{Ref. (C.19)}$$

      ▪ $$A_{total_{aft}} = (s + 1 \times h) \cdot c + (2 \times h) \cdot c_{strut_{aft}} \qquad \text{Ref. (C.20)}$$

         * $$c_{strut_{aft}} = \max\{c, \quad 1.2\ [m]\} \qquad \text{Ref. (6.11)}$$

   ○ $$F_{D,parasitic} = C_{D_0} \cdot \tfrac{1}{2}\rho V^2 \cdot A_{total}, \quad with: C_{D_0} = 0.01 \qquad \text{Ref. (C.23)}$$

   ○ $$F_{D,induced} = C_{Di} \cdot \tfrac{1}{2}\rho V^2 \cdot A \qquad \text{Ref. (C.24)}$$

      ▪ $$C_{Di} = \frac{C_L^2}{\pi \cdot AR} \cdot \left[\frac{AR}{AR_{eff}}\right], \quad with \left[\frac{AR}{AR_{eff}}\right] = 0.6 \qquad \text{Ref. (C.26)}$$

      ▪ $$A = s \cdot c \qquad \text{Ref. (6.1)}$$

   ○ $$F_{D,waves} = C_{Dw} \cdot \tfrac{1}{2}\rho V^2 \cdot A \qquad \text{Ref. (C.27)}$$

      ▪ $$C_{Dw} = 0.5 \cdot \frac{c}{h} \cdot \frac{C_L^2}{F_h^2} \cdot exp\left(\frac{-2}{Fn_h^2}\right) \qquad \text{Ref. (C.28)}$$

- $F_{D,interference} = \sum_{struts} C_{Dt} \cdot \frac{1}{2}\rho V^2 \cdot t^2$ Ref. (C.29)

  ○ $C_{Dt} = 17 \cdot (t/c)^2 - 0.05$ Ref. (C.30)

- $F_{D,spray} = \sum_{struts} C_{D_{spray}} \cdot t_{strut}^2 \cdot \frac{1}{2}\rho V^2, \qquad with\ C_{D_{spray}} = 0.24$ Ref. (C.31)

  ○ $t_{strut} = t$

  ○   In case of the propeller supporting aft struts:

      $t_{strut_{aft}} = \max\{t, \qquad 0.3\,[m]\}$ Ref. (6.10)

6.3.2 Battery Powered Ferry on Hydrofoils

The method that is described above can be used to estimate the resistance and energy consumption of the battery powered concept ferry, with a power and propulsion system mass as estimated in appendix A.1.10. The result is the blue solid curve that can be seen in figure 6.11 and 6.12. The two additional blue curves in these figures are from the estimation with a 10% margin on lift coefficient and the resistance (blue dashed curve), and with a 20% margin on the lift coefficient and the resistance (blue dash-dotted curve). A 10% or 20% higher lift coefficient can also be interpreted as a 10% or 20% lower total mass of the vessel.
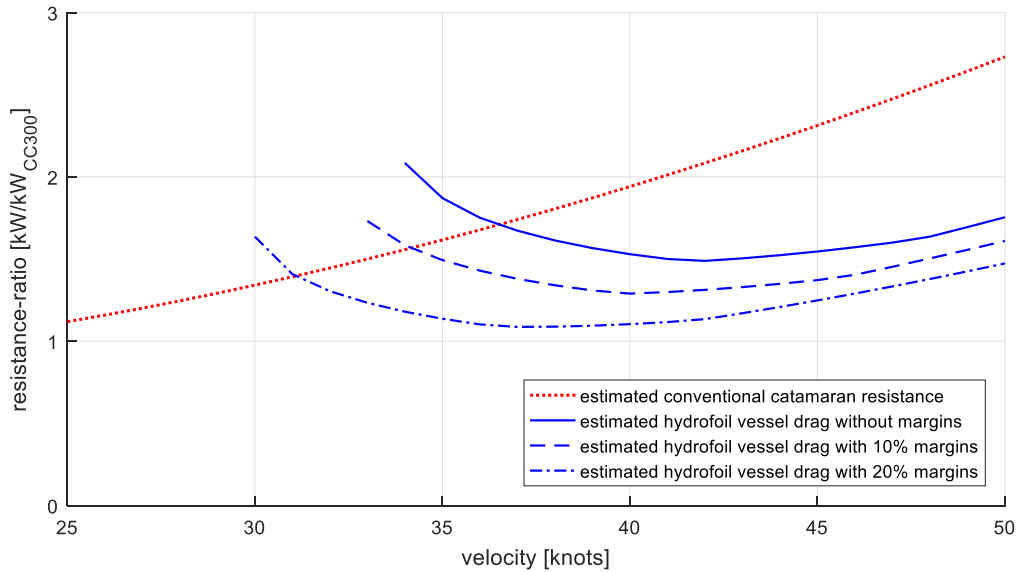
Figure 6.11: resistance estimation of the 39.5 m long battery powered carbon composite ferry (red dotted curve) and its hydrofoil version (blue curves), plotted against velocity. The resistance is normalized to the resistance of the CC300 at 30 knots. The margins are included as positive margins on the lift coefficient (higher C_L) and as negative margins on the resistance (lower F_D).

Resistance

Figure 6.11 shows that only the hydrofoil system with a 20% higher lift coefficient leads to a feasible result at a speed of 30 knots. The other two hydrofoils are too large, with too large 3D and interference effects that a feasible vessel does not exist at the design speed.

The resistance of the catamaran concept without hydrofoils is also plotted in the figure (red dotted curve), and it is estimated based on the method as described in the previous chapter (subparagraph

5.4.1). The result clearly shows that at a speed of around 45 knots, the design speed of many existing hydrofoil vessels [102] [110], the resistance of the hydrofoil vessel is around 40% lower than that of the 39.5 m long carbon composite catamaran. Another way to look at it is that the resistance of the hydrofoil vessel at 45 knots is roughly the same as that of the traditional catamaran at 32 knots. This shows that hydrofoils are more suited for speeds in excess of 40 knots.

Energy Consumption
Figure 6.12 shows the energy consumption of the hydrofoil vessel (blue curves), as well as of the comparable catamaran without hydrofoils (red dotted curve). In this figure it can be seen that the energy consumption at 45 knots of the hydrofoil ferry is around 30% lower than of the traditional catamaran. This difference is smaller than the difference in resistance, which is due to the difference in propulsor efficiency (around 17% [equation C.33]).

The target energy consumption (equation 5.3, see below) is also included in the figure (black dotted lines). The energy consumption falls well within the target region, which makes it look like this is might also be financially feasible. This is however not the case. First of all the target ratio is not really representative as it does not take the extra costs of the hydrofoil system into account. But more importantly, because the resistance ratio is higher than 1.0, as seen in figure 6.11, the electrical propulsion system must be more powerful, which means that the mass increases, thus the cycle starts all over again. Because the estimation diverges, no feasible solution exists for the battery powered ferry on hydrofoils.

$$\frac{E_{ESS}}{E_{CC300}} < \{0.8\text{-}1.4\} \qquad\qquad\qquad \text{Ref. (5.3)}$$
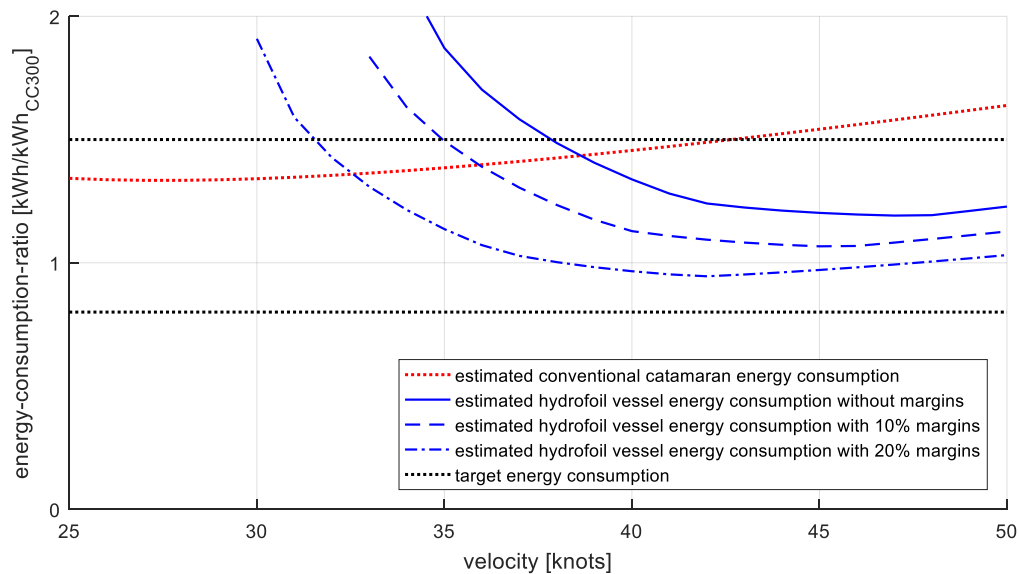
Figure 6.12: energy consumption estimation of the 39.5 m long battery powered carbon composite ferry (red dotted curve) and its hydrofoil version (blue curves), plotted against velocity. The energy consumption is normalized to the energy consumption of the CC300 at 30 knots, and the target energy consumption is included as well (black dotted lines). The margins are included as positive margins on the lift coefficient (higher C_L) and as negative margins on the resistance (lower F_D).

6.3.3 Hydrogen Powered Ferry on Hydrofoils

For the hydrogen powered version of the hydrofoil catamaran, a break-even point does exist. This means that the estimation method from figure 6.10 can be expanded to the method as seen in figure 6.13. It can be seen that the varying mass of the power and propulsion system (M_{PP}) leads to an additional iterative process.

Resistance

Figure 6.14 shows that at 30 knots, a feasible solution only exists if the lift coefficient is 20% higher (blue dash-dotted curve) than what is used in the estimation method (blue solid curve). It can also be seen that for higher speeds the resistance of the hydrofoil ferry is much lower than the catamaran without hydrofoils. For a design speed of 45 knots, the resistance of the hydrofoil ferry is around 60% lower than that of the traditional catamaran, but at 30 knots, the resistances are similar, when the 20% resistance margin is included.
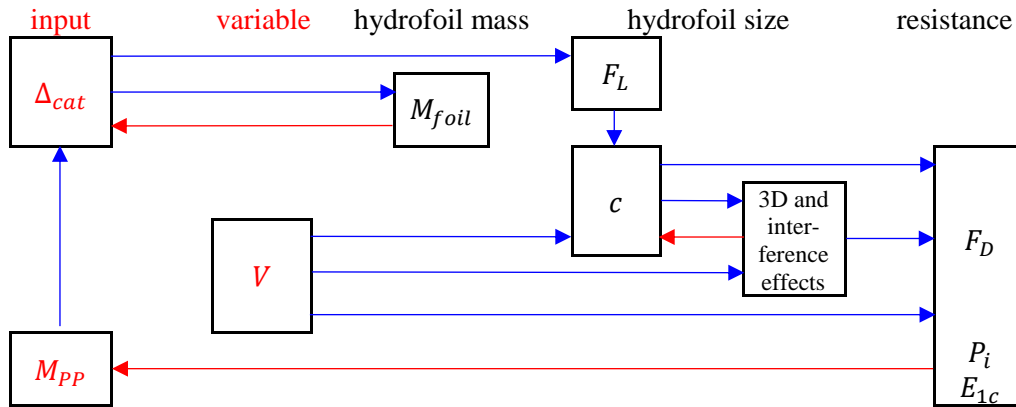
Figure 6.13: overview of the resistance estimation method for the hydrofoil supported ferry. The arrows indicate how the components are related to each other.
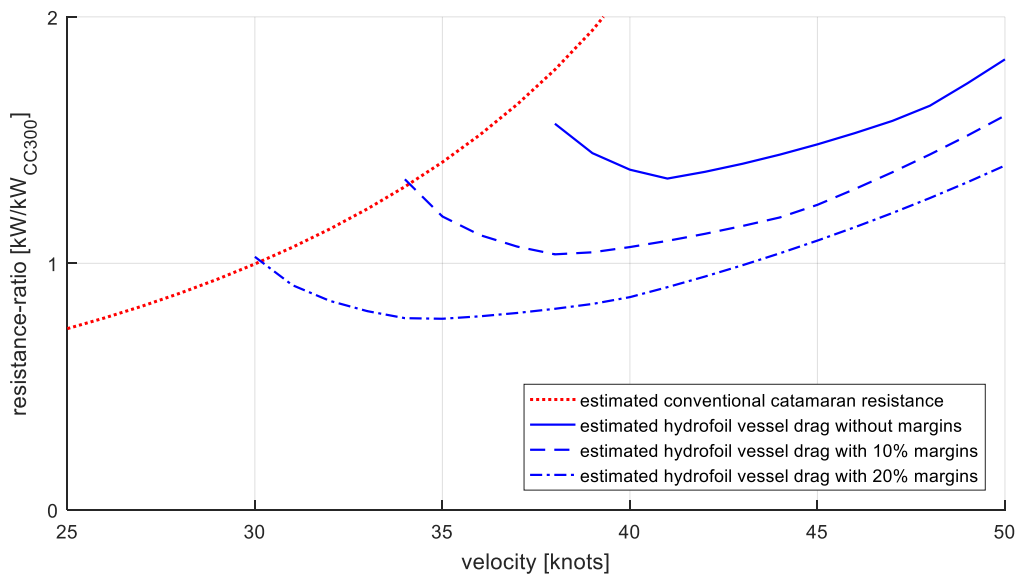
Figure 6.14: resistance estimation of the 39.5 m long hydrogen fuel cell powered carbon composite ferry (red dotted curve) and its hydrofoil version (blue curves), plotted against velocity. The resistance is normalized to the resistance of the CC300 at 30 knots. The margins are included as positive margins on the lift coefficient (higher C_L) and as negative margins on the resistance (lower F_D).

Energy Consumption

Figure 6.15 shows the energy consumption of the hydrofoil catamaran is barely below the target, which is indicated by the black dotted lines (equation 5.4 on the next page). Because the target is likely to move down to take the costs of the hydrofoil system into account, it can be concluded that a hydrofoil version of the hydrogen powered catamaran is also not a feasible solution.

$$\frac{E_{FC}}{E_{CC300}} < \{0.3\text{-}0.9\} \hspace{4cm} \text{Ref. (5.4)}$$
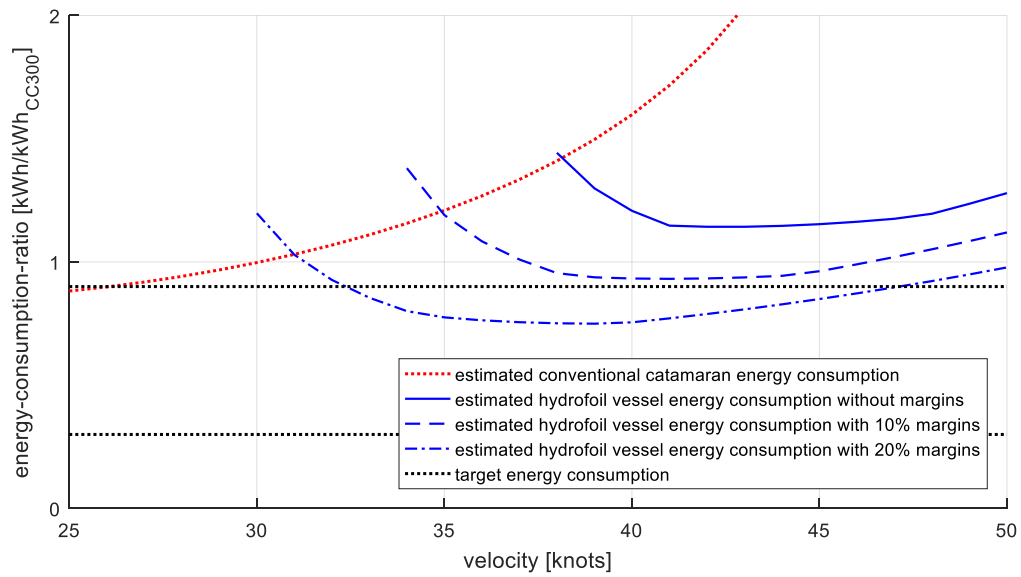
Figure 6.15: energy consumption estimation of the 39.5 m long hydrogen fuel cell powered carbon composite ferry (red dotted curve) and its hydrofoil version (blue curves), plotted against velocity. The energy consumption is normalized to the energy consumption of the CC300 at 30 knots, and the target energy consumption is included as well (black dotted lines). The margins are included as positive margins on the lift coefficient (higher C_L) and as negative margins on the resistance (lower F_D).

6.4 Conclusions on Hydrofoils

A severe reduction in resistance is desirable for both the battery powered and hydrogen powered concepts. Multiple fast ferries operate on hydrofoils, because such a ship type has a lower resistance at the design speed than a comparable ship without hydrofoils. Therefore, the following question was written at the beginning of this chapter:

> *How much can a hydrofoil system reduce the resistance*
> *and energy consumption of the electric concept ferry?*

The short answer is:

> *A hydrofoil system cannot reduce the resistance of the electric concept*
> *ferry at 30 knots, nor does it reduce the energy consumption.*

The large weight of the electric vessel requires a large hydrofoil system. Large hydrofoils suffer from large 3D and interference effects, which lower the effective lift coefficient. Because the effective lift coefficient is lower, the required size of the hydrofoil should be larger. If the size of the hydrofoil increases, the 3D and interference effects increase as well. This process can be repeated, but because it diverges, no feasible solution is found. Only the result with a 20% margin on the lift coefficient converges to a break-even point, but the resistance at this point is still higher than of the vessel without hydrofoils, despite the 20% resistance margin that is included as well.

Because it is not even close to a feasible option, it can be safely assumed that another ship type with hydrofoils, such as a monohull, is not an option either, if the displacement of the vessel is not significantly lower.

This chapter did show that at higher speeds, e.g. 45 knots, the resistance of a hydrofoil system is much lower than that of a similar vessel without hydrofoils. The relative resistance at higher speeds is much lower, but in absolute terms not so much. As a result, the energy consumption at higher speeds is also not much lower, compared to a conventional catamaran at 30 knots. Therefore, it can be concluded that hydrofoils are not suited for the electric concept ferry of this thesis.

7

Conclusions and Recommendations

Decreasing emissions has a positive effect on the global climate, as well as on the local air quality. Therefore, more and more vehicles are replaced by emission free electric vehicles. This transit to electric transportation also takes place in Shenzhen, a city in China where more than 12 million people live [16]. In 2018, Shenzhen became the first city in the world to have a 100% fully electric public bus fleet; with support from the government, they replaced all 16 thousand busses in a timespan of only eight years [9].

In the surrounding waters of Shenzhen, there are also many fast passenger ferries operational, such as CoCo Yacht's Coastal Cruiser 300. Because Shenzhen is motivated to go all-electric, it is desirable to replace these polluting diesel powered ferries with emission free versions.

This project is a case study for an emission free replacement for the Coastal Cruiser 300, operating between Shekou and Zhuhai, a crossing distance of 25 NM. The concept ferry is a catamaran that is capable of transporting 300 passengers with a speed of 30 knots.

Structure of this Chapter

The conclusion that can be drawn from this study can be found in **paragraph 7.1**, which also contains the main research question and its answer. This paragraph contains an overview of all conclusions from the previous chapters, followed by an overall conclusion in **subparagraph 7.1.5**. The final topic of this report is the recommendations, which can be found in **paragraph 7.2**.

7.1 Conclusions

During this thesis, the feasibility of an emission free replacement ferry for the Coastal Cruiser 300 was analysed. The main research question is the following:

How feasible is an emission free catamaran as a
replacement for the Coastal Cruiser 300, operating
as a fast passenger ferry in Shenzhen, China?

The short answer for the current situation, regarding the case study ferry crossing of 25 NM, is:

The hydrogen powered version is likely to be the better choice,
as the battery powered version is on the edge of feasibility.

The short answer for the expected future situation is:

The battery powered version is likely to be the better choice,
as al conventional concepts are feasible, but the costs are
possibly lower than that of the hydrogen powered ferry.

The general short answer for a fast ferry (30 knots, 300 passenger) is the following:

The battery powered concept ferry is feasible for shorter crossings (< 25 NM),
and the hydrogen powered concept is feasible under all analysed conditions.

7.1.1 Exploration of Emission Free Propulsion Methods

Currently most fast ferries operate on internal combustion engines that run on diesel fuel. In order to operate emission free, another propulsion method has to be installed on the vessel. The question is:

What are suitable methods of emission free propulsion,
and what is the main problem when implementing them into a ferry?

Two options remained after analysing different methods for emission free propulsion: battery powered and hydrogen fuel cell powered. Operating on supercapacitors is similar to operating on batteries, but because they are heavier and more expensive than batteries, supercapacitors were not chosen as an option. Solar cells were also not be implemented in the concept design, as their contribution is negligibly small.

   The main problem of batteries is its large mass, and the hydrogen powered ferry suffers from a large increase in fuel costs, as hydrogen is much more expensive than diesel fuel. So in both cases, the energy consumption must be sufficiently low.

   Costs related to the power and propulsion system were also analysed. It is however important to keep in mind that costs is not the most important aspect of the emission free ferry. The reduction in emissions might be worth the additional costs. Furthermore, it might lead to a reduction in indirect costs related to pollution.

7.1.2 Implementing the Electric Propulsion Systems into the Design

The next step was to combine the two electric propulsion systems with the design of the current Coastal Cruiser 300. Because energy consumption is an important aspect, the following question was raised:

What is the impact on energy consumption,
when implementing the emission free propulsion systems
into the design of the Coastal Cruiser 300,

and how does that impact the total costs?

A battery powered version is not feasible, because the weight of the vessel is too large, resulting in a too large increase in resistance and energy consumption. Thus a reduction in energy consumption is desirable to achieve a feasible battery powered fast ferry.

The hydrogen powered ferry is feasible, but the higher costs make a reduction in energy consumption desirable.

7.1.3 Analysis of Ways to Reduce the Energy Consumption

The desire to reduce the energy consumption has led to the following question:

How can the energy consumption of the electric concept ferry be reduced,
and what is the effect on the feasibility?

Energy consumption can be influenced by changes in design (i.e. elongated hull, lighter structure and improved system performance in the future), as well as by changes in the operational profile (i.e. sailing at a lower speed and operating on a shorter distance). The effect of changing these parameters was analysed for both the battery and hydrogen powered ferry.

Battery Powered Concept Ferry

In case of the battery powered catamaran, operating on the 25 NM crossing is only possible with an elongated hull. A lighter structure improves the feasibility of the elongated version, but it has no effect on the concept with the original length. Looking at costs, the battery powered ferry is likely to be more expensive than the diesel powered ferry, but this depends on the electricity price and diesel fuel price.

If the battery performance improves in the future, the feasibility increases. With 1,000 Wh/kg batteries, feasibility exists for all estimations, with a strong indication that operating on batteries is cost competitive with operating on diesel fuel.

Decreasing the design speed does not significantly reduce energy consumption, as the reduction in resistance is roughly proportional to the increase in travel time. Furthermore, without changing the timetable, the charging time at quay gets smaller if the travel time increases, making this option not feasible.

Operating on a shorter distance increases the feasibility. It can be advised to consider a battery powered ferry for short crossings, roughly shorter than 25 NM.

Hydrogen Powered Ferry

For the hydrogen powered ferry, all analysed concepts are feasible, but all are more expensive than the diesel powered ferry. The same is true in the future, when the fuel cell performance has improved.

Lowering the design speed also has little effect on the costs of the hydrogen powered ferry, for the same reason as it has little effect for the battery powered ferry.

Changing the design crossing's distance also does not have any significant impact on the total costs of the hydrogen powered ferry in comparison to the diesel powered ferry.

For the case study crossing of 25 NM, the hydrogen powered version is likely to be the better choice, as the battery powered version is on the edge of feasibility. So it can be advised to consider a hydrogen fuel cell powered ferry for long crossings, roughly longer than 25 NM.

As mentioned before, costs is not the most important aspect of this analysis. The reduction in pollution, and all other negative effects of emissions, might be worth the extra costs. Because the costs of the hydrogen powered ferry are likely to be higher than that of the battery powered version, it makes sense to only consider hydrogen for distances beyond 25 NM, which cannot be reached by the battery powered version.

7.1.4 Analysis of a Hydrofoil Supported Concept Catamaran

The final topic that was analysed in this project is the hydrofoil supported concept, because a more severe reduction in energy consumption is still desirable. Multiple fast ferries operate on hydrofoils, because these underwater wings can significantly lower the resistance. This raises the following question:

*How much can a hydrofoil system reduce the resistance
and energy consumption of the electric concept ferry?*

Compared to the existing hydrofoil vessels, there are two major differences: the electric concept ship has relatively more weight, and the design speed is lower. Both these differences require larger hydrofoils, which suffer from stronger 3D and interference effects. As a result, the effective lift coefficient goes down and no feasible solution exists.

The study shows that only at higher speeds, the hydrofoil has a positive impact on the resistance. But in absolute terms, this does not improve the energy consumption with respect to the electric version of the Coastal Cruiser 300 at 30 knots. It can therefore be concluded that hydrofoils are not suited for the electric concept ferry.

7.1.5 Overall Conclusion

This project was a case study for a 300 passenger ferry on a 25 NM crossings, operating at 30 knots. The results show that the battery powered concept is on the edge of feasibility, but for shorter crossings, the feasibility is higher. In general, a battery powered ferry, when feasible, is less expensive than a hydrogen powered ferry, but the latter is feasible over a larger range of distances.

So fast electric passenger ferries are feasible, but the direct costs are currently higher than for a comparable diesel powered ferry. The higher price can be seen as an investment, because it will improve the liveability on this planet, as well as limit the increase of the indirect costs of pollution, which is estimated to be over four trillion euro globally, each year. This shows that we have to pay the price either way. So the remaining question is:

Do we want to invest now, or pay for the damage afterwards?

…

7.2 Recommendations

This last paragraph before the appendices contains the recommendations that follow from this project.

7.2.1 Other Ferries, Other Routes

This thesis was a case study for a ferry route in Shenzhen, China. Though the results might also apply to other ferries on different locations around the world, it would be interesting to expand the analysis, e.g. combine varying speed with varying distances.

Looking at different passenger capacities would also be an interesting. In paragraph 2.1, the Coastal Cruiser 300 was chosen over the smaller Coastal Cruiser 199, but the same analysis can be done for the smaller ferry. This does however require some changes to the estimation, as it currently does not represent the CC199 with sufficient accuracy.

It would also be interesting to look at other ship types, as not all ferries are catamarans. Paragraph 5.3 indicated that it might be possible in the future to convert existing catamarans into electric ferries, this might also apply to existing monohulls for example.

7.2.2 Harbour Infrastructure

This thesis was mainly focussed on the ship itself; the quay was only looked at to see if it is possible to keep an electric ferry operational. Required adjustments must be identified, especially when there are plans to actually realize an electric ferry. The adjustments are likely to differ from quay to quay, depending on the already existing infrastructure in the harbour.

7.2.3 Lower Emission Fuels

This thesis was limited to a "zero emission" ferry. This is however not possible, as everything that humans do is accompanied with emissions, albeit indirectly. Though the pollution from battery production and recycling is relatively small, it is still there. Furthermore, if grey electricity or hydrogen is used that is created from fossil fuels, it might not reduce the overall pollution at all. So it might be interesting to make a comparison with clean fuels.

Internal combustion engines on hydrogen were already mentioned, but other options also exist, such as GTL (Gas to Liquid) and HVO (Hydrated Vegetable Oil), two EN 15940-norm fuels that are gaining popularity [112]. Because these fuels still have polluting exhaust gasses, it does not seem like a long-term solution. It might however be suited as a temporary solution, especially if they can be used with the currently installed diesel engines.

7.2.4 Future Propulsion Systems

In paragraph 5.3, the effect of the expected performance of future systems was analysed, but there might be other developments or breakthroughs that might be interesting to look at. Graphene for example is a material that is expected to significantly improve the performance of batteries.

7.2.5 Expended Financial Analysis

In this thesis, the costs were limited to the costs that are directly related to the propulsion system, both investment and operational costs, as explained in paragraph 3.6. This is however only a small part of the total costs of a ferry. It is sufficient for the purpose of comparing different concepts, but if such a vessel is really to be build, costs are important, as enough money has to be available.

Because the total cost of ownership is only known to the ferry operator, an extended financial analysis is not included in this report. But if it would be included, it would not significantly change the outcome of this study, it would only reduce the range of the cost ratios in the tables.

Costs related to changes to the harbour were also not taken into account, because this project was mainly focused on the ship itself. For the complete overview, it should be taken into account.

Also not taken into account are taxes, such as the carbon tax. If companies have to pay for the CO_2 they expel, it is likely to change the financial balance of the electric ferry.

A range of fuel and electricity prices was used in this report, which represents the current expected prices. The actual price differs from location to location, and it is also likely that prices will change in the future. These differences might fall within the price range of this report, but they might as well fall outside it; only an extended financial analysis can clarify this unknown.

7.2.6 Air Supported Vessel

A hydrofoil supported vessel was analysed in chapter 6, as these ship types were expected to result in a lower resistance. It turned out that this was not the solution for reducing the energy consumption, but there are other "exotic" ship types to look into.

The AiriEl, BB Green's fully electric demonstrator vessel, is an air supported vessel. They claim that the vessel requires 40% less power than a traditional catamaran, because the vessel runs on an air cushion. [12]

Another option is the surface effect ship, a vessel where the weight is also largely supported by an air cushion. An example is the Norwegian Skjold-class corvettes, which are 47 m long vessels with a 274 tonnes displacement that can reach speeds of over 60 knots [113].

It is however expected that the result is the same as for the hydrofoils: this ship type is suited for much higher speeds, but not for the design speed of 30 knots. The reason for this is the power required be the lift fans. In case of the Skjold-class corvettes [113], 1,400 kW is installed for the fans. This is small compared to the propulsion power of 12,000 kW that is required to reach the high speeds. But compared to the required power for a speed of only 30 knots, the difference is not so large, e.g. if the required propulsion power reduction is 40%, but the additional fan power is also 40%, the total result is no improvement at all.

Though it is not expected to improve much, a detailed estimation is required to confirm this.

7.2.7 Rules and Regulations

In this report it is mentioned that rules do not seem like a problem, but rules and regulations are an important factor for every new ship. Especially with new technology, it is an important point of attention. Depending on the location, rules and regulations might be different. So it is important to work with the local government regarding the rules and regulations.

7.2.8 Verification and Validation

All results in this report are estimation results. In order to check the accuracy and to verify the results, more detailed calculations have to be made.

It starts with the weight of all the components, better estimations can be made in collaboration with the manufacturers of these components. The actual structural weight can be better approximated with the use of computer software, e.g. FEM (Finite Element Method).

The actual resistance can be determined with CFD (Computational Fluid Dynamics) or physical model tests; this way verifying the estimation results from this project.

So some additional steps are required to verify the results from this report, but in order to fully validate the concept, a real vessel has to be build.

A

Mass and Displacement Approximation

The displacement of a ship can be split into lightship and deadweight. Lightship is constant for a vessel, and deadweight varies with different load conditions. This thesis looks at the ship in design condition, which means that the deadweight is constant as well in this analysis. Therefore, the displacement of the catamaran (Δ_{cat}) is not split into lightship and deadweight, but instead into the following three components:

$$\Delta_{cat} = M_S + M_{PP} + M_{add} \qquad\qquad (\text{ A.1 })$$

With:
- M_S, structural mass (hull and superstructure);
- M_{PP}, mass of the power and propulsion system;
- M_{add}, additional mass.

If the size of the vessel grows, the size of the structure grows as well. This means that the weight of the structure also increases.

In general, if the displacement of the ship design grows, the resistance grows as well. This means that components of the propulsion system, e.g. waterjet and engine, will increase in weight as well. In case of the electric ferry, the weight of the power and propulsion system also increases if the amount of batteries or hydrogen increases.

The additional mass takes all other mass components into account, such as interior arrangement, navigational equipment and the passengers on board. This mass component is constant in this analysis, as it is related to the mission of the vessel, which does not change in case of electric propulsion.

Structure of this Appendix
Appendix A.1 contains the mass approximation of the power and propulsion system, and the structural mass approximation is explained in **appendix A.2**.

A.1 Mass Approximation of the Power and Propulsion System

The components of the power and propulsion system of the electric ferry were discussed in chapter 3, and an overview can be seen in figure 3.8 below. This paragraph contains the weight estimation of each component, either as a function of installed power (P_i, equation B.38), or energy consumption of one crossing (E_{1c}, equation 3.2). These two variables are indicated in red to distinguish them from the constants that are used in this approximation. Furthermore, both are related to the resistance of the ferry (R), of which the estimation method will be discussed in appendix B.

$$P_i = 1.15 \times P_P \qquad\qquad\qquad \text{Ref. (B.38)}$$

$$E_{1c} = \frac{P_p}{\eta_{ED}} \cdot t_t + E_{aux} \qquad\qquad\qquad \text{Ref. (3.2)}$$

With:

$$P_P = \mathbf{X} \cdot R - \mathbf{X} \qquad\qquad\qquad \text{Ref. (B.37)}$$
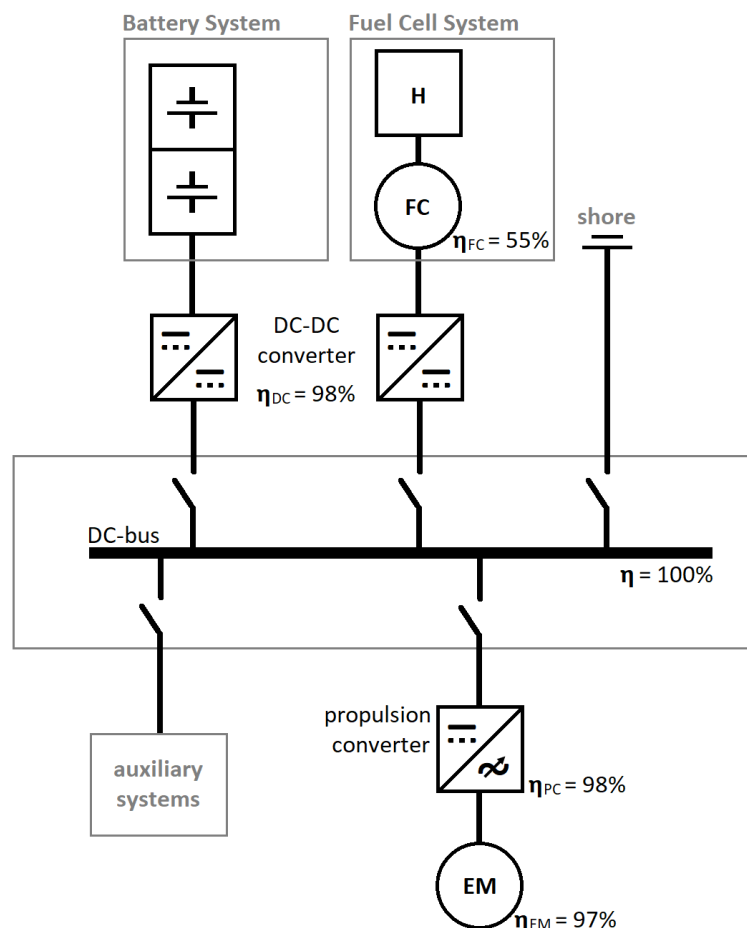
Ref. figure 3.8: line diagram of the electric propulsion system, both battery powered
and fuel-cell-battery powered, including the efficiencies of the
different components.

A.1.1 Waterjet Mass Approximation

More resistance requires more thrust and thus a larger waterjet system. The following relation is derived based on the installed power (P_i) in the Coastal Cruiser 199 and 300 [15], and the weight of the waterjets (M_{wj}) [114]:

$$M_{wj} = P_i \cdot \left[\frac{M_{wj}}{P_i}\right] - M_{wj0} \qquad\qquad (\text{ A.2 })$$

With:

- $\left[\frac{M_{wj}}{P_i}\right] = \text{X } kg/kW$;
- $M_{wj0} = \text{X } tonnes$.

Note that this expression contains a minus, which would mean that a low power waterjet could have a negative weight. The reason for this is that on a larger scale, the weight/power-ratio shows a more exponential relation [115]. For the power range used in this thesis, a linear relation is deemed accurate enough, based on the data from different manufacturers [115] [116].

A.1.2 Electric Motor Mass Approximation

The following ratio is used to estimate the weight of the electric motor, which is based on data of electric motor manufacturers [28] [27]:

$$M_{EM} = P_i \cdot \left[\frac{M_{EM}}{P_i}\right], \qquad with \left[\frac{M_{EM}}{P_i}\right] = 3.5 \ kg/kW \qquad\qquad (\text{ A.3 })$$

A.1.3 Propulsion Converter Mass Approximation

For estimating the weight, the following ratio is used [29]:

$$M_{PC} = P_i \cdot \left[\frac{M_{PC}}{P_i}\right], \qquad with \left[\frac{M_{PC}}{P_i}\right] = \text{X } kg/kW \qquad\qquad (\text{ A.4 })$$

In this equation, losses in the electric motor are neglected, as these are small enough that they do not affect the ratio.

A.1.4 Switchboard Mass Approximation

Since only direct current runs through the main switchboards, it is also known as DC-bus. The following ratio is used for estimating the weight of this component [29]:

$$\left[\frac{M_{SB}}{P}\right] = \text{X } kg/kW \qquad\qquad (\text{ A.5 })$$

The power (P) in this ratio is a function of installed propulsion power, auxiliary power (P_{aux}) and the efficiency of the electric motor ($\eta_{EM} = 97\%$ [27] [28]) and the propulsion converter ($\eta_{PC} = 98\%$ [29]):

$$P = \left(\frac{P_i}{\eta_{EM} \cdot \eta_{PC}} + P_{aux}\right) = \left(\frac{2.9 \ [MW]}{0.97 \cdot 0.98} + 0.1 \ [MW]\right) = 1.1 \times P_i \qquad\qquad (\text{ A.6 })$$

Battery Powered Ferry

The largest power that the DC-bus in the battery powered ferry has to handle occurs during charging. Fast charging requires 6.5 MW [subparagraph 3.3.4], which is over twice the installed power [15]:

$$\frac{P_{charge}}{P_i} = \frac{6.5 \, [MW]}{2.9 \, [MW]} \rightarrow P_{charge} = 2.2 \times P_i \qquad (\text{A.7})$$

Since the DC-bus of the battery powered ferry has to handle over twice the installed power, the mass/power-ratio will also be over twice as large as well:

$$M_{SB} = P_i \cdot \left[\frac{M_{SB}}{P_i}\right]_{ESS} \qquad (\text{A.8})$$

With:

$$\left[\frac{M_{SB}}{P_i}\right]_{ESS} = 2.2 \times 1.1 \times \mathbf{X} \, [kg/kW]$$

Fuel-Cell-Battery Powered Ferry
Batteries are added to the fuel cell system to handle fluctuating powers. They have 2/3 the power output of the fuel cell [subparagraph 3.5.4]. So the power that the DC-bus has to handle is (1+2/3) times P:

$$M_{SB} = P_i \cdot \left[\frac{M_{SB}}{P_i}\right]_{FC} \qquad (\text{A.9})$$

With:

$$\left[\frac{M_{SB}}{P_i}\right]_{FC} = (1 + 2/3) \times 1.1 \times \mathbf{X} \, [kg/kW]$$

A.1.5 DC-DC Converter Mass Approximation

The mass/power-ratio of the DC-DC converter is roughly the same as for the switchboard [29], thus the ratios are equal to the ones above:

$$M_{DC,ESS} = P_i \cdot \left[\frac{M_{DC}}{P_i}\right]_{ESS}, \qquad with \left[\frac{M_{DC}}{P_i}\right]_{ESS} = \mathbf{X} \, kg/kW \qquad (\text{A.10})$$

$$M_{DC,FC} = P_i \cdot \left[\frac{M_{DC}}{P_i}\right]_{FC}, \qquad with \left[\frac{M_{DC}}{P_i}\right]_{FC} = \mathbf{X} \, kg/kW \qquad (\text{A.11})$$

A.1.6 Energy Storage System Mass Approximation

The mass of battery system, known as the Energy Storage Systems (ESS), is approximated as a function of its energy capacity (E_{1c}/DOD):

$$M_{ESS} = \frac{E_{1c}}{DOD} \cdot \left[\frac{M_{ESS}}{E_C}\right] \qquad (\text{A.12})$$

With:
- $DOD = 50\%$, operational depth of discharge of the battery system [subparagraph 3.3.7];
- $\left[\frac{M_{ESS}}{E_C}\right] = 12.5 \, kg/kWh$, mass/capacity-ratio of the ESS [subparagraph 3.3.7].

A.1.7 Fuel-Cell-Battery Mass Approximation

A fuel cell system contains of multiple modules, similar to a battery system. The mass of a fuel cell module ranges from 1 to 5 kg/kW [17] [70]. A mass/power-ratio of 2.3 kg/kW is used for the fuel cell

modules, which is based on the Hydrogenics' HyPM-HD 30 Power Module [67], the same modules that were used as the basis SF-BREEZE feasibility study [13].

The weight of the total system is larger than of the weight of the modules alone. In case of battery systems, going from a battery module (90 Wh/kg [34]) to a battery pack (80 Wh/kg [19]) is a mass increase of 13%:

$$\frac{90\ [Wh/kg]}{80\ [Wh/kg]} = 1.13$$

Using the same ratio for the fuel cell system results in a mass/power-ratio of

$$1.13 \times 2.3\ [kg/kW] = 2.6\ kg/kW$$

The battery system has a mass/power ratio of 2.1 kg/kW, and it has 2/3 the power of the fuel cell [subparagraph 3.5.4]. To include the pipe system through which the hydrogen flows, a 5% margin is added to the weight, resulting in the following ratio:

$$\left[\frac{M_{FC}}{P}\right] = 1.05 \times (2.6 + 2/3 \times 2.1) = 4.2\ kg/kW \qquad\qquad (\text{ A.13 })$$

From this follows the following estimation equation for the weight of the fuel cell system (M_{FC}):

$$M_{FC} = \left(\frac{P_i}{\eta_{ED}} + P_{aux}\right) \cdot \left[\frac{M_{FC}}{P}\right] \qquad\qquad (\text{ A.14 })$$

With:

- $\eta_{ED} = 93\%$, electric powertrain efficiency [paragraph 3.1];
- $P_{aux} = 0.1\ MW$, auxiliary power consumption [21];
- $\left[\frac{M_{FC}}{P}\right] = 4.2\ kg/kW$.

A.1.8 Hydrogen Storage System Mass Approximation

The specific energy of hydrogen is 33 kWh/kg [17], and a hydrogen tank can contain around 5 wt% hydrogen [18]. So the specific energy of a hydrogen tank is:

$$\left[\frac{E_C}{M_{HS}}\right] = 33 \times 0.05 = 1.7\ kWh/kg \rightarrow \left[\frac{M_{HS}}{E_C}\right] = \frac{1}{1.7\ [kWh/kg]} = 0.6\ kg/kWh$$

An overcapacity is required to at least prevent running out of fuel, but it might also be desirable to make two crossings between refuelling, so only one refuelling station is required. In this project 2.5 is chosen as overcapacity factor, which is in line with the hydrogen fuelled ferry concept SF-BREEZE [13]. This overcapacity is inclueded in the equation by n_{HS}. The final thing to include is the efficiency of the fuel cell, which is 55% [67]. Based on this, the following expression is derived for the mass of the hydrogen storage (M_{HS}):

$$M_{HS} = n_{HS} \cdot \frac{E_{1c}}{\eta_{FC}} \cdot \left[\frac{M_{HS}}{E_C}\right] \qquad\qquad (\text{ A.15 })$$

With:

- $n_{HS} = 2.5$, energy capacity expressed in the number of crossings;
- $\eta_{FC} = 55\%$, efficiency of the fuel cell [67];

- $\left[\frac{M_{HS}}{E_C}\right] = 0.6 \ kg/kWh$ [17] [18].

A.1.9 Electric Cable and Shore Supply Mass Approximation

Energy is transferred in an electric propulsion system via electric cables. Due to the amount of power that is transferred between the components, large cables are required. As a result, the weight of the cables is too large to neglect.

Looking at the specifications of a DNV approved marine power cable, a single core cable with a 300 mm^2 cross sectional area has a weight of around 4 kg/m [117]. The current that this cable can handle is 600 amps [117], which is 360 kW at 600 volts:

$$P = U \times I = 600 \times 600 = 360 \ kVA$$

So the density of a cable line (ρ_{cable}) is $0.022 \ kg/kW/m$:

$$\rho_{cable} = \frac{2 \ [cables] \times 4 \ [kg/m/cable]}{360 \ [kW/cable]} = 0.022 \ kg/kW/m$$

Note that a two is added above, as there are two cables required to close the electrical circuit. The total mass of the cables (M_{cable}) is a function of this density, the power that it has to handle (P_{cable}) and the length of the cables (L_{cable}), as seen in A.16.

In this thesis the connection point that is required to charge the vessel at quay is also considered part of the electric cable system. It is included in the equation with $\rho_{shore \ connection}$, which is **X** kg/kW, based on both Coastal Cruisers [114]. This leads to the following expression:

$$M_{cable} = (\rho_{cable} \cdot L_{cable} + \rho_{shore \ connection}) \cdot P_{cable} \qquad\qquad (\text{A.16})$$

Battery Powered Ferry

Charging the batteries happens with roughly twice the installed propulsion power [subparagraph A.1.4], thus with one times the propulsion power per demi-hull:

$$P_{cable} = 2.2 \times P_i \ / \ 2 \ [demi\text{-}hulls] = 1.1 \times P_i$$

The length of the complete electric propulsion system is roughly 30 m, as seen in figure 3.4 from subparagraph 3.3.8 (also seen in the next page). An additional ten meters is required cross the overall beam of the ferry, thus the total cable length is 70 m:

$$L_{cable} = 30 \ [m/demi\text{-}hull] \times 2 \ [demi\text{-}hulls] + 10 \ [m] = 70 \ m$$

From this follows the weight of the electric cables, in case of the battery powered ferry:

$$M_{cable,ESS} = (0.022 \ [kg/kW/m] \times 70 \ [m] + \mathbf{X} \ [kg/kW]) \times P_i \qquad\qquad (\text{A.17})$$
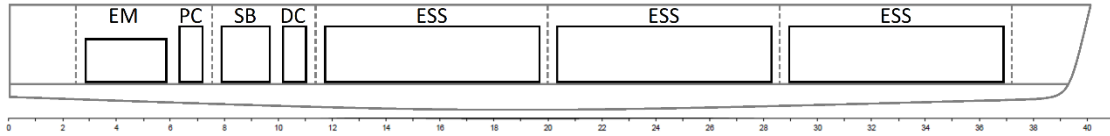
Ref. figure 3.4: side view of a demi-hull with an overview of the battery powered propulsion
system: electric motor (EM), propulsion converter (PC), switchboard (SB),
DC-DC converter (DC) and energy storage system (ESS).

Hydrogen Fuel-Cell-Battery Powered Ferry
Since the battery system is a lot smaller compared to the fully battery powered ferry, the power required
to charge the batteries is a lot smaller than the installed propulsion power. So the power that the cables
have to handle is the installed power divided by two, as there are two demi-hulls:

$$P_{cable} = P_i \ / \ 2 \ [demi\text{-}hulls] = \frac{1}{2} \cdot P_i$$

The length over which the cables have to run is also smaller; roughly 20 m, as seen in figure 3.7 below.
The ten additional meters to cross the overall beam of the ferry is again required for charging at quay,
thus the total length is 50 m:

$$L_{cable} = 20 \ [m/demi\text{-}hull] \times 2 \ [demi\text{-}hulls] + 10 \ [m] = 50 \ m$$

From this follows the weight of the electric cables, in case of the hydrogen fuel cell powered ferry:

$$M_{cable,FC} = (0.022 \ [kg/kW/m] \times 50 \ [m] + \mathbf{X} \ [kg/kW]) \times \frac{1}{2} \cdot P_i \qquad (\ A.18 \ )$$
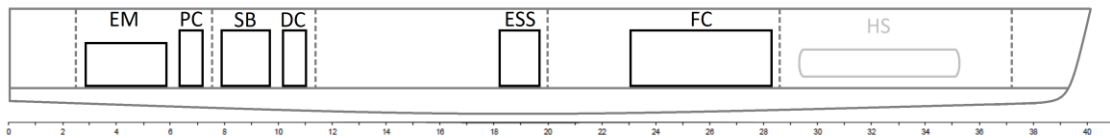
 Ref. figure 3.7: side view of a demi-hull with an overview of the hydrogen fuel-cell-battery
powered propulsion system: electric motor (EM), propulsion converter (PC),
switchboard (SB), DC-DC converter (DC), fuel cell system (FC), battery
system (ESS) and hydrogen storage tank (HS).

A.1.10 Total Mass of the Power and Propulsion System
The total mass of the power and propulsion system is simply the summation of all its individual
components. Since only the main components are discussed above, five percent is added to account for
additional components, such as foundations [114].

A.2 Structural Mass Approximation

In this paragraph, the estimation method is derived for the structural mass, which consists of the hull and the superstructure of the vessel.

A.2.1 Structural Mass of the Enlarged Ship Concept Designs

For the study on the Enlarged Ship Concept, the resistance was measured for three different ship lengths [118]. Length and displacement of these three ships is seen in table A.1. Design 2600 is the "base boat", and the other designs have an elongated hull, while keeping the beam and depth of the ship constant. All other components in the design remained constant as well, thus the weight of the superstructure also remains constant.

This means that only the weight of the hull changed, and thus the displacement of the vessel (Δ) can be split into two parts: the mass of the hull (M_{hull}), and additional mass (M_{add}) that accounts for all other components on board:

$$\Delta = M_{hull} + M_{add} \qquad\qquad\qquad\qquad (A.19)$$

Table A.1: waterline length (L) and displacement (Δ) of the different designs of the Enlarged Ship Concept study. [118]

design	2600	3500	4100	
L	23.4	31.6	36.9	m
Δ	970	1058	1115	kN

Because the only parameter that changes between the three designs is the length of the boat, it makes sense to look at the displacement in relation to the length of the vessel (L). From this follows a constant ratio (the largest difference is only 0.2%):

$$\frac{\Delta_{4100} - \Delta_{3500}}{L_{4100} - L_{3500}} \approx \frac{\Delta_{4100} - \Delta_{2600}}{L_{4100} - L_{2600}} \approx \frac{\Delta_{3500} - \Delta_{2600}}{L_{3500} - L_{2600}} = 10.7\ kN/m \qquad (A.20)$$

This result suggests that the mass of the hull is only a function of the length of the vessel, with the ratio as derived in equation A.20:

$$M_{hull} = L \cdot \left[\frac{M_{hull}}{L}\right], \qquad with\ \left[\frac{M_{hull}}{L}\right] = 10.7\ kN/m \qquad (A.21)$$

Using equations A.19 and A.21 leads to the results as seen in table A.2, which also shows that the ratio between the hull mass and the displacement decreases as the ship size grows, i.e. the hull mass is stronger related to size than to displacement.

Table A.2: displacement (Δ) [118], hull mass (M_{hull}), additional mass (M_{add}) and hull mass – displacement ratio of the different designs of the Enlarged Ship Concept study.

design	2600	3500	4100	
Δ	970	1058	1115	kN
M_{hull}	250	338	395	kN
M_{add}	720	720	720	kN
M_{hull}/Δ	26%	24%	22%	

A.2.2 Structural Mass of the Coastal Cruiser 199 and 300

In case of the Coastal Cruiser 199 and 300, both the hull mass and superstructure mass are different.

Hull Mass

The hull depth (D) of the Coastal Cruiser 199 and 300 is the same, but the length and overall beam (B_{oa}) are different [53] [71]. When all three main dimensions are included, equation A.21 expands into the following expression:

$$M_{hull} = L \cdot B_{oa} \cdot D \cdot \left[\frac{M_{hull}}{L \cdot B_{oa} \cdot D}\right] \qquad (\text{A.22})$$

The hull-mass/main-dimensions-ratio is the roughly the same for both Coastal Cruisers (the difference is 1.2%) [114] [53] [71]:

$$\left[\frac{M_{hull}}{L \cdot B_{oa} \cdot D}\right]_{CC199} \approx \left[\frac{M_{hull}}{L \cdot B_{oa} \cdot D}\right]_{CC300} = \mathbf{X} \, kg/m^3 \qquad (\text{A.23})$$

The hull mass of the Coastal Cruiser 199 is 20% of its displacement [114], while the hull mass of the CC300 is 18% [114] of its displacements. So the ratio between the hull mass and the displacement also decreases as the ship size grows. This is in line with the findings of the enlarged ship concept [subparagraph B.1.1]. It also confirms that the hull mass is related stronger to size rather than displacement.

Superstructure Mass

Both the Coastal Cruiser 199 and Coastal Cruiser 300 have two passenger decks, thus the construction height is similar. The superstructure is as wide as the overall beam of the vessel, thus the CC300 has a wider superstructure than the CC199. The length of the CC300's superstructure (L_{ss}) is also much longer than that of the CC199, which is required as it can carry a hundred more passengers. [53] [71]

The ratio between the mass of the superstructure (M_{ss}) and its dimensions differs 4% between the two Coastal Cruisers [114] [53] [71]:

$$\left[\frac{M_{ss}}{L_{ss} \cdot B_{oa}}\right]_{CC199} \approx \left[\frac{M_{ss}}{L_{ss} \cdot B_{oa}}\right]_{CC300} = \mathbf{X} \, kg/m^2 \qquad (\text{A.24})$$

Total Structural Mass

Combining equations A.22 and A.25 results in an expression for estimating the total structural weight (M_S):

$$M_S = L \cdot B_{oa} \cdot D \cdot \left[\frac{M_{hull}}{L \cdot B_{oa} \cdot D}\right] + L_{ss} \cdot B_{oa} \cdot \left[\frac{M_{ss}}{L_{ss} \cdot B_{oa}}\right] \qquad (\text{A.25})$$

Using this equation to estimate the total structural weight of the Coastal Cruiser 199 leads to an overestimation of only 0.3%, and for the Coastal Cruiser 300 the error with this estimation method is 0.6%. [114]

Due to this small error, this method is deemed accurate enough for the estimation purposes in this thesis.

A.2.3 Structural Mass Estimation of the Electric Catamaran

The estimation method for estimating the mass of the hull is already derived (equation A.22). Estimating the weight of the superstructure has yet to be determined though.

The size of a ferry's superstructure is mainly dependent on the mission requirements, e.g. in order to carry a hundred more passengers, the Coastal Cruiser 300 has a larger superstructure than the Coastal Cruiser 199. Since the electric ferry has the same passenger capacity as the CC300, the size of the superstructure does not need to change. However, the superstructure also contributes to the structural strength of the ferry. For that reason, if the length of the ferry increases, the length of the superstructure has to increase as well, in order to cope with the additional loads. For that reason it is assumed that the length of the superstructure changes with the same rate as the length of the ferry ($L_{ss} \sim L$).

With this assumption, equation A.25 simplifies to the following expression:

$$M_S = L \cdot B_{oa} \cdot \left(D \cdot \left[\frac{M_{hull}}{L \cdot B_{oa} \cdot D} \right] + \left[\frac{M_{ss}}{L \cdot B_{oa}} \right] \right) \qquad (\text{A.26})$$

With [71] [114]:

$$\left[\frac{M_{hull}}{L \cdot B_{oa} \cdot D} \right] = \mathbf{X} \, kg/m^3, \qquad \left[\frac{M_{ss}}{L \cdot B_{oa}} \right] = \mathbf{X} \, kg/m^2$$

The overall beam stays constant as there is no need to change it, because the hull separation does not significantly affect the resistance according to appendix B.4.2.

Hull Depth Estimation

A few additional assumptions must be made in order to estimate the structural weight.

The freeboard of the ferry remains constant, as the current freeboard is already optimized for its operation. That means that the hull depth only increases if the draft increases, which happens if the main dimensions of the ferry remain constant, while the displacement increases. This means that the draft has to be linked to the displacement of the ferry.

The displacement of a demi-hull (∇) is equal to the product of the block coefficient (C_B), the length (L), the beam (B) and the draft (T) of that demi-hull:

$$\nabla = C_B \cdot L \cdot B \cdot T \qquad (\text{A.27})$$

From appendix B.2.2 will follow that the block coefficient (C_B) and beam/draft-ratio (B/T) have a minimal influence on the resistance. It can therefore be assumed that the block coefficient and demi-hull beam are constant. This leads to the following relation between demi-hull displacement, length and draft:

$$\left. \begin{array}{l} \nabla = C_B \cdot L \cdot B \cdot T \\ C_B = constant \\ B = constant \end{array} \right\} \nabla \sim L \cdot T \qquad (\text{A.28})$$

This relation can be used to derive the following expression in which the draft is a function of displacement, length and the length-draft/displacement-ratio:

$$\frac{\nabla}{\nabla} = \frac{L \cdot T}{L \cdot T} \rightarrow T = \frac{\nabla}{L} \cdot \left[\frac{L \cdot T}{\nabla} \right] \qquad (\text{A.29})$$

The depth of the hull is the draft plus the freeboard height (H). Using this results in the following expression:

$$D = H + T = H + \frac{\color{red}\nabla}{\color{red}L} \cdot \left[\frac{L \cdot T}{\nabla} \right]$$ (A.30)

With [71] [114]:

$$H = \mathbf{X}\, m, \qquad \left[\frac{L \cdot T}{\nabla} \right] = \mathbf{X}\, m^{-1}$$

Complete Structural Mass Estimation

Substituting equation A.30 into equation A.26 leads to the following estimation equation for the structural weight of the ferry:

$$M_S = L \cdot B_{oa} \cdot \left(\left(H + \frac{\color{red}\nabla}{\color{red}L} \cdot \left[\frac{L \cdot T}{\nabla} \right] \right) \cdot \left[\frac{M_{hull}}{L \cdot B_{oa} \cdot D} \right] + \left[\frac{M_{ss}}{L \cdot B_{oa}} \right] \right)$$ (A.31)

This equation contains the following constants:
- $B_{oa} = 10.3\, m$ [15];
- $H = 2.1\, m$ [15];
- $\left[\frac{L \cdot T}{\nabla} \right] = \mathbf{X}\, m^{-1}$;
- $\left[\frac{M_{hull}}{L \cdot B_{oa} \cdot D} \right] = \mathbf{X}\, kg/m^3$;
- $\left[\frac{M_{ss}}{L \cdot B_{oa}} \right] = \mathbf{X}\, kg/m^2$.

The two variables in the equation are indicated in red:
- $\color{red}L$, waterline length of the vessel;
- $\color{red}\nabla$, displacement of the catamaran ($\nabla = \Delta_{cat}/\rho/2$);

Because structural mass is dependent on the displacement, and vice versa, this method is an iterative process. The influence on each other small though, so a few iterations will already lead to a balance between structural weight and displacement.

B

Derivation of the Equations for the Catamaran Resistance Estimation

The weight of the electric powered system is larger than the diesel powered system [appendix A.1.10], thus the displacement of the vessel is larger as well. A larger hull does have an impact on resistance, so a relation has to be derived that relates resistance to displacement of the ferry. In this thesis, the following equation is used to estimate the hull resistance (R_{hull}) of the electric ferry:

$$R_{hull} = (C_F + C_R) \cdot \frac{1}{2}\rho V^2 \cdot S \qquad\qquad\qquad (\text{ B.1 })$$

With:

- C_F, the frictional resistance coefficient;
- C_R, the residual resistance coefficient;
- ρ, the seawater density;
- V, design speed of the ferry;
- S, wetted surface area.

The seawater density is independent on the design of the ferry, thus it is a constant in this analysis ($\rho = 1{,}025\ kg/m^3$). The design speed is constant as well ($V = 30\ knots = 30 \cdot 1{,}852/3{,}600\ m/s$). The other three variables have to be estimated. This will be discussed in this appendix.

Structure of this Appendix
The frictional resistance coefficient is discussed in **appendix B.1**, followed by the residual resistance coefficient **appendix B.2**. The estimation for the wetted surface area can be found in **appendix B.3**. The complete overview of the total resistance is discussed in **appendix B.4**, in which also is explained how the propulsion power and energy consumption is related to the resistance.

B.1 Frictional Resistance Coefficient

The frictional resistance coefficient takes the friction between the water and the hull into account. It can be calculated using the ITTC-57 formula (equation B.2), which is dependent on Reynolds number (equation B.3), which is a function of ship's velocity (V), length of the vessel (L), and viscosity of the water (v).

$$C_F = \frac{0.075}{(\log_{10} Rn - 2)^2}$$
(B.2)

$$Rn = \frac{V \cdot L}{v}$$
(B.3)

Like the design speed of the ferry, the viscosity of water is independent of the design of the vessel, so it is constant in this estimation ($v = 1.2 \cdot 10^{-6} \, m^2/s$). This means that the frictional resistance coefficient is only a function of length of the ferry, according to equation B.4. This is also illustrated in figure B.1.

$$C_F = \frac{0.075}{\left(\log_{10}\left(\frac{V}{v} \cdot L\right) - 2\right)^2}$$
(B.4)

With:
- $V = 30 \cdot 1{,}852/3{,}600 \, m/s$;
- $v = 1.2 \cdot 10^{-6} \, m^2/s$.
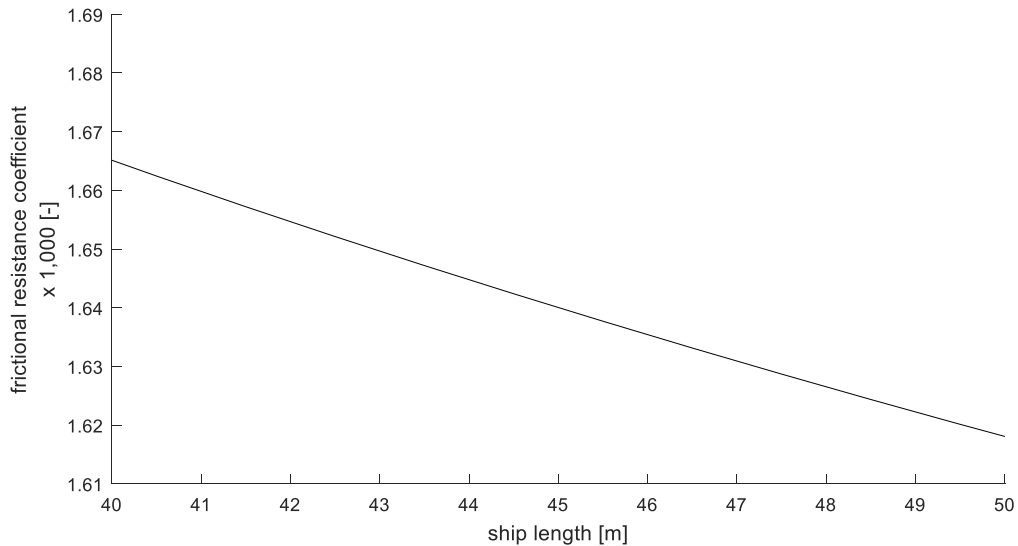
Figure B.1: frictional resistance plotted against length of the ferry, according to equation B.4.

B.2 Residual Resistance Coefficient

Besides skin friction, there are other resistance components, such as pressure resistance and wave making resistance. Al these components together are represented by the residual resistance coefficient, which is dependent on the hull shape and the Froude number (Fn), a dimensionless expression for the ship's velocity (V):

$$Fn = \frac{V}{\sqrt{g \cdot L}}$$
(B.5)

Both velocity and gravitational acceleration (g) are constant, so Froude number is only dependent on the length of the ferry.

How the resistance changes with the hull characteristics has to be estimated. For this purpose, a resistance analysis of a systematic demi-hull series is used, as such a study contains information on how changes in hull characteristics affect the resistance. Two criteria were important for the choice of systematic demi-hull analysis:

- The study had to be representative, i.e. the hull characteristics of CoCo Yachts' Coastal Cruiser 300 must fall within the range of hull characteristics of the systematic demi-hull series;
- The study must provide insight in the effect of a longer hull, i.e. the slenderness ratio has to go higher than that of the Coastal Cruiser 300.

Based on these criteria, the analysis of X.P. Pham, K. Kantimahanthi and P.K. Sahoo was chosen [119]. Their goal was to obtain a speed independent prediction equation. For that purpose they did a regression analysis on the residual resistance coefficients that they obtained via the software package SHIPFLOW. The analysis and prediction equation is not very useful for this thesis, because it is not accurate enough due to its speed independency. The generated data however is useful, which contains the residual resistance coefficient for 18 demi-hull models, four demi-hull separation ratios (0.2 to 0.5) and 12 Froude numbers (0.4 to 1.5).

Table B.1 contains the characteristics of the 18 demi-hull models. The closest match with the Coastal Cruiser 300, based on these characteristics, is model M8. Using this model to estimate the residual resistance coefficient of the Coastal Cruiser 300 results in an over estimation of over 10%, compared to the known values if this vessel [120].

So the value of the residual resistance coefficient is not representative for the Coastal Cruiser, and thus neither for its future electric version, as the resistance coefficient is much higher. Despite this, the data is still useful, as it contains information on how the resistance is influenced by the main demi-hull characteristics.

Table B.1: characteristics of the models of the systematic catamaran demi-hull series of X.P. Pham, K. Kantimahanthi and P.K. Sahoo. [119]

Models	M1	M2	M3	M4	M5	M6	M7	M8	M9	M10	M11	M12	M13	M14	M15	M16	M17	M18
C_B	0.50	0.50	0.50	0.50	0.50	0.55	0.55	0.55	0.55	0.55	0.60	0.60	0.60	0.60	0.60	0.60	0.55	0.59
L/B	10.40	10.40	15.60	20.80	20.80	10.40	15.60	15.60	15.60	20.60	10.40	10.40	15.60	15.60	20.80	20.80	13.00	17.20
B/T	1.50	2.50	2.00	1.50	2.50	2.00	1.50	2.00	2.50	2.00	1.50	2.50	1.50	2.00	1.50	2.50	1.86	1.60
$L/\nabla^{1/3}$	6.69	7.93	9.67	10.62	12.58	7.13	8.49	9.35	10.08	11.33	6.30	7.47	8.24	9.09	9.98	11.86	8.07	9.12
S/L^2	0.16	0.12	0.09	0.08	0.06	0.14	0.11	0.09	0.08	0.07	0.17	0.13	0.11	0.09	0.08	0.06	0.11	0.10

B.2.1 Excluding Models from the Systematic Demi-Hull Analysis

The following four demi-hull characteristics where presented for the 18 models, as seen in table B.1:

- Block coefficient (C_B);
- Length/beam-ratio (L/B);
- Beam/draft-ratio (B/T);

- Slenderness ration ($L/\nabla^{1/3}$).

An important thing to keep in mind is that these characteristics are demi-hull characteristics, which means that B is the demi-hull beam, not the overall beam of the catamaran, and ∇ is the displacement volume of one demi-hull, not of the whole catamaran (∇_{cat}):

$$\nabla_{cat} = 2 \cdot \nabla \qquad\qquad\qquad\qquad\qquad\qquad\qquad\qquad (\text{ B.6 })$$

Of the characteristics above, the slenderness ratio is the most important factor for resistance. It is why the catamaran exists; two demi-hulls have less resistance than one monohull, because they are more slender, more streamlined. For this reason it makes sense to plot the residual resistance coefficients, against slenderness ratio, as seen in figure B.2. This figure shows some deviating coefficients that are either higher or lower than both their neighbouring data points, while they are expected to be in between the values of their neighbouring data points. Looking at the characteristics, it is not possible to explain these anomalies, as the characteristics do not deviate much from their neighbouring models when ordered from lowest to highest slenderness ratio. The paper does not contain an explanation for these results, but a reason might be better or worse optimized hull forms, unexplained hull interactions, or errors in the analysis.
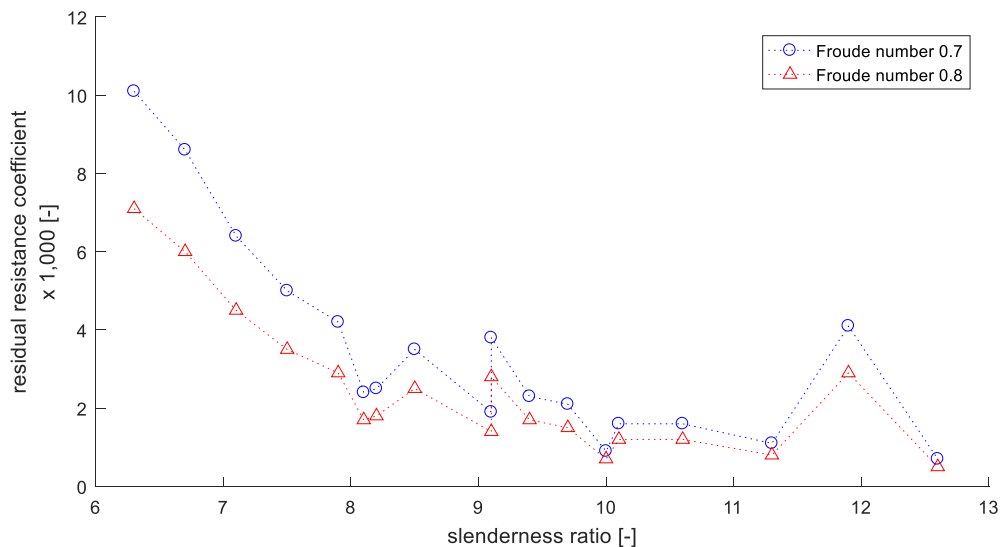
Figure B.2: residual resistance coefficient for different slenderness ratios, for all 18 demi-hulls, for a hull separation ratio of 0.2. [119]

To better predict the resistance, the deviating models are left out of the analysis. This results in the plot as seen in figure B.3. Table B.2 contains the remaining demi-hull models with their characteristics and their residual resistance coefficients, ordered from lowest to highest slenderness ratio.

Note that the focus in these figures and tables is on a demi-hull separation ratio 0.2 and Froude numbers 0.8, as this closely matches the operation of the Coastal Cruiser 300. Because the electric ferry might increase in length, a Froude number of 0.70 is also included as the lower limit, which corresponds to a ship length of 49.6 meters. Vessels longer than this are not acceptable due to operational limits [21].
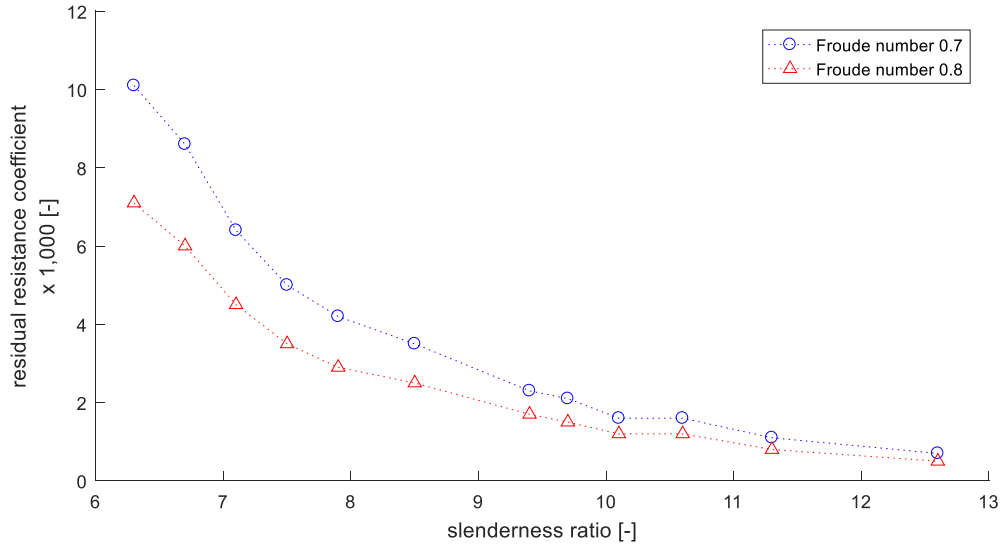
Figure B.3: residual resistance coefficient for different slenderness ratios, for models M11, M1, M6, M12, M2, M7, M8, M3, M9, M4, M10 and M5 (from left to right), for a hull separation ratio of 0.2. [119]

Table B.2: demi-hull characteristics and residual resistance coefficients (for $b/L = 0.2$) of the remaining models of the systematic study, ordered from lowest to highest slenderness ratio.   [119]

$L/\nabla^{1/3}$	6.3	6.7	7.1	7.5	7.9	8.5	9.4	9.7	10.1	10.6	11.3	12.6
$Model$	M11	M1	M6	M12	M2	M7	M8	M3	M9	M4	M10	M5
C_B	0.60	0.50	0.55	0.60	0.50	0.55	0.55	0.50	0.55	0.50	0.55	0.50
L/B	10.4	10.4	10.4	10.4	10.4	15.6	15.6	15.6	15.6	20.8	20.6	20.8
B/T	1.5	1.5	2.0	2.5	2.5	1.5	2.0	2.0	2.5	1.5	2.0	2.5
S/L^2	0.17	0.16	0.14	0.13	0.12	0.11	0.09	0.09	0.08	0.08	0.07	0.06
C_R x1,000												
Fn = 0.7	10.1	8.6	6.4	5.0	4.2	3.5	2.3	2.1	1.6	1.6	1.1	0.7
Fn = 0.8	7.1	6.0	4.5	3.5	2.9	2.5	1.7	1.5	1.2	1.2	0.8	0.5

B.2.2 Demi-Hull Characteristics and Residual Resistance Coefficient

When looking at the characteristics of the model hulls (table B.2), it can be noted that there are three other parameters besides slenderness ratio ($L/\nabla^{1/3}$) that determine the hull form and thus the resistance: block coefficient (C_B), length/beam-ratio (L/B) and beam/draft-ratio (B/T). These four parameters are not independent of each other, as they can be related to each other.

Block coefficient is defined as the displacement volume divided by the volume of a block with the same dimensions as the hull:

$$C_B = \frac{\nabla}{L \cdot B \cdot T}$$

(B.7)

So the block coefficient contains all four variables of the other hull characteristics, which suggest that they can be related to each other in the following way:

$$(C_B)^\alpha = \left(\frac{\nabla}{L \cdot B \cdot T}\right)^\alpha = \left(\frac{L}{\nabla^{\frac{1}{3}}}\right)^\beta \cdot \left(\frac{L}{B}\right)^\gamma \cdot \left(\frac{B}{T}\right)^\delta \qquad (\text{ B.8 })$$

Regrouping each variable leads to the following expressions and values:

$$\nabla^\alpha = \nabla^{-\frac{1}{3}\beta} \rightarrow \beta = -3\alpha \qquad (\text{ B.9 })$$

$$L^{-\alpha} = L^\beta \cdot L^\gamma \rightarrow \gamma = -\alpha - \beta = -\alpha - (-3\alpha) = 2\alpha \qquad (\text{ B.10 })$$

$$B^{-\alpha} = B^{-\gamma} \cdot B^\delta \rightarrow \delta = -\alpha + \gamma = -\alpha + (2\alpha) = \alpha \qquad (\text{ B.11 })$$

The draft can be used to check the value of δ:

$$T^{-\alpha} = T^{-\delta} \rightarrow \delta = \alpha \qquad (\text{ B.12 })$$

The smallest integer value of α is 1, and thus $\beta = -3$, $\gamma = 2$ and $\delta = 1$. Equation B.8 can be rewritten as a function of slenderness ratio, and when these values are used as well, the result is as follows:

$$\left(L/\nabla^{1/3}\right)^3 = \frac{(L/B)^2 \cdot (B/T)}{C_B} \qquad (\text{ B.13 })$$

The equation above gives a good insight into how each characteristic influences the demi-hull slenderness ratio, and thus the resistance:
- The length-beam ratio has the most influence, as this is the only variable that is squared;
- A higher length-beam ratio results in a higher slenderness ratio;
- A higher beam-draft ratio results in a higher slenderness ratio;
- A lower block coefficient results in a higher slenderness ratio.

A high beam-draft ratio combined with a low block coefficient results in a lower resistance than a demi-hull with a low B/T-ratio and a high C_B. This is illustrated in figure B.4. The same data points can also be plotted against slenderness ratio, as is done in figure B.5. This figure shows that the slenderness ratio has by far the most impact on the resistance, as the difference due to the other factors is decreased to only four percent or less.

This confirms that the slenderness ratio is the most important factor for resistance, when comparing different hulls of the same family. The other three demi-hull characteristics (length-beam ratio, beam-draft ratio and block coefficient) can be altered to optimize the hull for resistance, but without changing the slenderness ratio, the improvements are only minor.

It can be concluded that for a family of demi-hulls, the slenderness ratio is the most dominant factor for determining the resistance. Molland et al. also concluded that slenderness ratio is the most significant hull parameter with respect to resistance [100]. This means that the residual resistance coefficient of a catamaran can be estimated with sufficient accuracy when using the slenderness ratio as the only hull characteristic. Thus only the length and displacement are required for the resistance estimation at a certain speed.
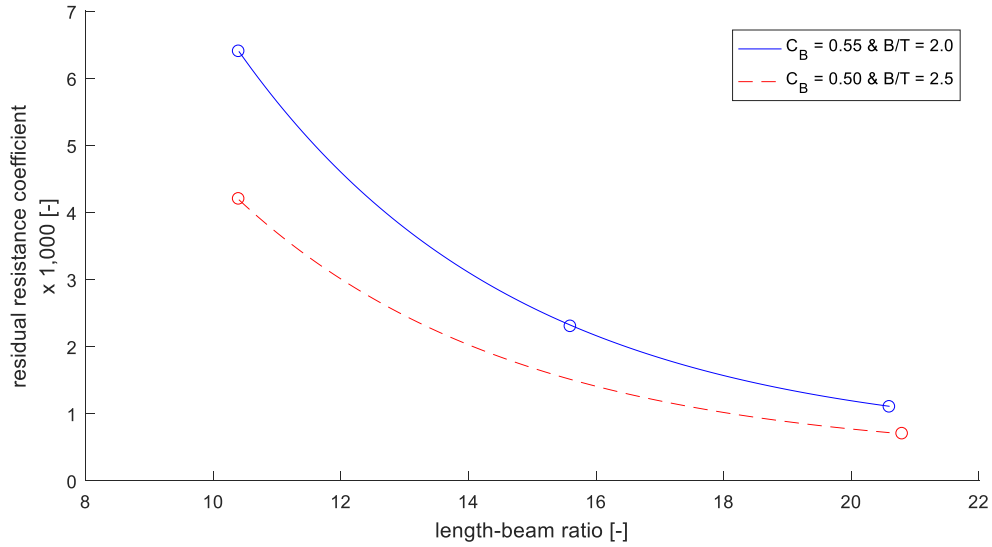
Figure B.4: residual resistance coefficient for different length-beam ratios, for a block coefficient of 0.55 and a beam-draft ratio of 2.0 (solid blue curve), and for $C_B = 0.50$ and $B/T = 2.5$ (dashed red curve), both for $Fn = 0.7$ [119]. The two curves are created with equation B.15 and B.17.
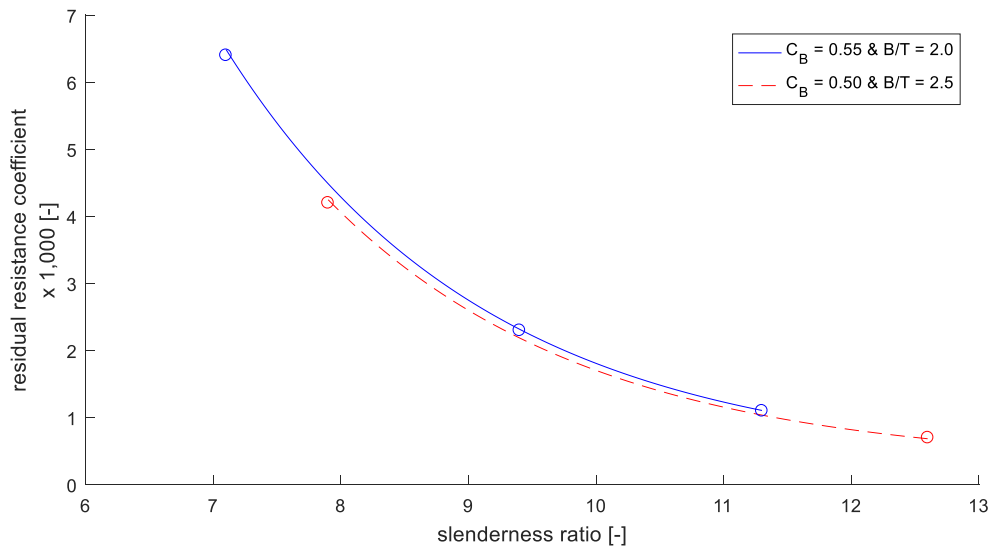
Figure B.5: residual resistance coefficient for different slenderness ratios for a block coefficient of 0.55 and a beam-draft ratio of 2.0 (solid blue curve), and for $C_B = 0.50$ and $B/T = 2.5$ (dashed red curve), both for $Fn = 0.7$ [119]. The two curves are created with equation B.16 and B.18.

B.2.3 Exponential Fitted Function

The curves in figure B.4 and B.5 are created with an exponential function of the following form:

$$C_{R.i} = a + b \cdot \exp(-c \cdot x), \qquad with \ x = L/B \ or \ x = L/\nabla^{1/3} \tag{B.14}$$

The reason this type of function is chosen is that it shows the best fit the data points; not only with the data of the systematic analysis that is discussed up until now, but also of the study of Molland et al. that will be discussed in the next subparagraph.

The subscript i in the expression indicates the Froude number, e.g. $i = 7$ indicates $Fn = 0.7$, and $C_{R.8}$ is the residual resistance coefficient at Froude number 0.8.

As there are three unknows (a, b and c), at least three data points are required for such an exponential curve. The blue curves in the two figures are plotted with the following equations that are determined with the three data points:

$$C_{R.7} \times 1,000 = 0.55 + 64 \cdot \exp(-0.23 \cdot L/B), for\ C_B = 0.55, B/T = 2.0 \qquad (\ B.15\ )$$

$$C_{R.7} \times 1,000 = 0.32 + 2.0 \cdot 10^2 \cdot \exp\left(-0.49 \cdot L/\nabla^{1/3}\right), for\ C_B = 0.55, B/T = 2.0 \qquad (\ B.16\ )$$

The red dashed curves in the two figures are derived from the two equations above, as two data points is not enough to determine all three unknowns. a and b were changed to fit the curve through the two data points, while c was kept constant. This resulted in the following two equations:

$$C_{R.7} \times 1,000 = 0.35 + 42 \cdot \exp(-0.23 \cdot L/B), for\ C_B = 0.50, B/T = 2.5 \qquad (\ B.17\ )$$

$$C_{R.7} \times 1,000 = 0.29 + 1.9 \cdot 10^2 \cdot \exp\left(-0.49 \cdot L/\nabla^{1/3}\right), for\ C_B = 0.50, B/T = 2.5 \qquad (\ B.18\ )$$

Exponential functions can also be fitted through the data points of all remaining models, as seen in figure B.6. The following equations are used for respectively the solid blue curve and dashed red curve:

$$C_{R.7} \times 1,000 = 0.32 + 2.5 \cdot 10^2 \cdot \exp\left(-0.52 \cdot L/\nabla^{1/3}\right) \qquad (\ B.19\ )$$

$$C_{R.8} \times 1,000 = 0.18 + 1.5 \cdot 10^2 \cdot \exp\left(-0.49 \cdot L/\nabla^{1/3}\right) \qquad (\ B.20\ )$$
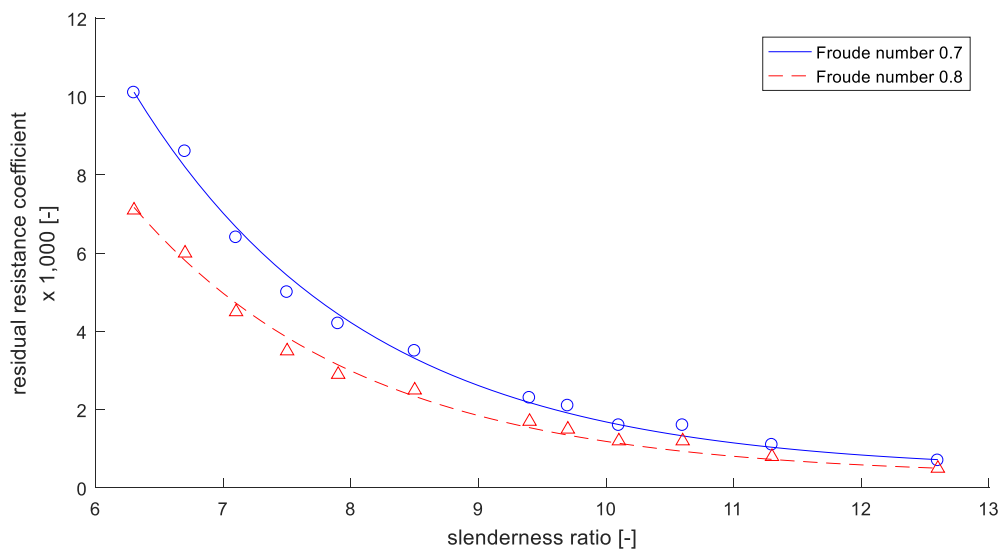
Figure B.6: residual resistance coefficient for different slenderness ratios, for models M11, M1, M6, M12, M2, M7, M8, M3, M9, M4, M10 and M5 (from left to right), for a hull separation ratio of 0.2 [119]. The two curves are created with equation B.19 and B.20.

A comparison between the data points and the estimation curve can be seen table B.3 and B.4. These tables also contain the relative error in percentage and the absolute error.

Looking at Froude number 0.7 (table B.3), all relative errors, with the exception of slenderness ratio 10.6, are 10% or less. At Froude number 0.8 (table B.4), the relative errors are slightly larger; 13% or less, with the exception of slenderness ratio 10.6. In both cases, the absolute error is less than $\pm 0.4 \times 1,000$, with an average of only $\pm 0.2 \times 1,000$. In subparagraph B.2.1 was already discussed that the data of the study showed some deviation in the residual resistance coefficients. It is therefore expected that the errors will be smaller if the demi-hulls would be better optimized.

Table B.3: comparison between residual resistance coefficients of the data [119] and of the estimation (equation B.19), for Froude number 0.7 (and $b/L = 0.2$).

slenderness ratio	$C_{R.7} \times 1,000$		relative error	absolute error [$\Delta C_R \times 1,000$]
	data	estimated		
6.3	10.1	10.1	0%	0.0
6.7	8.6	8.2	-5%	-0.4
7.1	6.4	6.7	5%	0.3
7.5	5.0	5.4	8%	0.4
7.9	4.2	4.4	5%	0.2
8.5	3.5	3.3	-6%	-0.2
9.4	2.3	2.2	-4%	-0.1
9.7	2.1	1.9	-10%	-0.2
10.1	1.6	1.6	0%	0.0
10.6	1.6	1.3	-19%	-0.3
11.3	1.1	1.0	-9%	-0.1
12.6	0.7	0.7	0%	0.0
		Average	$\pm 6\%$	± 0.2

Table B.4: comparison between residual resistance coefficients of the data [119] and of the estimation (equation B.20), for Froude number 0.8 (and $b/L = 0.2$).

slenderness ratio	$C_{R.8} \times 1,000$		relative error	absolute error [$\Delta C_R \times 1,000$]
	data	estimated		
6.3	7.1	7.2	1%	0.1
6.7	6.0	5.8	-3%	-0.2
7.1	4.5	4.7	4%	0.2
7.5	3.5	3.8	9%	0.3
7.9	2.9	3.1	7%	0.2
8.5	2.5	2.3	-8%	-0.2
9.4	1.7	1.5	-12%	-0.2
9.7	1.5	1.4	-7%	-0.1
10.1	1.2	1.1	-8%	-0.1
10.6	1.2	0.9	-25%	-0.3
11.3	0.8	0.7	-13%	-0.1
12.6	0.5	0.5	0%	0.0
		average	$\pm 8\%$	± 0.2

B.2.4 Molland et al.'s Systematic Demi-Hull Series

A.F. Molland, J.F. Wellicome and P.R. Couser analysed a systematic demi-hull series in 1994 [121]. Relevant data from this study can be seen in table B.5, and plotting this data is done in figure B.7 and B.8. It can be seen in these figures that at lower slenderness ratio, the demi-hull models of Molland et al. have lower resistances than those of Pham et al. [119]. Furthermore, the exponential curves (created with equation B.21 and B.22) that are fitted through the four data points have 0% error. This shows that an exponential equation seems to be the right choice to represent the residual resistance coefficient as function of slenderness ratio.

$$C_{R.7} \times 1,000 = 1.9 + 1.9 \cdot 10^2 \cdot \exp\left(-0.61 \cdot L/\nabla^{1/3}\right) \qquad (\text{ B.21 })$$

$$C_{R.8} \times 1,000 = 2.1 + 6.7 \cdot 10^2 \cdot \exp\left(-0.87 \cdot L/\nabla^{1/3}\right) \qquad (\text{ B.22 })$$

Table B.5: relevant characteristics and residual resistance coefficients of the models of the systematic demi-hull series, for $b/L = 0.2$.   [121]

$L/\nabla^{1/3}$	6.3	7.4	8.5	9.5
$Model$	3b	4a	5a	6a
C_B	0.40	0.40	0.40	0.40
L/B	7.0	10.4	12.8	15.1
B/T	2.0	1.5	1.5	1.5
C_R x1,000				
Fn = 0.7	6.0	4.0	3.0	2.5
Fn = 0.8	4.9	3.2	2.5	2.3
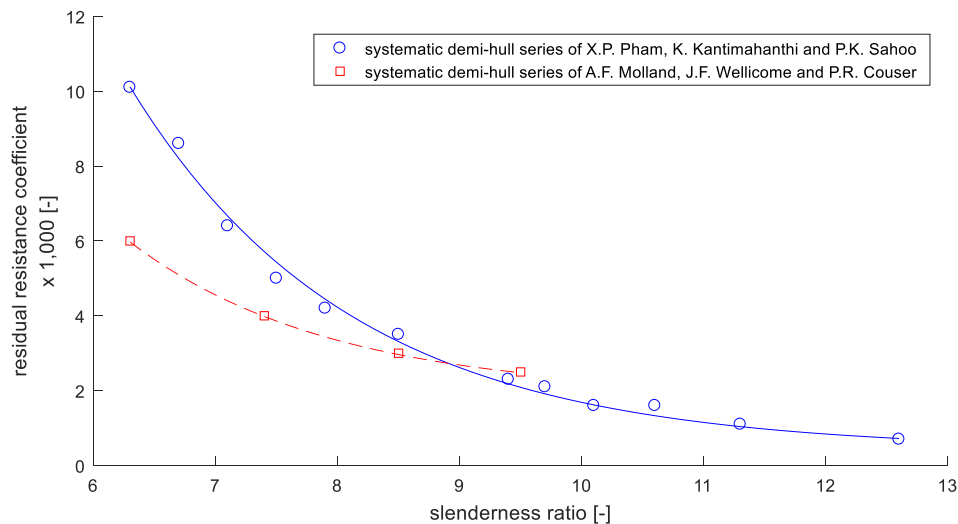
Figure B.7: residual resistance coefficient at Froude number 0.7 for different slenderness ratios for the systematic demi-hull series of Pham et al. [119] (red dashed curve) and Molland et al. [121] (blue solid curve).
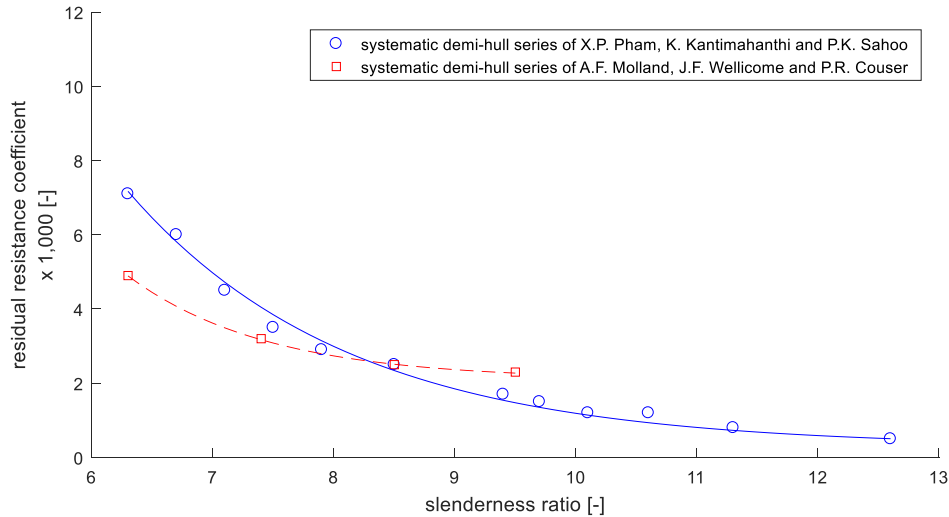
Figure B.8: residual resistance coefficient at Froude number 0.8 for different slenderness ratios for the systematic demi-hull series of Pham et al. [119] (red dashed curve) and Molland et al. [121] (blue solid curve).

B.2.5 Exponential Curve Fitted Through the Lowest Data Points

The following conclusions are drawn from the analysis in this appendix:

- The residual resistance coefficient can be estimated based on slenderness as only demi-hull parameter, for catamarans of the same family;
- An exponential equation results in a good estimation of the residual resistance coefficient;
- An optimized hull form (e.g. the CC300 hull) has a lower resistance than either systematic demi-hull series.

So the goal is to derive an exponential equation that goes through the data point of the Coastal Cruiser 300. The fact that both Coastal Cruisers have a lower residual resistance coefficient than either systematic demi-hull series leads to the expectation that the C_R of a Coastal Cruiser family would be lower over the whole range of slenderness ratios. However, how much lower is unknown. So instead the equation is based on the three lowest points that are known to be reachable:

- The systematic demi-hull series of A.F. Molland, J.F. Wellicome and P.R. Couser has the lowest C_R at low slenderness ratio ($L/\nabla^{1/3} = 6.3$);
- The Coastal Cruiser 300 has the lowest C_R at medium slenderness ratio;
- The systematic demi-hull series of X.P. Pham, K. Kantimahanthi and P.K. Sahoo has the lowest C_R at high slenderness ratio ($L/\nabla^{1/3} = 12.6$).

These chosen data points are used to form the exponential functions as seen in equation B.23 and B.24, for Froude number 0.7 and 0.8 respectively. These two equations are also plotted in figure B.9.

$$C_{R.7} \cdot 1{,}000 = 0.43 + 115 \cdot \exp\left(-0.48 \cdot L/\nabla^{1/3}\right) \tag{B.23}$$

$$C_{R.8} \cdot 1{,}000 = 0.26 + 90 \cdot \exp\left(-0.47 \cdot L/\nabla^{1/3}\right) \tag{B.24}$$
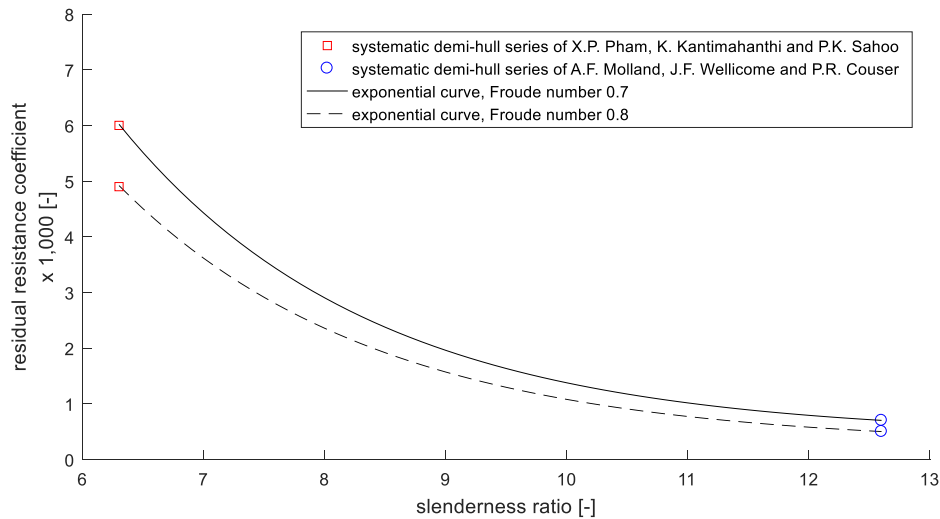
Figure B.9: estimated residual resistance coefficient at Froude number 0.7 (solid curve, equation B.23) and 0.8 (dashed curve, equation B.24), plotted against different slenderness ratios. Also plotted are the used data points of the systematic demi-hull series of Pham et al. [119] (red squares) and Molland et al. [121] (blue circles).

B.2.6 Varying Waterline Length

The previous subparagraph indicated that there is sufficient information for a residual resistance equation that can be used to estimate the resistance based on slenderness ratio. This is however only the case for Froude number 0.7 and 0.8, as there are no data points between these Froude numbers [119].

Interpolating over Froude Number

Estimating the values in between these Froude numbers can be done by interpolation. One way of interpolation is linear interpolation between the Froude numbers:

$$C_R = \frac{(0.8 - Fn) \cdot C_{R.7} + (Fn - 0.7) \cdot C_{R.8}}{0.8 - 0.7} \qquad (\text{ B.25 })$$

In this equation the residual resistance coefficient (C_R) is expressed as a function of Froude number (Fn) and the residual resistance coefficient at $Fn = 0.7$ and 0.8 ($C_{R.7}$ and $C_{R.8}$ respectively). The result is not so accurate, as seen in seen in figure B.10. In this figure, as well as in figure B.11, the data points of model M8 from the study of Pham et al. are used, as listed in table B.6. This table also contains the waterline length (L) corresponding to the Froude numbers, as calculated with the following equation:

$$L = \left(\frac{V}{Fn}\right)^2 / g = \left(\frac{30 \cdot \frac{1,852 \left[\frac{knots}{m/s}\right]}{3,600}}{Fn}\right)^2 / 9.81 \qquad (\text{ B.26 })$$

Table B.6: residual resistance coefficients for different Froude numbers for Model M8 of the study of Pham et al. [119]

Fn	0.6	0.7	0.8	0.9	1.0	1.1	1.2	1.3	1.4	1.5
$L\ [m]$	67.4	49.6	37.9	30.0	24.3	20.1	16.9	14.4	12.4	10.8
$C_R \times 1,000$	3.4	2.3	1.7	1.3	1.0	0.9	0.8	0.7	0.6	0.5

Figure B.10: residual resistance coefficient for different Froude numbers for model M8 (slenderness ratio of 9.4) [119], including a line that is interpolated between, and extrapolated outside, the data points of Froude number 0.7 and 0.8 (dashed line, equation B.25). The data points use for extrapolation can be recognized by an 'x'.

Interpolating over Waterline Length

If the design speed is constant, the Froude number is only dependent on length of the ferry. Therefore the residual resistance coefficient can also be written as a function of ship length (L). In that case, it can be linearly interpolated over ship length instead of Froude number, as is done in equation B.27. This method is more accurate, as seen in figure B.11; a significant difference only occurs at a very high length. It is deemed accurate enough that this way of linear interpolation is used in this thesis.

$$C_R = \frac{(L_{0.8} - L) \cdot C_{R.7} + (L - L_{0.7}) \cdot C_{R.8}}{L_{0.8} - L_{0.7}} \qquad (\text{ B.27 })$$

With $L_{0.8} = 37.9\ m$ (the length at Froude number 0.8), $L_{0.7} = 49.6\ m$ (length at Froude number 0.7), and $C_{R.7}$ and $C_{R.8}$ can be calculated with equation B.23 and B.24.

When looking at the systematic demi-hull study of Molland et al., the same interpolation method can be applied. Model 6 of the study has a slenderness ratio that is the closest match with the CC300, and with model M8 that is used above [121]. The data of two versions of this model are listed in table B.7.

Figure B.12 and B.13 show that linear interpolation between the waterline lengths of Froude numbers 0.7 and 0.8 is indeed a sufficiently accurate interpolation method.

Table B.7: residual resistance coefficients for different Froude numbers for Model 6a and 6c of the study of Molland et al. [121]

	Fn	0.6	0.7	0.8	0.9	1.0
Model 6a	$C_R \times 1,000$	4.59	3.19	2.53	2.11	2.03
Model 6b	$C_R \times 1,000$	4.15	3.08	2.05	2.17	2.07

Figure B.11: residual resistance coefficient for different ship lengths for model M8 (slenderness ratio of 9.4) [119], including a line that is interpolated between, and extrapolated outside, the data points of Froude number 0.7 and 0.8 (dashed line, equation B.27). The data points use for extrapolation can be recognized by an 'x'.
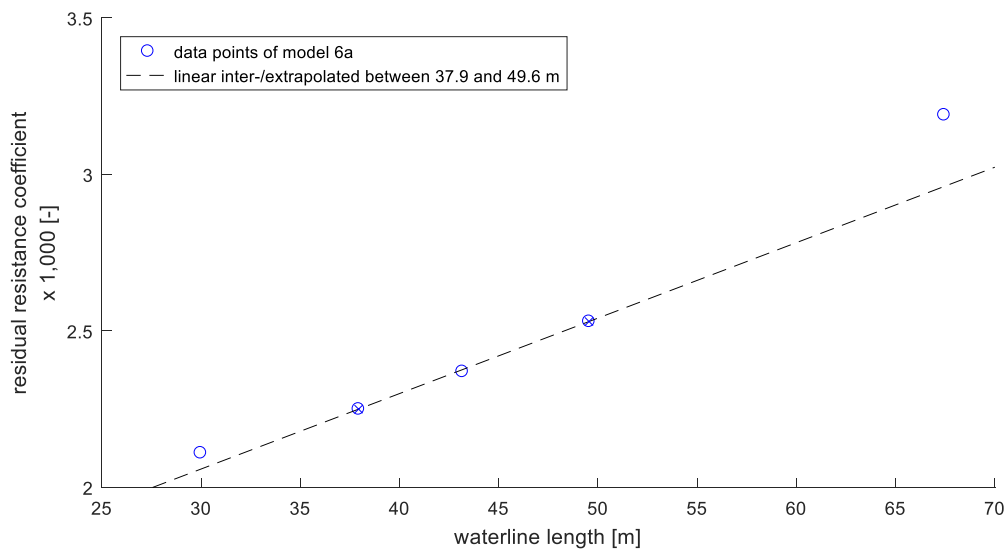
Figure B.12: residual resistance coefficient for different ship lengths for model 6a (slenderness ratio of 9.5) [121], including a line that is interpolated between, and extrapolated outside, the data points of Froude number 0.7 and 0.8 (dashed line, equation B.27). The data points use for extrapolation can be recognized by an 'x'.
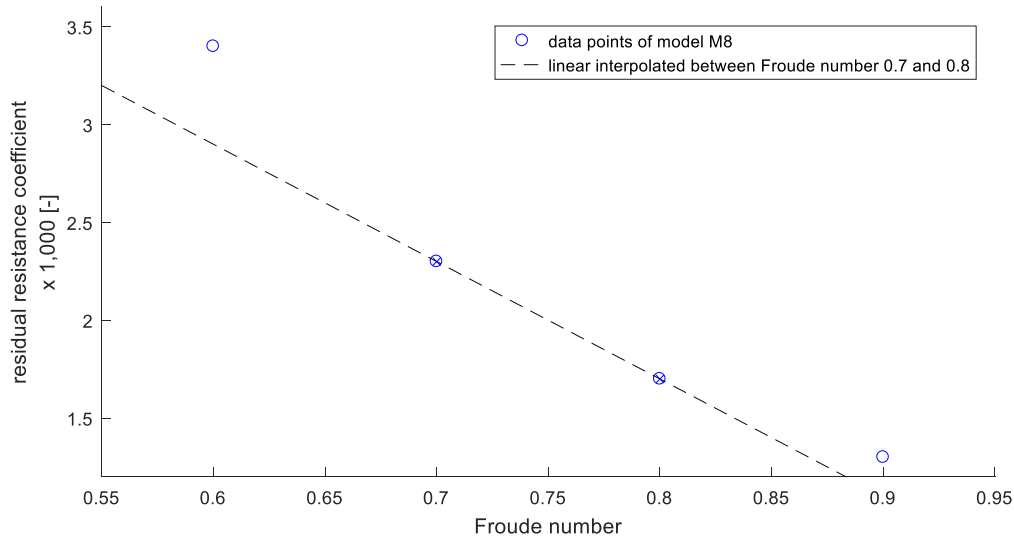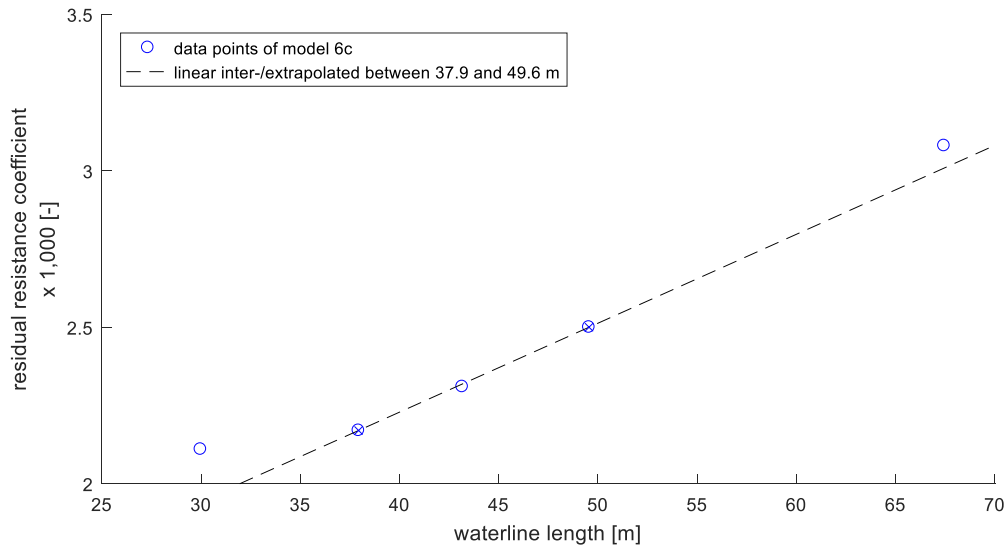
Figure B.13: residual resistance coefficient for different ship lengths for model 6b (slenderness ratio of 9.5) [121], including a line that is interpolated between, and extrapolated outside, the data points of Froude number 0.7 and 0.8 (dashed line, equation B.27). The data points use for extrapolation can be recognized by an 'x'.

B.2.7 Varying Velocity

In paragraph 5.4, the effect of sailing at a lower speed is analysed. Linear interpolation between waterline lengths changes to extrapolation when the velocity changes. As seen in figures B.11 to B.13, the estimation method gets less accurate when it is extrapolated. Therefore another method is used: extrapolation based on velocity.

With equation B.23 and B.24, the residual resistance coefficient can be calculated for Froude number 0.7 and 0.8 respectively. This means that for each waterline length (39.5 and 46.5 m), the residual resistance coefficient can be estimated for two velocities. This can be seen in table B.8, where the speed is calculated with the following equation:

$$V\,[knots] = Fn \cdot \sqrt{gL} \,/\, \frac{3{,}600}{1{,}852} \left[\frac{knots}{m/s}\right]$$

(B.28)

Table B.8: speed of the vessel as a function of waterline length (L) and Froude number (Fn).

		39.5	46.5	m
$Fn = 0.7$	$V_{0.7}$	26.8	29.1	knots
$Fn = 0.8$	$V_{0.8}$	30.6	33.2	knots

Extrapolating over Velocity

Extrapolating outside the velocities of table B.8 is done with the following inter-/extrapolation equation:

$$C_R = \frac{(V_{0.8}^{-2.8} - V^{-2.8}) \cdot C_{R.7} + (V^{-2.8} - V_{0.7}^{-2.8}) \cdot C_{R.8}}{V_{0.8}^{-2.8} - V_{0.7}^{-2.8}}$$

(B.29)

In this equation, $V_{0.7}$ and $V_{0.8}$ are the velocities that corresponds to Froude number 0.7 and 0.8 respectively, as listed in table B.8. $C_{R.7}$ and $C_{R.8}$ are the residual resistance coefficients that corresponds to Froude number 0.7 and 0.8, which can be calculated with equations B.23 and B.24.

It can be noted that equation B.29 is not linear inter-/extrapolation, but to the power '-2.8'. Figure B.14 illustrates that this is a sufficient estimation method. The data points in this figure are the residual resistance coefficients as listed in table B.6, combined with equation B.28, and the concept waterline lengths of waterline 39.5 and 46.5 m.

The equation for interpolation over length (equation B.27) can also be altered by adding a power to it. This does however not lead to a satisfying result; the relation between resistance and length is more complicated than between resistance and velocity.
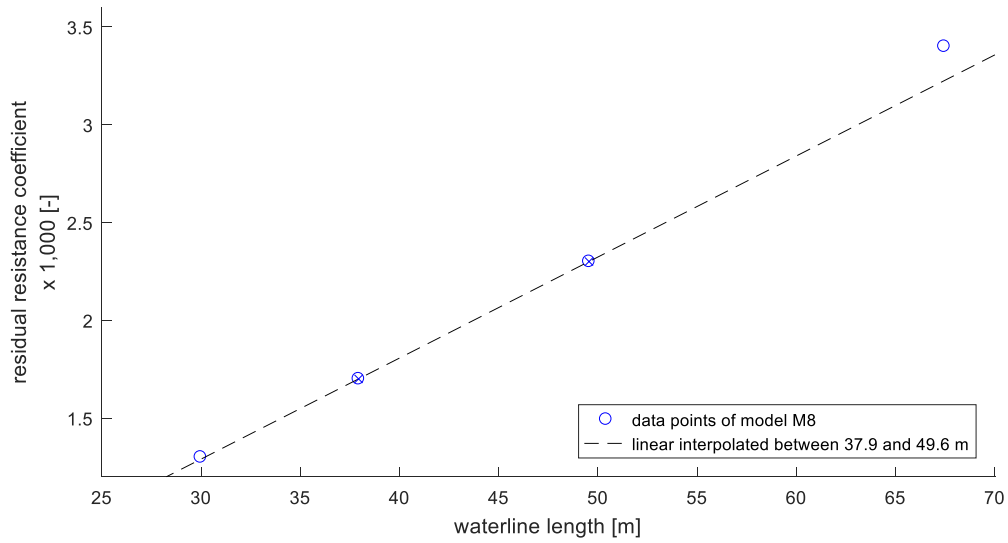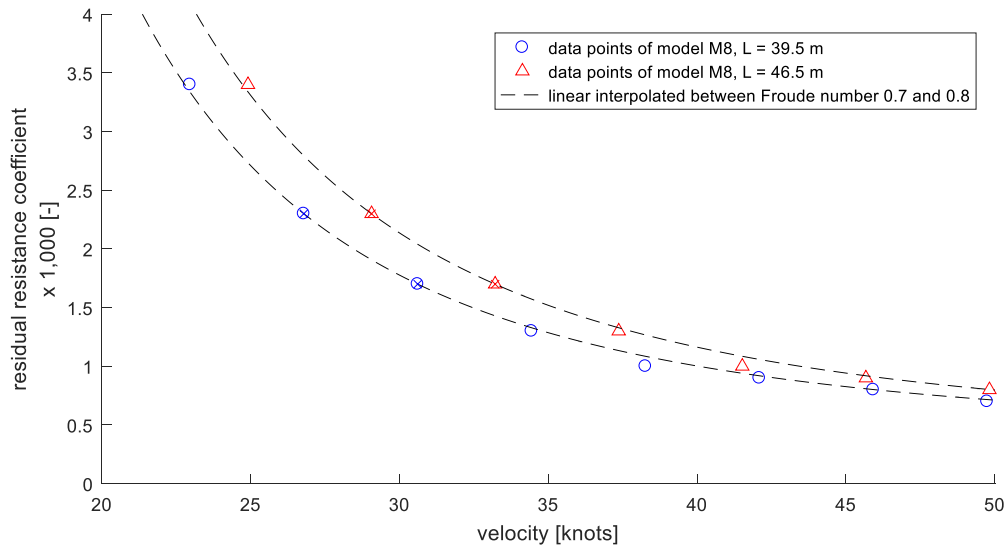

Figure B.14: residual resistance coefficient for different velocities for model M8 (slenderness ratio of 9.4) [119], including a curve that is interpolated between, and extrapolated outside, the data points of Froude number 0.7 and 0.8 (dashed line, equation B.29). The data points use for extrapolation can be recognized by an 'x'.

The extrapolation method can also be used with the study of Molland et al.. Figure B.15 shows that for model 6a, the velocity extrapolation method is reasonably accurate at higher velocities and figure B.16 shows that for model 6b, the extrapolation is reasonably accurate for lower velocities. These results might introduce some doubts about the estimation method. However, when using equation B.29 in combination with the estimation equations for the residual resistance coefficients (equation B.23 and B.24), the result for the Coastal Cruiser 300 is accurately matched, as seen in figure B.17. The power '-2.8' is also chosen as this has the best match with the CC300.

It should be mentioned that this interpolation method is valid for Froude numbers above roughly 0.5. Around this Froude number lies the peak of residual resistance coefficient [121]. This can also be seen in figure B.18, and it means that if the speed is reduced below this point, the residual resistance coefficient will decrease with decreasing speed instead of increase. Froude number 0.5 corresponds to around 20 knots for the concept ferry, as calculated with equation B.28:

$$V = 0.5 \cdot \sqrt{9.81 \cdot \{39.5\text{-}46.5\}} \times \frac{3{,}600}{1{,}852} \left[\frac{knots}{m/s}\right] = \{19\text{-}21\}\, knots$$
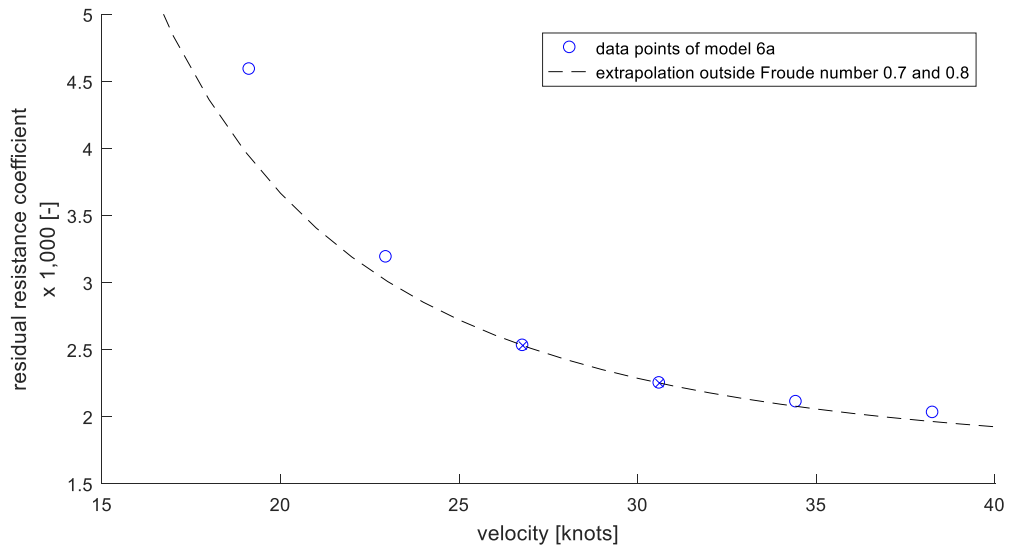
Figure B.15: residual resistance coefficient for different velocities for model 6a (slenderness ratio of 9.5) [121], including a line that is interpolated between, and extrapolated outside, the data points of Froude number 0.7 and 0.8 (dashed line, equation B.29). $L = 39.5\ m$. The data points use for extrapolation can be recognized by an 'x'.
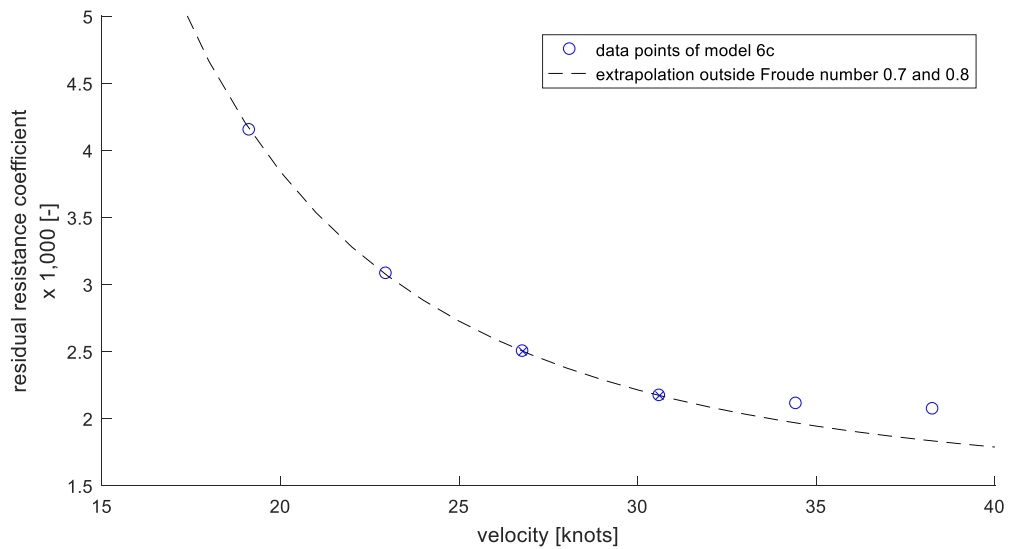
Figure B.16: residual resistance coefficient for different velocities for model 6b (slenderness ratio of 9.5) [121], including a line that is interpolated between, and extrapolated outside, the data points of Froude number 0.7 and 0.8 (dashed line, equation B.29). $L = 39.5\ m$. The data points use for extrapolation can be recognized by an 'x'.
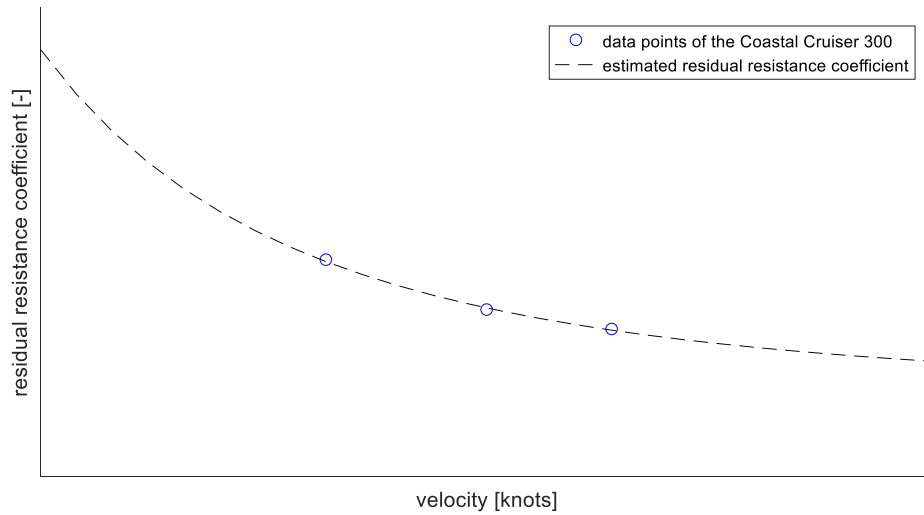
Figure B.17: residual resistance coefficient of the Coastal Cruiser 300 for different velocities [120],
and estimated residual resistance coefficient (dashed line, equations B.29).
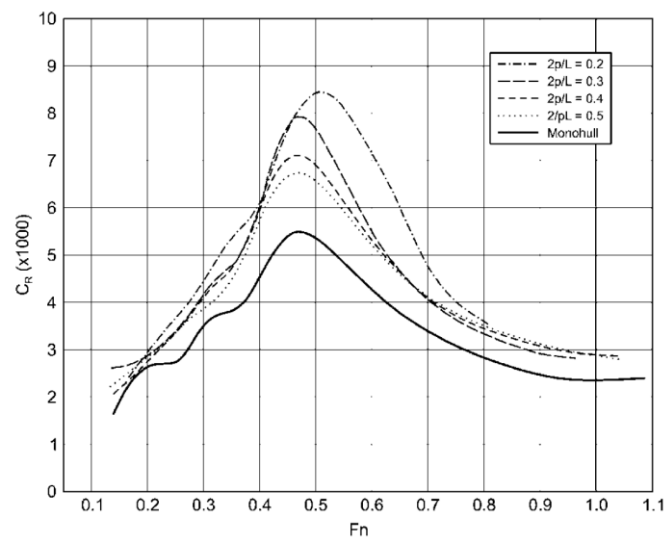
Figure B.18: residual resistance coefficient of model 4b of   [100]
the systematic demi-hull series of Molland et al.

B.3 Wetted Surface Area

The wetted surface area (S) is an important factor in estimating the resistance ($R = C_T \cdot \frac{1}{2}\rho V^2 \cdot S$). Not only the displacement, but also the hull shape determines the wetted surface area.

The data of the systematic demi-hull series (table B.2) contains a ratio between wetted surface area and length of the vessel (S/L^2). This can be combined with the slenderness ratio to obtain the wetted surface area as a ratio of displacement:

$$S/\nabla^{2/3} = (S/L^2) \cdot \left(L/\nabla^{1/3}\right)^2 \tag{B.30}$$

Plotting this ratio is done in figure B.19, which shows that a linear line can be fitted through these data points (created with equation B.31). There seems to be some deviation between the data points, but one must keep in mind that this is due to lack of accuracy, as the wetted-surface-area/length-ratio is only expressed by two decimals, which in some cases results in only one significant number (e.g. $S/L = 0.09$, for $L/\nabla^{1/3} = 9.4$).

$$\left(S/\nabla^{2/3}\right)_{model} = 0.41 \cdot \left(L/\nabla^{1/3}\right) + 4.3 \tag{B.31}$$

If the slenderness ratio of the Coastal Cruiser 300 is used with equation B.31 to calculate the wetted-surface-area/displacement-ratio, the result is 5% higher than the real wetted surface area of the Coastal Cruiser 300 [120]. The real ratio of the CC199 is also 5% lower than when estimated with this equation [122]. Compensating for this leads to the following result:

$$S/\nabla^{2/3} = (100\% - 5\%) \times \left(S/\nabla^{2/3}\right)_{model} = 0.39 \cdot \left(L/\nabla^{1/3}\right) + 4.1 \tag{B.32}$$

This equation can be rewritten to an expression for the wetted surface area as a function of the length and displacement of the vessel, which is done in equation B.33. Note that a two is added to the equation, as there are two demi-hulls, and the displacement in these equations is the volume of one demi-hull.

$$S = 2 \cdot \left(S/\nabla^{2/3}\right) \cdot \nabla^{2/3} = 0.78 \cdot L \cdot \nabla^{1/3} + 8.2 \cdot \nabla^{2/3} \tag{B.33}$$
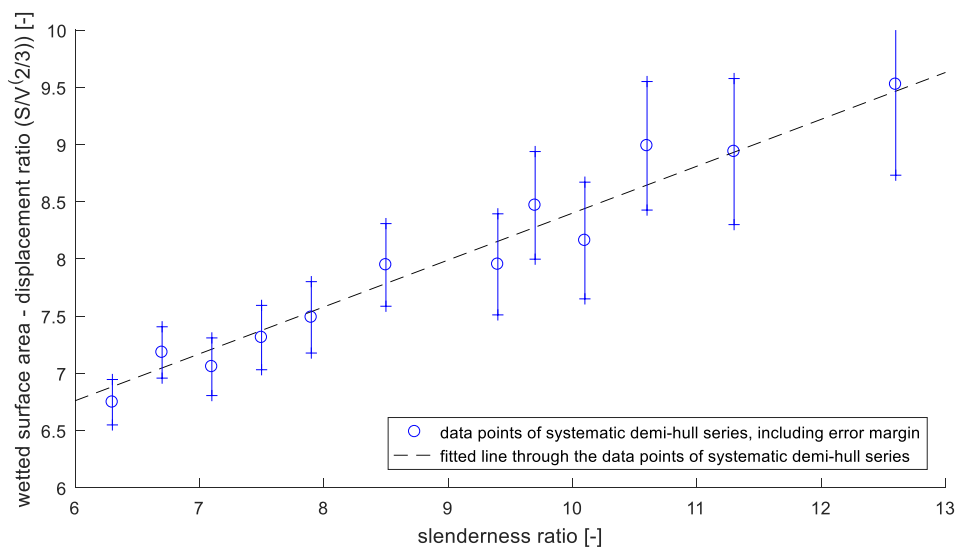
Figure B.19: wetted-surface-area/displacement-ratio ($S/\nabla^{2/3}$), for different slenderness ratios. The data points with their error margin are blue, and the black dashed line that is fitted through these points is created with equation B.31.

B.4 Total Ship Resistance, Propulsion Power and Energy Consumption

Up until now, only the hull resistance (R_{hull}) was discussed in the appendix, which is the largest part of the total resistance of a ship (R). Other parts are appendage drag (R_{app}) and air resistance (R_{air}):

$$R = R_{hull} + R_{app} + R_{air} \qquad\qquad (\text{ B.34 })$$

Appendage Drag

Because the ferry is a catamaran with waterjet propulsion, there are no rudders, propeller shaft struts, or stabilizer fins. Thus there are no appendages that contribute to the resistance of the ferry, so there is no appendage drag: $R_{app} = 0\ kN$.

Air Resistance

Air resistance does play a role, but since no significant changes will be made to the part of the ferry that contributes to this resistance component, it is kept constant for the design speed of 30 knots ($R_{air_{30\ knots}} = \mathbf{X}\ kN$). In case of the Coastal Cruiser 300, the air resistance is less than 5% of the total resistance [120]. So even if this resistance component changes for the electric ferry, its impact is small enough that a constant value is sufficient for this estimation method.

When the velocity of the ship changes, the air resistance changes as well. Like other resistance components, the air resistance is a function of the velocity squared, thus it can be estimated using the velocity ratio squared:

$$R_{air} \sim V^2 \rightarrow R_{air} = R_{air_{30\ knots}} \cdot \left(\frac{V\ [knots]}{30\ [knots]}\right)^2 \qquad\qquad (\text{ B.35 })$$

B.4.1 Overview of the Resistance Estimation Equations

In this thesis, the following equations are used for estimating the resistance of the catamaran ferry:

$$R = (C_F + C_R) \cdot \frac{1}{2}\rho V^2 \cdot S + R_{air} \qquad\qquad (\text{ B.36 })$$

With:

- $$C_F = \frac{0.075}{\left(\log_{10}\left(\frac{V}{\nu} \cdot L\right) - 2\right)^2} \qquad\qquad \text{Ref. (B.4)}$$

- $$C_R = \frac{(L_{0.8} - L) \cdot C_{R.7} + (L - L_{0.7}) \cdot C_{R.8}}{L_{0.8} - L_{0.7}} \qquad\qquad \text{Ref. (B.27)}$$

    - $$C_{R.7} \cdot 1{,}000 = 0.43 + 115 \cdot \exp\left(-0.48 \cdot L/\nabla^{1/3}\right) \qquad\qquad \text{Ref. (B.23)}$$

    - $$C_{R.8} \cdot 1{,}000 = 0.26 + 90 \cdot \exp\left(-0.47 \cdot L/\nabla^{1/3}\right) \qquad\qquad \text{Ref. (B.24)}$$

- $$S = 0.78 \cdot L \cdot \nabla^{1/3} + 8.2 \cdot \nabla^{2/3} \qquad\qquad \text{Ref. (B.33)}$$

- $$R_{air} = R_{air_{30\ knots}} \cdot \left(\frac{V\ [knots]}{30\ [knots]}\right)^2 \qquad\qquad \text{Ref. (B.35)}$$

These equations contain the following constants:

- $\rho = 1,025 \, kg/m^3$;
- $V = 30 \cdot 1,852/3,600 \, m/s$;
- $v = 1.2 \cdot 10^{-6} \, m^2/s$;
- $L_{0.7} = 49.6 \, m$;
- $L_{0.8} = 37.9 \, m$;
- $R_{air_{30 \, knots}} = \mathbf{X} \, kN$.

The two input variables in the equations are indicated in red:
- L, waterline length of the vessel;
- ∇, displacement of one demi-hull ($\nabla = \Delta_{cat}/\rho/2$).

Varying Speed

If instead of the length of the vessel, the speed is a variable (V, indicated in blue), equation B.27 above is replaced by equation B.29:

$$C_R = \frac{(V_{0.8}^{-2.8} - V^{-2.8}) \cdot C_{R.7} + (V^{-2.8} - V_{0.7}^{-2.8}) \cdot C_{R.8}}{V_{0.8}^{-2.8} - V_{0.7}^{-2.8}}$$

Ref. (B.29)

The velocity values ($V_{0.7}$ and $V_{0.8}$) are listed in table B.8.

Ref. table B.8: speed of the vessel as a function of waterline length (L) and Froude number (Fn).

		39.5	46.5	m
$Fn = 0.7$	$V_{0.7}$	26.8	29.1	knots
$Fn = 0.8$	$V_{0.8}$	30.6	33.2	knots

The table header first column is L.

B.4.2 Hull Interference

The waves that are generated by one demi-hull interfere with those of the other demi-hull. This is called the hull interference. In general, the closer the hulls are together, the larger the interference, and therefore the larger the resistance. This also follows from the systematic demi-hull series study of X.P. Pham, K. Kantimahanthi and P.K. Sahoo [119]. Other studies also indicate a higher resistance when the demi-hulls are closer together [123] [124]. However, hull interference is not in all cases negative, as some configurations result in no interference, or even positive interference effects [121] [124]. What all these studies show is that hull interference is a very complex process that it is influenced by many factors. That fact that the studies show that it is possible to have no hull interference, suggests that interference effects can be neglected.

The Coastal Cruiser 199 [53] has a lower hull separation ratio than either the CC300 [71] or the systematic demi-hull series [119]. Since it is lower, it might be expected that the hull resistance is much higher due to interference effects. However, the known resistance [122] is only 1.5% higher than what follows from the estimation. So there is no significant increase in resistance due to the smaller hull separation ratio; the difference might as well be the result of the difference between the demi-hull characteristics of the CC199 and the CC300, as the latter has a higher B/L-ratio, a lower B/T-ratio and a higher block coefficient [53] [71].

Based on this knowledge, it is concluded that the changes in the interference effects can be safely neglected in this estimation method. The residual resistance coefficients of both the demi-hull series, as well as both Coastal Cruisers, are including the interference effects. So it is taken into account as a constant factor.

B.4.3 Estimating the Installed Propulsion Power

The mass of the power and propulsion system is related to the installed propulsion power. So in order to estimate it, the installed power has to be related to the resistance of the ferry.

The required propulsion power (P_P) has a linear relation with the resistance of the ferry (R), based on data from the waterjets of the Coastal Cruiser 300 [125]:

$$P_P = \mathbf{X} \cdot R - \mathbf{X} \tag{B.37}$$

This expression is valid for a velocity of 30 knots, and it includes shaft and gearbox losses. The Coastal Cruiser 199 has smaller waterjets installed, but the same relation can be derived from that waterjet data [126].

One of the design requirements [paragraph 2.3] is a 15% margin between the installed propulsion power (P_i) and required propulsion power:

$$P_i = 1.15 \times P_P = \mathbf{X} \cdot R - \mathbf{X} \tag{B.38}$$

B.4.4 Estimating Energy Consumption

The energy consumption of the ferry is discussed in subparagraph 3.2, where the following relation was derived for the energy consumption of one crossing (E_{1c}):

$$E_{1c} = \frac{P_p}{\eta_{EP}} \cdot t_t + E_{aux} \tag{Ref. (3.2)}$$

With:

- $\eta_{EP} = 93\%$, efficiency of the electric powertrain [paragraph 3.1];
- $t_t = 50/60 \; hour$, time at transit speed [21];
- $E_{aux} = 0.1 \; MWh$, auxiliary energy consumption [21].

Equations 3.2 and B.38 can be used to link energy consumption to installed power:

$$E_{1c} \approx \frac{P_i}{1.15 \times 93\%} \times \left(\frac{50 \; [minutes]}{60 \; [minutes/hour]} \right) = 0.8 \; [kWh/kW] \times P_i \tag{B.39}$$

Note that auxiliary energy consumption is neglected in this expression. Because it is a constant, as well as a very small part of the total energy consumption, it can safely neglected for the determination of the target energy consumption ratio, which is done in paragraph 3.6.

Varying Speed

If design speed changes, the transit time changes as well. The following equation is used to calculate the time at transit speed:

$$t_t = \frac{25 \; [NM]}{V \; [knots]} \tag{B.40}$$

C

Hydrofoils: Mass, Lift and Drag Approximation

This appendix contains the mass, lift and drag estimation of the hydrofoil system. The result of this appendix will be used in chapter 6.

Structure of this Appendix
Appendix C.1 is about the mass estimation, **appendix C.2** about the lift coefficient and size estimation, and **appendix C.3** is about the resistance of the hydrofoil system.

C.1 Hydrofoil Mass Approximation

The lift that a hydrofoil has to generate is determined by the mass of the vessel. So first, the mass of the hydrofoil system has to be estimated, as this is a part of the total mass as well. Estimating the mass of the hydrofoil system (M_{foil}) can be done with following equation, which is derived by A. Rufolo, based on estimations from several hydrofoil designers [111]:

$$M_{foil} = \left(0.020 + 0.031 \sqrt{\frac{\Delta_{cat}}{100}} \right) \cdot \Delta_{cat} \qquad\qquad (\text{ C.1 })$$

This is a rough estimation, but for the estimation purpose in this thesis it is sufficient. The displacement can be written as the catamaran displacement without foils (Δ_0) plus the mass of the foil system (M_{foil}):

$$\Delta_{cat} = \Delta_0 + M_{foil} \qquad\qquad (\text{C.2})$$

With:

$$\Delta_0 = M_S + M_{PP} + M_{add} \qquad\qquad (\text{C.3})$$

With:

- M_S, structural mass (hull and superstructure);
- M_{PP}, mass of the power and propulsion system;
- M_{add}, additional mass.

A more detailed explanation of these three mass components can be found in appendix A.

C.2 Hydrofoil Lift Coefficient and Size Approximation

The lift of a hydrofoil (F_L) can be calculated with the following equation:

$$F_L = C_L \cdot \tfrac{1}{2}\rho V^2 \cdot A \qquad\qquad \text{Ref. (6.3)}$$

With:

- C_L, the lift coefficient;
- ρ, the fluid density ($1{,}025\ kg/m3$ for seawater);
- V, speed of the ferry;
- A, planform area of the foils.

The concept hydrofoil ferry has two hydrofoils, and each support half the weight of the vessel. This way the size of each foil can be determined:

$$A = \frac{F_L}{C_L \cdot \tfrac{1}{2}\rho V^2}, \qquad with\ F_L = \frac{\Delta_{cat}}{2} \cdot g \qquad\qquad (\ C.4\ )$$

In this approximation, a rectangular hydrofoil is considered, which means that the planform area is the product of the span (s) and the chord length (c):

$$A = s \cdot c \qquad\qquad \text{Ref. (6.1)}$$

The total span of each hydrofoil is equal to the overall beam of the vessel. Because not the whole area is effectively used, due to the presence of struts, an effective span of nine meter is assumed (s = 9 m). Because the span is fixed, the planform area is only determined by the chord length.

In paragraph 6.2, the free-stream lift coefficient (C_{L_0}) was determined to be 0.8. This value is valid for a foil in infinite fluid. Some factors affect this value. This subparagraph discussed three components are of importance for determining the effective lift coefficient:

- Finite span;
- Foil-foil interference;
- Water surface effects.

It must be mentioned here that this is an iterative process. If the effective lift coefficient is smaller, the area of the foil has to be larger to generate the same amount of lift (equation C.4). Because the hydrofoil is larger, the interference effects are larger as well, thus the area has to increase again. This process continuous until a break-even point is found. This is not necessarily the case, as the process can also diverge, than no feasible chord length exists.

C.2.1 Finite Foil Span

A real foil has a finite span, and thus a finite aspect ratio (AR), which is determined for a rectangular foil as the span divided by the chord length:

$$AR = \frac{s}{c} \qquad\qquad \text{Ref. (6.2)}$$

Due to the finite span, 3D effects occur that have a negative impact on the lift; the lower the aspect ratio, the lower its effective lift coefficient. This is also the reason why gliders have long and narrow wings, i.e. high aspect ratio wings, as these aircraft require a high lift/drag-ratio.

Søding presents an expression for estimating the lift coefficient of a low aspect ratio wing [100], which can be written as follows:

$$\frac{C_L}{C_{L_0}} = \frac{AR \cdot (AR + 1)}{(AR + 2)^2} \qquad\qquad\qquad\qquad (\text{ C.5 })$$

The negative effect of a limited aspect ratio can be limited by applying foil end-plates, which increase the effective aspect ratio. According to Dubs, the effect of end-plates can be estimated with the method as seen in figure C.1 [127]. In case of the catamaran, the largest part of the foil is located between the two centre planes of the demi-hulls, and the struts also act as foil-end-plates. Thus b is the demi-hull separation and h the foil submersion. This results in a ratio (AR/AR_{eff}) of 0.6.
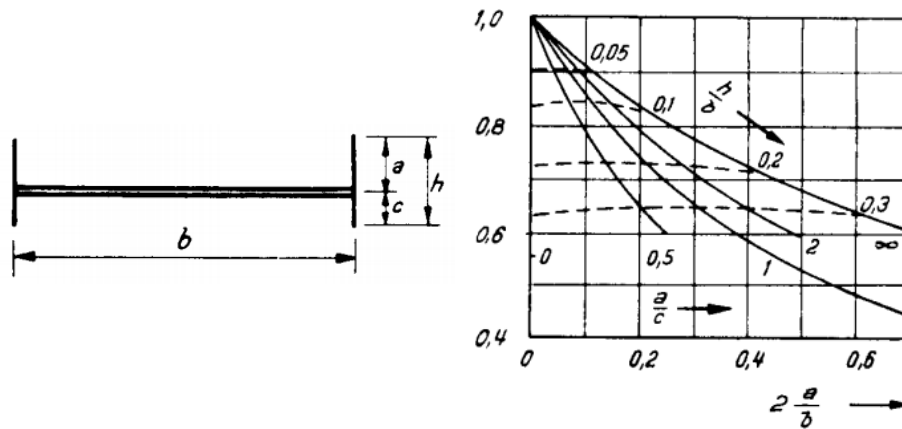
Figure C.1: front view of a wing with winglets (on the left), and the   [127]
corresponding ratio between the aspect ratio and effective
aspect ratio (AR/AR_{eff}).

Combining the two 3D effects results in the following expression:

$$\left[\frac{C_L}{C_{L_0}}\right]_{AR} = \frac{AR_{eff} \cdot (AR_{eff} + 1)}{\left(AR_{eff} + 2\right)^2}, \qquad with: AR_{eff} = \frac{AR}{0.6} \qquad (\text{ C.6 })$$

C.2.2 Foil-Foil Interference

The flow around the aft foil is disturbed by the presence of the forward foil. This influences the lift coefficient of the aft foil. An import factor is the creation of waves by the front foil, that affects the flow direction at the aft foil, i.e. the angle of attack changes and thus the lift changes [100]. This process is too complex to implement in this thesis, so instead a constant value will be used. Based on a study from Wetzel and Maxwell [128], a reduction of 25% in lift is assumed for the aft foil:

$$\left[\frac{C_L}{C_{L_0}}\right]_{foil\text{-}foil} = 0.75 \qquad\qquad\qquad\qquad (\text{ C.7 })$$

C.2.3 Water Surface Effect

The final interference effect is caused by the presence of the water surface. Hough and Moran analysed the free-surface effect [100]. This can be seen in figure C.2, where the effect of the free-surface is plotted against submergence Froude number (Fn_h, equation C.8), for different submergence/chord-length-ratios (h/c).

$$Fn_h = \frac{V}{\sqrt{g \cdot h}} \qquad\qquad (\text{ C.8 })$$
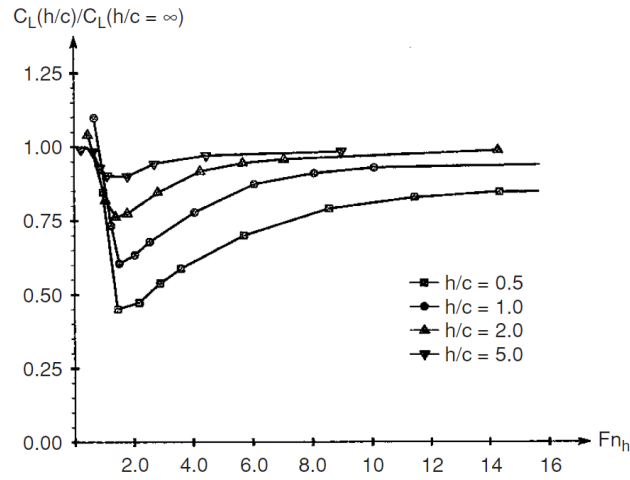
Figure C.2: effect of the free-surface on the lift coefficient, [100]
plotted against submergence Froude number,
for different submergence/chord-length-ratios.

The foil submergence (h) was determined to be 2.5 m in paragraph 6.2. The range of interest that follows from this submergence is between submergence Froude number 3 and 5, which corresponds to a speed between 29 and 48 knots, as calculated with the equation C.8.

The submergence ratios that are of interest lie between 1.0 to 5.0, which correspond to a chord length of between 0.5 and 2.5 m.

Based on figure C.2 and the ranges as described above, the following equation is derived for the estimation of the surface effect (C_L/C_{L_0}):

$$\left[\frac{C_L}{C_{L_0}}\right]_{water\text{-}surface} = \exp(-0.2 \cdot c) \cdot \left(\frac{Fn_h}{2}\right)^{c/8} \qquad\qquad (\text{ C.9 })$$

C.2.4 Size and Lift Coefficient Limitation of the Hydrofoil

The higher the design velocity, the smaller the required planform area of the hydrofoil. This can be seen with equation C.4. If the hydrofoil becomes too small, it is not strong enough anymore to carry the weight of the vessel. Therefore, for higher design speeds, it makes more sense to limit the lift coefficient of the hydrofoil, i.e. decrease the angle of attack of the hydrofoil.

So the lift coefficient is also determined by the maximum size of the hydrofoils, which can be determined by the maximum allowable aspect ratio of the foil. Hoerner et al. derived an expression to estimate the aspect ratio between the struts ($"AR"_{max}$) [103]:

$$"AR"_{max} = 0.96 \sqrt{\frac{\sigma}{f} \cdot \frac{t/c}{\sqrt{F_L/A}}} \qquad\qquad (\text{ C.10 })$$

With:

- σ, yield stress ($\sigma \approx 200\ MPa$ for aluminium [129]);
- f, safety factor ($f = 1.15$ [103]);
- t/c, thickness ratio of a foil. ($t/c = 0.12$ in case of the NACA 64_1-212 [105]);
- F_L/A, foil loading.

It must be mentioned that the original equation was created for empirical units; '11.5' is changed into '0.96' to use the formula with SI-units.

The foil loading is determined by area of the hydrofoil, which is the span times the chord length (equation 6.1). Because the span is fixed ($s = 9\ m$), equation C.10 can be rewritten from a function of planform area to a function of chord length:

$$"AR"_{max} = 0.96 \sqrt{\frac{\sigma}{f} \cdot \frac{t/c}{\sqrt{F_L/s}}} \cdot \sqrt{c} \qquad\qquad (\ C.11\ )$$

Two struts are located at the centre plane of the demi-hulls, and one strut is placed in the centre plane of the catamaran. Thus the aspect ratio between the struts is half the demi-hull separation divided by the chord length of the foil, and it should not be larger than the maximum allowable aspect ratio:

$$AR \leq "AR"_{max} \rightarrow \frac{b/2}{c} \leq 0.96 \sqrt{\frac{\sigma}{f} \cdot \frac{t/c}{\sqrt{F_L/s}}} \cdot \sqrt{c} \qquad\qquad (\ C.12\ )$$

Equation C.12 can be rewritten to an expression of minimum hydrofoil chord length:

$$c_{min} = \left(\frac{1.92}{b} \cdot \sqrt{\frac{\sigma}{f} \cdot \frac{t/c}{\sqrt{F_L/s}}} \right)^{-3/2} \qquad\qquad (\ C.13\ )$$

From this minimum chord length follows the minimum planform area, and thus the maximum lift coefficient:

$$A_{min} = s \cdot c_{min} \qquad\qquad (\ C.14\ )$$

$$C_{L,max} = \frac{F_L}{\frac{1}{2}\rho V^2 \cdot A_{min}} \qquad\qquad (\ C.15\ )$$

C.2.5 Overview of Foil Sizing and Lift Coefficient Estimation Equations

As mentioned before, estimating the size and lift coefficient of the hydrofoil system is an iterative process, because the lift coefficient determines the size of the foil, and the size of the foil determines the magnitude of the interference effects and thus of the lift coefficient. As long as the ratio of velocity-over-weight is high enough, the iterative process converges.

Chord Length of the Hydrofoils
The chord length of each hydrofoil can be estimated as follows:

$$c = \frac{A}{s}, \qquad with\ s = 9\ m \qquad\qquad (\ C.16\ )$$

With:

$$A = \frac{F_L}{C_L \cdot \frac{1}{2}\rho V^2}, \qquad with: F_L = \frac{\Delta_{cat}}{2} \cdot g \qquad\qquad Ref.\ (\ C.4\ )$$

Note that the displacement of the catamaran is divided by two, as each foil carries half the weight.

Lift Coefficient of the Hydrofoil System
Combining the interference effects with the free stream lift coefficient leads to the following expressions for estimating the lift of the forward and aft foil respectively:

$$C_{L,forward} = \min\left\{\left(C_{L_0} \cdot \left[\frac{C_L}{C_{L_0}}\right]_{water\text{-}surface}\right), \quad C_{L,max,forward}\right\} \qquad (\text{ C.17 })$$

$$C_{L,aft} = \min\left\{\left(C_{L_0} \cdot \left[\frac{C_L}{C_{L_0}}\right]_{water\text{-}surface} \cdot \left[\frac{C_L}{C_{L_0}}\right]_{foil\text{-}foil}\right), \quad C_{L,max,aft}\right\} \qquad (\text{ C.18 })$$

With:

- $C_{L_0} = 0.8$

- $\left[\frac{C_L}{C_{L_0}}\right]_{water\text{-}surface} = \exp(-0.2 \cdot c) \cdot \left(\frac{Fn_h}{2}\right)^{c/8}$ Ref. (C.9)

- $\left[\frac{C_L}{C_{L_0}}\right]_{foil\text{-}foil} = 0.75$ Ref. (C.7)

- $C_{L,max} = \dfrac{F_L}{\tfrac{1}{2}\rho V^2 \cdot A_{min}}$ Ref. (C.15)

    ○ $A_{min} = s \cdot c_{min}$ Ref. (C.14)

    ○ $c_{min} = \left(\dfrac{1.92}{b} \cdot \sqrt{\dfrac{\sigma}{f}} \cdot \dfrac{t/c}{\sqrt{F_L/s}}\right)^{-3/2}$ Ref. (C.13)

C.3 Hydrofoil System Drag Approximation

The drag of the hydrofoil system can be split into multiple components, and the total resistance is the summation of all these components:

- Frictional drag;
- Parasitic drag;
- Induced drag;
- Wave making drag;
- Interference drag;
- Spray drag.

Most of these components are related to area, just like the resistance of the ship itself. However, in case of hydrofoils, there are two areas used for estimating the resistance: planform area (A) and total area of the system (A_{total}), both explained below. There are also some resistance components are related to the foil thickness.

Because the resistance coefficient is often different for forward and aft foil, the two foil systems will be handled separately and the summation of their individual resistances is the total resistance.

Planform Area

The planform area is simply the span times the chord length of the hydrofoil:

$$A = s \cdot c$$ Ref. (6.1)

Total Area

The total area also includes the area of the struts. The height of the struts under water is equal to the hydrofoil submergence ($h = 2.5\ m$). The forward foil has three equal struts, all with the same chord length as the hydrofoil they support ($c_{forward}$). Thus the total area of the forward foil system is:

$$A_{total_{forward}} = (s + 3 \times h) \cdot c_{forward}$$ (C.19)

The aft foil also has three struts, but the size of two of them have a minimal chord length of 1.2 m to support the propulsion system, as discussed in subparagraph 6.2.4. This leads to the following expression:

$$A_{total_{aft}} = (s + 1 \times h) \cdot c + (2 \times h) \cdot c_{strut_{aft}}$$ (C.20)

With:

$$c_{strut_{aft}} = \max\{c, \qquad 1.2\ [m]\}$$ Ref. (6.11)

C.3.1 Friction Drag

The friction drag coefficient can be calculated using the ITTC-57 formula, similar as is done for the ship itself (equation B.2). The Reynolds number is different though, as it is not a function of the length of the vessel, but of the chord length of the foil (c):

$$Rn_c = \frac{V \cdot c}{\nu}$$ (C.21)

With:

- V, the speed of the ferry;
- ν, the viscosity of seawater ($1.2 \cdot 10^{-6}\ m^2/s$).

$$C_F = \frac{0.075}{(\log_{10} Rn - 2)^2}$$ Ref. (B.2)

The frictional drag is simply a function of this coefficient and the total area:

$$F_{D,friction} = C_F \cdot \tfrac{1}{2}\rho V^2 \cdot A_{total}$$ (C.22)

C.3.2 Parasitic Drag

The parasitic drag is related to the pressure distribution over the foil. In subparagraph 6.1.3, a parasitic drag coefficient (C_{D_0}) of 0.01 was mentioned, which is in line with the value mentioned by Hoerner et al. [103]. With this value the parasitic drag can be calculated:

$$F_{D,parasitic} = C_{D_0} \cdot \tfrac{1}{2}\rho V^2 \cdot A_{total}, \qquad with\text{:} C_{D_0} = 0.01$$ (C.23)

C.3.3 Induced Drag

The 3D effects of a foil on the resistance is taken into account with the induced drag, which is only a function of the planform area, as the struts do not generate lift:

$$F_{D,induced} = C_{Di} \cdot \tfrac{1}{2}\rho V^2 \cdot A$$ (C.24)

The induced drag coefficient (C_{Di}) of a fully submerged foil is a function of the lift coefficient (C_L) and the aspect ratio (AR) of the foil [103]:

$$C_{Di} = \frac{C_L^2}{\pi \cdot AR}$$ (C.25)

Foil-end-plates and struts increase the effective aspect ratio [127]. This changes equation C.25 into the following expression:

$$C_{Di} = \frac{C_L^2}{\pi \cdot AR} \cdot \left[\frac{AR}{AR_{eff}}\right], \qquad with \left[\frac{AR}{AR_{eff}}\right] = 0.6$$ (C.26)

The ratio of 0.6 was determined in subparagraph C.2.1

C.3.4 Wave Making Drag

The lift of a hydrofoil deforms the free-surface, i.e. waves are generated. Both Faltinsen [100] and Hoerner [130] have derived the following equation for estimating the wave making drag of a hydrofoil:

$$F_{D,waves} = C_{Dw} \cdot \tfrac{1}{2}\rho V^2 \cdot A$$ (C.27)
With:

$$C_{Dw} = 0.5 \cdot \frac{c}{h} \cdot \frac{C_L^2}{F_h^2} \cdot exp\left(\frac{-2}{Fn_h^2}\right)$$ (C.28)

C.3.5 Interference Drag

Two interference drags are considered: foil-foil interference and foil-strut interference.

Foil-Foil Interference
A foil might experience interference drag if it is located in the downwash of another foil. In case of the concept ferry the distance between the struts is large enough ($x/c > 10$) that no noticeable interference drag occurs [130].

Foil-Strut Interference
Interference drag does occur on each connection between foil and strut. This drag is not a function of area, but a function of foil thickness squared (t^2) [130]:

$$F_{D,interference} = \sum_{struts} C_{Dt} \cdot \tfrac{1}{2}\rho V^2 \cdot t^2 \qquad\qquad (\text{C.29})$$

With:

$$C_{Dt} = 17 \cdot (t/c)^2 - 0.05 \qquad\qquad (\text{C.30})$$

C.3.6 Spray Drag
Due to the relatively high Froude numbers at which a strut operates, the waves that are created by the struts break up, forming a "spray". The following empirical function, derived by Hoerner, is used to estimate the spray drag [130]:

$$F_{D,spray} = \sum_{struts} C_{D_{spray}} \cdot t^2 \cdot \tfrac{1}{2}\rho V^2, \qquad with\ C_{D_{spray}} = 0.24 \qquad\qquad (\text{C.31})$$

C.3.7 Drag Estimation Overview and Energy Consumption Estimate
An overview of the equations of this paragraph can be seen on the next page.

Using the equations as mentioned in this appendix for the Coastal Cruiser 300 on hydrofoils, sailing 30 knots, results in the following contributions of each resistance component:

Table C.1: contribution of each resistance component, as estimated for the Coastal Cruiser 300 with hydrofoils at a design speed of 30 knots.

Frictional drag	12%
Parasitic drag	47%
Induced drag	14%
Interference drag	7%
Wave making drag	11%
Spray drag	9%

Energy Consumption
Energy consumption is proportional to resistance and travel time, and the latter becomes smaller if speed increases. Thus the following proportionality exists:

$$\frac{E_{1c_{hydrofoil}}}{E_{1c_{CC300}}} \approx \frac{R_{hydrofoil}}{R_{CC300}} \cdot \frac{V_{CC300}}{V_{hydrofoil}} \qquad\qquad (\text{C.32})$$

Another factor to take into account is the propulsor efficiency. The efficiency of a conventional waterjet is in the order of 70% [107], and the propeller propulsion was determined to be in the order of 60%

[paragraph 6.2.3]. This means that if the resistance of the hydrofoil vessel is equal to that of the conventional catamaran, its energy consumption is around 17% higher:

$$\frac{\eta_{CC300}}{\eta_{hydrofoil}} = \frac{70\%}{60\%} = 1.17 \qquad (\text{ C.33 })$$

Taking this into account results in the following expression for the energy consumption:

$$\frac{E_{1c_{hydrofoil}}}{E_{1c_{CC300}}} \approx \frac{R_{hydrofoil}}{R_{CC300}} \cdot \frac{V_{CC300}}{V_{hydrofoil}} \cdot \frac{\eta_{CC300}}{\eta_{hydrofoil}} \qquad (\text{ C.34 })$$

Overview of the Hydrofoil System Drag Estimation Equations

$$F_D = \left(F_{D_{foil}}\right)_{forward} + \left(F_{D_{foil}}\right)_{aft} + F_{D,interference} + F_{D,spray} \qquad (\text{ C.35 })$$

With:

- $F_{D_{foil}} = F_{D,friction} + F_{D,parasitic} + F_{D,induced} + F_{D,waves}$ (C.36)

  With:

  - $F_{D,friction} = C_F \cdot \frac{1}{2}\rho V^2 \cdot A_{total}$ Ref. (C.22)

    - $C_F = \dfrac{0.075}{(\log_{10} Rn - 2)^2}$ Ref. (B.2)

      * $Rn = \dfrac{V \cdot c}{\nu}$ Ref. (C.21)

    - $A_{total_{forward}} = (s + 3 \times h) \cdot c_{forward}$ Ref. (C.19)

    - $A_{total_{aft}} = (s + 1 \times h) \cdot c + (2 \times h) \cdot c_{strut_{aft}}$ Ref. (C.20)

      * $c_{strut_{aft}} = \max\{c, \quad 1.2\,[m]\}$ Ref. (6.11)

  - $F_{D,parasitic} = C_{D_0} \cdot \frac{1}{2}\rho V^2 \cdot A_{total}, \quad with: C_{D_0} = 0.01$ Ref. (C.23)

  - $F_{D,induced} = C_{Di} \cdot \frac{1}{2}\rho V^2 \cdot A$ Ref. (C.24)

    - $C_{Di} = \dfrac{C_L^2}{\pi \cdot AR} \cdot \left[\dfrac{AR}{AR_{eff}}\right], \quad with \left[\dfrac{AR}{AR_{eff}}\right] = 0.6$ Ref. (C.26)

    - $A = s \cdot c$ Ref. (6.1)

  - $F_{D,waves} = C_{Dw} \cdot \frac{1}{2}\rho V^2 \cdot A$ Ref. (C.27)

$$\blacksquare \quad C_{Dw} = 0.5 \cdot \frac{c}{h} \cdot \frac{C_L^2}{F_h^2} \cdot exp\left(\frac{-2}{Fn_h^2}\right)$$

Ref. (C.28)

- $F_{D,interference} = \sum_{struts} C_{Dt} \cdot \frac{1}{2}\rho V^2 \cdot t^2$

Ref. (C.29)

  ○ $C_{Dt} = 17 \cdot (t/c)^2 - 0.05$

Ref. (C.30)

- $F_{D,spray} = \sum_{struts} C_{D_{spray}} \cdot t_{strut}^2 \cdot \frac{1}{2}\rho V^2, \quad with \ C_{D_{spray}} = 0.24$

Ref. (C.31)

  ○ $t_{strut} = t$

  ○ In case of the propeller supporting aft struts:

  $t_{strut_{aft}} = \max\{t, \quad 0.3 \ [m]\}$

Ref. (6.10)

Bibliography

[1]   National Climate Assessment, „Extreme Weather," 2014. [Online]. Available: https://nca2014.globalchange.gov/highlights/report-findings/extreme-weather.   [Accessed March 2019].

[2]   J. Cook, N. Oreskes, P. Doran, A. W. en B. Verheggen, „Consensus on consensus: a synthesis of consensus estimates on human-caused global warming," *Environmental Research Letters,* vol. 11, nr. 4, 2016.

[3]   NASA Climate Change website, „Graphic: Carbon dioxide hits new high," [Online]. Available: https://climate.nasa.gov/climate_resources/7/graphic-carbon-dioxide-hits-new-high/. [Accessed January 2019].

[4]   S. Arrhenius, „On the Influence of Carbonic Acid in the Air upon the Temperature of the Ground," *Philosophical Magazine and Journal of Science,* vol. 41, pp. 237-276, 1896.

[5]   C. Pope III en D. Dockery, „Health Effects of Fine Particulate Air Pollution: Lines that Connect," *Journal of the Air & Waste Management Association,* vol. 56, nr. 6, pp. 709-742, 2006.

[6]   European Union, „Science for Environment Policy; What are the health costs of environmental pollution?," Publications Office, Luxembourg, Luxembourg, 2018.

[7]   S. Cohen, „The Human and Financial Cost of Pollution," 23 October 2017. [Online]. Available: https://blogs.ei.columbia.edu/2017/10/23/the-human-and-financial-cost-of-pollution/. [Accessed July 2019].

[8]   URBANET, „The world urban population," 25 August 2016. [Online]. Available: https://www.urbanet.info/world-urban-population/. [Accessed January 2019].

[9]   L. Poon, „How China Took Charge of the Electric Bus Revolution," 8 May 2018. [Online]. Available: https://www.citylab.com/transportation/2018/05/how-china-charged-into-the-electric-bus-revolution/559571/. [Accessed December 2018].

[10]   SupercapTech.com, „Supercapacitor electric boat : Ar Vag Tredan operates in France," 18 September 2013. [Online]. Available: https://www.supercaptech.com/supercapacitor-electric-boat-ar-vag-tredan-operates-in-france. [Accessed December 2018].

[11]   P. Marx, „Norway is Showing the World How to Electrify Transportation," 5 February 2018. [Online]. Available: https://medium.com/@parismarx/norway-is-showing-the-world-how-to-electrify-transportation-c6bf4806c00b. [Accessed December 2018].

[12]   Green City Ferries with Horizon 2020 partners, „This is BB GREEN," 2018. [Online]. Available: http://bbgreen.eu/. [Accessed May 2019].

[13]   J. Pratt en L. Klebanoff, „Feasibility of the SF-BREEZE: a Zero-Emission, Hydrogen Fuel Cell, High-Speed Passenger Ferry," Sandia National Laboratories, Albuquerque, New Mexico, USA, 2016.

[14]   T. Stensvold, „Tester skalamodell av batteridrevet hurtigbåt," 24 April 2019. [Online]. Available: https://www.tu.no/artikler/tester-skalamodell-av-batteridrevet-hurtigbat/463521?key=iWlxDGbd. [Accessed May 2019].

[15]   CoCo Yachts, „CoCo Yachts - Plenty Ships sign contract for one Coastal Cruiser 199 and one Coastal Cruiser 300 with Peng Xing Shipping Company," [Online]. Available: https://www.cocoyachts.com/. [Accessed December 2018].

[16]   World Population Review, „Shenzhen Population 2019," 30 November 2018. [Online]. Available: http://worldpopulationreview.com/world-cities/shenzhen-population/. [Accessed January 2019].

[17] L. van Biert, M. Godjevac, K. Visser en A. Purushothaman Vellayani, „A review of fuel cell systems for maritime applications," *Journal of Power Sources,* vol. 327, 2016.

[18] U.S. DRIVE Partnership, „Target Explanation Document: Onboard Hydrogen Storage for Light-Duty Fuel Cell Vehicles," 2017. [Online]. Available: https://www.energy.gov/sites/prod/files/2017/05/f34/fcto_targets_onboard_hydro_storage_explanation.pdf. [Accessed January 2019].

[19] Corvus Energy, „High Energy Density is the Key to Economical Electric & Hybrid Energy Storage Systems," 12 September 2017. [Online]. Available: https://corvusenergy.com/high-energy-density-is-the-key-to-economical-electric-hybrid-energy-storage-systems/. [Accessed January 2019].

[20] Yu Media Group d.o.o., „Monthly weather forecast and Climate Shenzhen, China," [Online]. Available: https://www.weather-atlas.com/en/china/shenzhen-climate. [Accessed July 2019].

[21] ST|CoCo Yachts, *160802_Operational Profile_CC-300_PX1. [Unpublished Excel document],* Gorinchem, 2019.

[22] ST | CoCo Yachts, *ferry lines Shenzhen, time tables and distances. [Unpublished Excel document],* Gorinchem, 2019.

[23] M. Zhou, „Shekou and Zhuhai Ferry Schedules," [Online]. Available: http://www.shenzhenparty.com/ferry/shekou-zhuhai. [Accessed December 2018].

[24] M. Ciniviz en H. Köse, „Hydrogen Use in Internal Combustion Engine: a Review," *International Journal of Automotive,* vol. 1, nr. 1, pp. 1-15, 2012.

[25] Omnagen Ltd., „NOx emissions – formation, reduction and abatement," 2017. [Online]. Available: https://clean-carbonenergy.com/nox-emissions.html. [Accessed February 2019].

[26] F. Un-Noor, P. S., M.-P. L., M. Mollah en E. Hossain, „A Comprehensive Study of Key Electric Vehicle (EV) Components, Technologies, Challenges, Impacts, and Future Direction of Development," *Energies,* vol. 10, nr. 8, 2017.

[27] Siemens, *ac-motors; Large Drives; Three-phase synchronous motors based on permanent magnet technology,* Nürnberg, Germany, 2007.

[28] ABB, *Low voltage Water cooled motors,* 2011.

[29] ST|CoCo Yachts, *180301_US100_R_ES [Unpublished Excel document],* Gorinchem, 2019.

[30] MTU, „Diesel Engines 12V/16V 2000 M72 for Vessels with High Load Factors (1B)," September 2007. [Online]. Available: https://www.transdiesel.com/app_docs/mtu%2012v&16v2000m72.pdf. [Accessed January 2019].

[31] Corvus Energy, „World's First All-Electric Car Ferry," [Online]. Available: https://corvusenergy.com/marine-project/mf-ampere-ferry/. [Accessed December 2018].

[32] T. Stensvold, „Nå lader batterifergen mer enn hun trenger," 13 May 2015. [Online]. Available: https://www.tu.no/artikler/na-lader-batterifergen-mer-enn-hun-trenger/223419. [Accessed December 2018].

[33] B. Perry, „High capacity battery packs," [Online]. Available: https://library.e.abb.com/public/82b8e284d5fdc935c1257a8a003c26a4/ABB%20Generations_22%20High%20capacity%20battery%20packs.pdf. [Accessed December 2018].

[34] Corvus Energy, „AT6500 High Performance Energy Storage," Corvus Energy, 22 May 2015. [Online]. Available: https://corvusenergy.com/wp-content/uploads/2015/09/Corvus-Energy-AT6500_MAY-2015.pdf. [Accessed December 2018].

[35] XALT Energy, „XPAND Rack System (XRS) - For Marine and Grid," 25 September 2018. [Online]. Available: https://www.xaltenergy.com/wp-content/uploads/2018/09/XRS.pdf. [Accessed February 2019].

[36] G. Pistoia, Batteries for Portable Devices, Amsterdam, The Netherlands: Elsevier B.V., 2005.

[37] Cavotec SA, „E-charging," 2017. [Online]. Available: http://www.cavotec.com/en/your-applications/ports-maritime/e-charging. [Accessed May 2019].

[38] M. Kane, „World's Largest Electric Ferries: 4.16 MWh Battery, 10 MW Charging," 28 Sebtember 2016. [Online]. Available: https://insideevs.com/worlds-largest-electric-ferries-to-be-equipped-with-pbesxalt-energys-4-16-mwh-battery-packs/. [Accessed December 2018].

[39] „Global Solar Atlas," 2018. [Online]. Available: https://globalsolaratlas.info/. [Accessed December 2018].

[40] V. Aggarwal, „What are the most efficient solar panels on the market?," 5 November 2018. [Online]. Available: https://news.energysage.com/what-are-the-most-efficient-solar-panels-on-the-market/. [Accessed December 2018].

[41] GVT, „Completely Electric-propelled Inland Vessels; Port-liner Builds Emission-free Sailing Barges in 2018," 12 Februari 2018. [Online]. Available: https://www.gvt.nl/nl/nieuws/completely-electric-propelled-inland-vessels. [Accessed December 2018].

[42] C. Fortuna, „Tesla shuts down battery swap program in favor of Superchargers, for now," 6 November 2016. [Online]. Available: https://www.teslarati.com/tesla-shuts-down-battery-swap-program-for-superchargers/. [Accessed December 2018].

[43] XALT Energy, „XALT 60Ah High Power Lithium-Ion LTO Cell," 13 August 2018. [Online]. Available: https://www.xaltenergy.com/wp-content/uploads/2019/02/60Ah-LTOHP.pdf. [Accessed November 2018].

[44] XALT Energy, „XALT 75 Ah High Power (HP) Lithium Ion Cell," 6 September 2018. [Online]. Available: https://www.xaltenergy.com/wp-content/uploads/2018/09/75Ah-HP.pdf. [Accessed November 2018].

[45] XALT Energy, „XALT 56 Ah High Power (HP) Lithium Ion Cell," 14 May 2018. [Online]. Available: https://www.xaltenergy.com/wp-content/uploads/2018/05/56Ah-HP.pdf. [Accessed February 2019].

[46] XALT Energy, „XALT 63 Ah Ultra High Energy (UHE) Lithium Ion Cell," 13 August 2018. [Online]. Available: https://www.xaltenergy.com/wp-content/uploads/2018/08/63Ah_UHE.pdf. [Accessed November 2018].

[47] *Gewichten batterijen [email from N. Kleijweg, received at 29 April 2019].*

[48] M. Rodriguez-Achach, „Will Supercapacitors Ever Replace Batteries?," 19 January 2017. [Online]. Available: https://hackaday.com/2017/01/19/will-supercapacitors-ever-replace-batteries/. [Accessed December 2018].

[49] SupercapTech.com, „Battery VS Supercapacitor," 21 May 2016. [Online]. Available: https://www.supercaptech.com/battery-vs-supercapacitor. [Accessed January 2019].

[50] Woodbank Communications Ltd., „Calendar Life and Cycle Life," 2005. [Online]. Available: https://www.mpoweruk.com/life.htm. [Accessed May 2019].

[51] Northern Arizona Wind & Sun, „Deep Cycle Battery Frequently Asked Questions," 2014. [Online]. Available: https://www.solar-electric.com/learning-center/batteries-and-charging/deep-cycle-battery-faq.html. [Accessed May 2019].

[52] S. Choi en H. Lim, „Factors that affect cycle-life and possible degradation mechanisms of a Li-ion cell based on LiCoO2," *Journal of Power Sources,* vol. 111, nr. 1, pp. 130-136, 2002.

[53] CoCo Yachts, *160801-1000-001 General Arrangement CC-199 2016.11.30 [Unpublished Excel document],* Gorinchem, 2016.

[54] M. Romare en L. Dahllöf, „The Life Cycle Energy Consumption and Greenhouse Gas Emissions from Lithium-Ion Batteries," IVL Swedish Environmental Research Institute Ltd., Stockholm, Sweden, 2017.

[55] J. Rhodes, „Nuclear and wind power estimated to have lowest levelized CO2 emissions," The University of Texas at Austin, 7 November 2017. [Online]. Available: https://energy.utexas.edu/news/nuclear-and-wind-power-estimated-have-lowest-levelized-co2-emissions. [Accessed January 2019].

[56] E. Apostolaki-Iosifidou, P. Codani en W. Kempton, „Measurement of power loss during electric vehicle charging and discharging," *Energy,* vol. 127, pp. 730-742, 2017.

[57] BP p.l.c., „BP Statistical Review of World Energy," 2019. [Online]. Available: https://www.bp.com/content/dam/bp/business-sites/en/global/corporate/pdfs/energy-economics/statistical-review/bp-stats-review-2019-electricity.pdf. [Accessed July 2019].

[58] M. Ernst, „Carbon Footprint 2016; Erasmus University Rotterdam," Arcadis Nederland B.V., Rotterdam, The Netherlands, 2018.

[59] S. Muthu, The Carbon Footprint Handbook, Boca Raton, Florida, USA: Taylor & Francis Group, LLC, 2016.

[60] SupercapTech.com, „Supercapacitor electric boat : Ar Vag Tredan operates in France," 18 September 2013. [Online]. Available: https://www.supercaptech.com/supercapacitor-electric-boat-ar-vag-tredan-operates-in-france. [Accessed December 2018].

[61] Ecolopop, „Ar Vag Tredan / Lorient : premier bateau à passagers au monde à zéro émission de CO2," [Online]. Available: http://www.ecolopop.info/2013/10/ar-vag-tredan-lorient-premier-bateau-a-passagers-au-monde-a-zero-emission-de-co2/16812. [Accessed January 2019].

[62] K. Field, „Hydrogen Fuel Cell & Battery Electric Vehicles — Technology Rundown," 11 August 2018. [Online]. Available: https://cleantechnica.com/2018/08/11/hydrogen-fuel-cell-battery-electric-vehicles-technology-rundown/. [Accessed December 2018].

[63] IRENA, „Hydrogen from renewable power: Technology outlook for the energy transition," International Renewable Energy Agency, Abu Dhabi, 2018.

[64] D. Astiaso Garcia, F. Barbanera, F. Cumo, U. De Matteo en B. Nastasi, „Expert Opinion Analysis on Renewable Hydrogen Storage Systems Potential inEurope," *Energies,* vol. 9, nr. 11, 2016.

[65] A. Ådnanes, „Energy efficiency and fuel consumption of marine and offshore vessels - Technical possibilities and a case study," November 2010. [Online]. Available: http://www02.abb.com/global/seitp/seitp202.nsf/0/e1e06068666a4ed1c12577fb00073e9d/$file/Electric+Distribution.pdf. [Accessed January 2019].

[66] N. Sirosh, *Hydrogen Composite Tank Program,* Irvine, California, USA: QUANTUM Technologies WorldWide, Inc, 2002.

[67] Hydrogenics Corporation, „HyPM-HD 30 Power Module," December 2016. [Online]. Available: http://www.hydrogenics.com/wp-content/uploads/HyPM-30-Spec-Sheet.pdf. [Accessed May 2019].

[68] Ballard Power Systems, „Ballard Powered Fuel Cell Electric Bus Achieves 25,000 Hours of Revenue Operation," 29 August 2017. [Online]. Available: http://ballard.com/about-ballard/newsroom/news-releases/2017/08/29/ballard-powered-fuel-cell-electric-bus-achieves-25-000-hours-of-revenue-operation. [Accessed June 2019].

[69] J. Bauman en M. Kazerani, „A Comparative Study of Fuel-Cell–Battery, Fuel-Cell–Ultracapacitor, and Fuel-Cell–Battery–Ultracapacitor Vehicles," *IEEE TRANSACTIONS ON VEHICULAR TECHNOLOGY,* vol. 57, nr. 2, pp. 760-769, 2008.

[70] T. Tronstad, H. Åstrand, G. Haugom en L. Langfeldt, „Study on the use of fuel cells in shipping," DNV GL, 2017.

[71] CoCo Yachts, *160802-1000-001 General Arrangement CC-300 Rev. H 2018.03.--- [Unpublished PDF document],* Gorinchem, 2018.

[72] Honda North America, „Honda FCX Clarity Fuel Cell Vehicle Lease Program Begins with First Customer Delivery," 25 July 2008. [Online]. Available: https://hondanews.com/releases/honda-fcx-clarity-fuel-cell-vehicle-lease-program-begins-with-first-customer-delivery?query=clarity+2008. [Accessed July 2019].

[73] Hydrogen Europe, „Hydrogen safety," 2017. [Online]. Available: https://hydrogeneurope.eu/hydrogen-safety. [Accessed July 2019].

[74] A. Sveshnikova, K. Abrosimov, A. Khayrullina en A. Ustinov, „Effect of ambient air conditions on PEM fuel cell performance," *Journal of Renewable and Sustainable Energy,* vol. 9, nr. 4, 2017.

[75] R. Roy en N. Braathen, „The Rising Cost of Ambient Air Pollution thus far in the 21st Century: Results from the BRIICS and the OECD Countries - Environment Working Paper No. 124," OECD Environment Directorate, Paris, France, 2017.

[76] TNO, „D2.8 / D2.9 Standardized model and cost/benefit assessment for right-size engines and hybrid configurations," 2018.

[77] Moteurs Leroy-Somer SAS, „Environmental Product Declaration," 2017. [Online]. Available: http://www.leroy-somer.com/documentation_pdf/4951_en.pdf. [Accessed June 2019].

[78] S. Eaves en J. Eaves, „A cost comparison of fuel-cell and battery electric vehicles," *Journal of Power Sources,* vol. 130, pp. 208-212, 2004.

[79] K. Reddi, A. Elgowainy, N. Rustagi en E. Gupta, „Impact of hydrogen SAE J2601 fueling methods on fueling time of light-duty fuel cell electric vehicles," [Online]. Available: https://www.osti.gov/pages/servlets/purl/1389635. [Accessed December 2018].

[80] N. Saito, „The economic analysis of commercial ships with hydrogen fuel cell through case studies," World Maritime University, Malmö, Sweden, 2018.

[81] M. Adachi, H. Kosaka, T. Fukuda, S. Ohashi en K. Harumi, „Economic analysis of trans-ocean LNG-fueled container ship," *Journal of Marine Science andTechnology,* vol. 19, nr. 4, pp. 470-478, 2014.

[82] R. Kochhan, S. Fuchs, B. Reuter, P. Burda, S. Matz en M. Lienkamp, „An Overview of Costs for Vehicle Components, Fuels and Greenhouse Gas Emissions," 2014.

[83] Element Energy Limited, „Update on European hydrogen bus activity," September 2018. [Online]. Available: http://zebconference.com/wp-content/uploads/2018/04/2_Madden.pdf. [Accessed June 2019].

[84] „Bunker Index," January 2019. [Online]. Available: https://bunkerindex.com/index.php. [Accessed January 2019].

[85] van Wijk, A., „Green Hydrogen Economy in the Northern Netherlands," December 2016. [Online]. Available: https://www.deingenieur.nl/uploads/media/5880bffadd9af/Green%20Hydrogen%20Economy%20in%20Northern%20Netherlands.pdf. [Accessed May 2019].

[86] IRENA, „Renewable Power Generation Costs in 2017," International Renewable Energy Agency, Abu Dhabi, 2018.

[87] Gurit, „Composite technology for work boats – Can composites pay their way?," April 2015. [Online]. Available: https://www.gurit.com/Our-Business/Composite-Engineering/Technical-forum. [Accessed June 2019].

[88] Turner & Townsend, „International construction market survey 2018," 2018.

[89] MBH Media, Inc., „Exchange-Rates.org; Exchange Rates; Convert US Dollars to Euros," May 2019. [Online]. Available: https://exchange-rates.org/converter/USD/EUR/1. [Accessed May 2019].

[90] Brødrene Aa, „Rygerkatt," [Online]. Available: https://www.braa.no/fast-ferries/rygerkatt. [Accessed May 2019].

[91] Brødrene Aa, „Zhong Shan 6," [Online]. Available: https://www.braa.no/fast-ferries/zhong-shan-6. [Accessed May 2019].

[92] M. Masuelli, Introduction of Fibre-Reinforced Polymers − Polymers and Composites: Concepts, Properties and Processes, London, UK: IntechOpen Limited, 2013, pp. 3-40.

[93] J. Kuzjatkin, „Structural Weight Optimisation of a Carbon Fibre Ferry," KTH Royal Institute of Technology, 2014.

[94] T. Hertzberg, „LASS, Lightweight Construction Applications at Sea," SP Technical Research Institute of Sweden, Borås, Sweden, 2009.

[95]   M. Kane, „Innolith Claims It's On Path To 1,000 Wh/kg Battery Energy Density," 4 April 2019. [Online]. Available: https://insideevs.com/news/343771/innolith-claims-its-on-path-to-1000-wh-kg-battery-energy-density/. [Accessed June 2019].

[96]   imec, „Next-Generation Solid-state Batteries," [Online]. Available: https://www.imec-int.com/drupal/sites/default/files/2018-04/imec-solid-state-batteries.pdf. [Accessed July 2019].

[97]   H. Degans, „Imec, partner in EnergyVille, doubles energy density of its solid-state batteries to 400Wh/liter," 18 June 2019. [Online]. Available: https://www.imec-int.com/en/articles/imec-partner-in-energyville-doubles-energy-density-of-its-solid-state-batteries-to-400Wh-liter. [Accessed July 2019].

[98]   C. Barchasz, V. Tarnopolskyi, L. Picard, D. Bloch, S. Patoux en S. Perraud, „Progress and challenges Generation 4," 11 January 2018. [Online]. Available: https://europa.eu/sinapse/webservices/dsp_export_attachement.cfm?CMTY_ID=0C46BEEC-C689-9F80-54C7DD45358D29FB&OBJECT_ID=230DABFD-90AB-8F7D-083EF5BD909DD025&DOC_ID=9C5B92E3-C93C-4321-7C5F116966494AD1&type=CMTY_CAL. [Accessed July 2019].

[99]   U.S. Department of Energy, „DOE Technical Targets for Fuel Cell Systems and Stacks for Transportation Applications," [Online]. Available: https://www.energy.gov/eere/fuelcells/doe-technical-targets-fuel-cell-systems-and-stacks-transportation-applications. [Accessed June 2019].

[100]   O. Faltinsen, Hydrodynamics of High-Speed Marine Vehicles, Cambridge, UK: Cambridge University Press, 2005.

[101]   M. Zhou, „Shekou and Hong Kong Airport Ferry Schedules," [Online]. Available: http://www.shenzhenparty.com/ferry/shekou-hong-kong-airport. [Accessed June 2019].

[102]   Shun Tak-China Travel Ship Management Limited, „FOILCAT," [Online]. Available: https://www.turbojet.com.hk/en/vessel-information/foilcat.aspx. [Accessed June 2019].

[103]   S. Hoerner, W. Michel, L. Ward en T. Buermann, Hydrofoil Handbook; Volume I; Design of Hydrofoil Craft, New York, New York, USA: Bath Iron Works Corp. by Gibbs and Cox, Inc., 1954.

[104]   I. Abbott en A. Doenhoff, Theory of Wing Sections; Including a Summary of Airfoil Data, Mineola, New York, USA: Dover Publications, 1949, 1959.

[105]   I. Abbott en A. Doenhoff, „National Advisory Committee for Aeronautics | Summary of Airfoil Data," Langley Memorial Aeronautical Laboratory, Langley Field, Virginia, USA, 1945.

[106]   Klein Woud, H., Stapersma, D., *Selected Chapters of Design of Auxiliary Systems, Shafting and Flexible Mounting,* Delft: TU Delft, 2016.

[107]   ST | CoCo Yachts, *Waterjets: Overview of Different Systems [Unpublished Word document],* Gorinchem, 2019.

[108]   Marine Jet Power, „Designer's Guide; MJP CSU; MJP DRB," [Online]. Available: https://marinejetpower.com/uploads/2019/03/MJP-DRB-CSU-Designers-Guide.pdf. [Accessed May 2019].

[109]   R. Johnston, „Hydrofoils," *Naval Engineers Journal,* vol. 97, nr. 2, pp. 142-199, 1985.

[110]   T. Timoleon, „Norway The Hydrofoil Years," *Classic Fast Ferries,* October 2003.

[111]   A. Rufolo, „Foil Weigth Saving and Hydrofoil Performance," *Naval Engineers Journal,* vol. 78, nr. 5, pp. 905-913, 1966.

[112]   G. Vreemann en T. v. Stok, „Het antwoord is niet altijd ja," *Grondig,* vol. 4, pp. 28-33, 2018.

[113]   Navy Recognition, „Skjold class coastal Corvette fast attack craft Surface effect ship Catamaran twin Hull patrol boat P960 P961 Storm P962 Skudd P963 Steil P964 Glimt P965 Gnist Royal Norwegian Navy RNoN Umoe Mandal datasheet pictures photos video specifications," 5 September 2011. [Online]. Available: https://www.naval-technology.com/projects/skjold/. [Accessed July 2019].

[114] ST | CoCo Yachts, *160801-02_CC-199-300-WBD-dl [Unpublished Excel document],* Gorinchem, 2019.

[115] Marine Jet Power, „MJP CSU Waterjets - Product data sheet," 16 April 2013. [Online]. Available: https://www.mshs.com/pdf/Products/MJP/MJP_CSU_ProdSheet%20Apr13.pdf. [Accessed April 2019].

[116] Wärtsilä Corporation, „Wärtsilä Waterjets," September 2016. [Online]. Available: https://cdn.wartsila.com/docs/default-source/product-files/gears-propulsors/waterjets/brochure-o-p-waterjets.pdf.

[117] Eland Cables, „BFOU 0.6/1kV Power Cable," March 2014. [Online]. Available: https://www.elandcables.com/handlers/downloadpdf.ashx?url=/media/39499/bfou-0-6-1kv-power-cable.pdf. [Accessed February 2019].

[118] J. Keuning en J. Pinkster, „Further design and seakeeping investigations into the "Enlarged Ship Concept"," in *Fourth International Conference on Fast Sea Transportation, FAST '97*, Sydney, Australia, 1997.

[119] X. Pham, K. Kantimahanthi en P. Sahoo, „Wave Resistance Prediction of Hard-Chine Catamarans through Regression Analysis," Australian Maritime College, Dept. of Naval Architecture & Ocean Engineering, Launceston, Australia, 2015.

[120] ST | CoCo Yachts, *160802_sim_2017.05.19_CC-300_PX1 [Unpublished Excel document],* Gorinchem, 2019.

[121] A. Molland, J. Wellicome en P. Couser, „Resistance Experiments on a Systematic Series of High Speed Displacement Catamaran Forms: Variation of Length-Displacement Ratio and Breadth-Draught Ratio," University of Southampton, Southampton, 1994.

[122] ST | CoCo Yachts, *160801_sim_CC-199 [Unpublished Excel document],* Gorinchem, 2019.

[123] R. Broglia, B. Jacob, S. Zaghi, F. Stern en A. Olivieri, „Experimental investigation of the interference effects for high-speed catamarans," *Ocean Engineering,* vol. 76, pp. 75-85, 2014.

[124] R. Yeung, „Interference Resistance of Multi-Hulls per Thin-Ship Theory," in *20th International Workshop on Water Waves & Floating Bodies*, Longyearbyen, Spitsbergen, Norway, 2005.

[125] Marine Jet Power, *P173672 - CC300 Reintjes 2.96 [Unpublished Excel document],* 2017.

[126] Marine Jet Power, *CC - 199 Reintjes_1 650DD [Unpublished Excel document],* 2017.

[127] D. Scholz, „7 Wing Design," in *Aircraft Design*, Hamburg, Germany, Hamburg University of Applied Sciences, 2015.

[128] J. Wetzel en W. Maxwell, „Tandem Interference Effects of Flat Noncavitating Hydrofoils," St. Anthony Falls Hydraulic Laboratory, Minneapolis, Minnesota, USA, 1962.

[129] W. J. Callister, Materials Science and Engineering; An Introduction, Hoboken, New Jersey, USA: John Wiley & Sons, Inc., 2007.

[130] S. Hoerner, Fluid-Dynamic Drag, 1965.